DEPTH-INTEGRATED FREE-SURFACE FLOW WITH NON-HYDROSTATIC FORMULATION

A DISSERTATION SUBMITTED TO THE GRADUATE DIVISION OF THE

UNIVERSITY OF HAWAI‘I AT MĀNOA IN PARTIAL FULFILLMENT

OF THE REQUIREMENTS FOR THE DEGREE OF

DOCTOR OF PHILOSOPHY

IN

OCEAN AND RESOURCES ENGINEERING

MAY 2012

By

Yefei Bai

Dissertation Committee:

Kwok Fai Cheung, Chairperson
Marcelo H. Kobayashi
Eva-Marie Nosal
Geno Pawlak
Michelle H. Teng

We certify that we have read this dissertation and that, in our opinion, it is satisfactory in scope and quality as a dissertation for the degree of Doctor of Philosophy in Ocean and Resources Engineering.

DISSERTATION COMMITTEE

_____
Chairperson

_____

_____

_____

_____

Acknowledgments

I would like to make a grateful acknowledgment to my advisor Prof. Kwok Fai Cheung, who has been guiding my study and research since I enrolled in the Department of Ocean and Resources Engineering, University of Hawai‘i at Mānoa in 2005. He is the only one who gave me the opportunity to study abroad and that changed my life. I learned disciplinary knowledge from his classes, improved my professional writing skills through his devoted guidance, built career capabilities through a variety of funded research projects, and broadened my horizon in coastal engineering through his insights. I'll treasure these experiences for the rest of my life. I would also like to thank Profs. Marcelo Kobayashi, Geno Pawlak, Eva-Marie Nosal, and Michelle Teng for joining my dissertation committee and the suggestions and comments on my research.

It was full of obstacles during the seven years when I tried to reach this important landmark of my life. However, it is my pleasure to mention that there were always people who would help me overcome each difficulty. Thank you, Drs. Dandridge Greeson and John C. Wiltshire, for helping me prepare my second qualify exam. Thank you, Prof. Miguel Canals, for helping me improve my English and blend in campus life. Thank you, Drs. Yoshiki Yamazaki and Volker Roeber, for sharing incisive understanding in wave modeling. Thank you, Drs. Yong Wei, Liujuan Tang, Yongyan Wu and Liang Ge, for taking care of me when I just arrived in Hawaii. Thank you, Mr. Jacob Tyler, for helping me understand American culture. I would also want to deliver my thanks to the lovely former and current ORE members, Mr. Alex Sánchez, Ms. Sophie Munger, Ms. Megan Craw, Mr. Pablo Duarte-Quiroga, Mr. Justin Stopa, Mr. Troy Heitmann,

Mr. Michael Cynn, Mr. Masoud Hayatdavoodi, Mr. Richard Carter, Dr. Das Suvabrata, Mr. Shailesh Namekar, Dr. Ning Li, Mr. Abdulla Mohamed, Mr. Lei Yan, Dr. Jinfeng Zhang, Ms. Edith Katada, and Ms. Natalie Nagai. It is my pleasure to have you all in my life.

I would like to send my gratitude to my honorific parents, Mr. Yinxi Bai and Ms Zhenhua Zhang. Thank you for being there in China all the time to back me up no matter I am happy or sad, no matter I am right or wrong, and no matter I rise or fall. Special appreciation will be sent to my father-in-law Mr. Xin Zhang and mother-in-law Ms Dongmei Chen who confidently trust me in taking care of their daughter. Finally, my heart goes to my lovely wife, Ms. Chenchen Zhang, the only person worthy of my company in the world.

The research work in this dissertation was funded in part by the Office of Naval Research through Grant No. N00014-02-1-0903 and the National Tsunami Hazard Mitigation Grant No. NA09NWS4670016.

Abstract

This dissertation presents the formulation of depth-integrated wave propagation and runup models from a system of governing equations for two-layer non-hydrostatic flows. The conventional two-layer non-hydrostatic formulation is re-derived from the continuity and Euler equations in non-dimensional form to quantify contributions from nonlinearity and dispersion and transformed into an equivalent integrated system, which separately describes the flux and dispersion-dominated processes. The formulation includes interfacial advection to facilitate mass and momentum exchange over the water column. This equation structure allows direct implementation of a momentum conserving scheme and a moving waterline technique to model wave breaking and runup without interference from the dispersion processes. The non-hydrostatic pressure, however, must be solved at the layer interface and the bottom simultaneously from the pressure Poisson equation, which involves a non-symmetric 9-band sparse matrix for a two-dimensional vertical plane problem. A parameterized non-hydrostatic pressure distribution is introduced to reduce the computational costs and maintain essential dispersion properties for modeling of coastal processes. The non-hydrostatic pressure at mid flow depth is expressed in terms of the bottom pressure with a free parameter, which is optimized to match the exact linear dispersion relation for the water depth parameter up to $kd = 3$. This reduces the integrated two-layer formulation to a hybrid system with unknown non-hydrostatic pressure at the bottom only and a tridiagonal matrix in the pressure Poisson equation. The hybrid system reduces to a one-layer model for a linear distribution of the non-hydrostatic pressure.

Fourier analysis of the governing equations of the two-layer, hybrid, and one-layer systems yield analytical expressions of the linear dispersion and shoaling gradient as well as the super and sub-harmonics transfer functions. The two-layer system reproduces the linear dispersion relation within a $5\,\%$ error for water depth parameter up to $kd = 11$. The hybrid system with an optimized free parameter yields the same dispersion relation as the extended Boussinesq equations. The one-layer system shows a major improvement of the dispersion properties in comparison to the classical Boussinesq equations, but is not sufficient to model coastal wave transformation. The linear shoaling gradient serves as analytical tool to measure wave transformation over a plane slope although it is secondary compared to the linear dispersion relation. In comparison to second-order wave theory, the two-layer system shows overall underestimation of the nonlinearity, while the hybrid system reasonably describes the super and sub-harmonics for kd ranging from 0 to 3.

The two-layer, hybrid, and one-layer systems share common numerical procedures. A staggered finite difference scheme discretizes the governing equations in the horizontal dimension and the Keller box scheme reconstructs the non-hydrostatic terms in the vertical direction. A semi-implicit scheme integrates the depth-integrated flow in time with the non-hydrostatic pressure determined from a Poisson-type equation. Numerical results are verified and validated through a series of numerical and laboratory experiments selected to measure model capabilities in wave dispersion, shoaling, breaking, runup, drawdown, and overtopping. The two-layer model shows good performance in handling these processes through its integrated structure, but slightly underestimates the wave height in shoaling. The hybrid model provides comparable results with the two-layer system in general and slightly improved performance in shoaling calculations due to better approximation of nonlinearity. The one-layer model exhibits stable and robust performance even when the wave characteristics are beyond its applicable range.

Table of Contents

List of Tables

List of Figures

Chapter 1

Introduction

The propagation of ocean waves from deep water to the shore involves a sequence of physical processes with different spatial and temporal scales. Dispersion, which must be balanced by nonlinearity, plays an important role for wave transformation from deep to intermediate water. The flow becomes flux dominated in shallow water and exhibits shock-related hydraulic processes arising from wave breaking. The resulting sheet flow runs up on the beach and returns to the ocean as drawdown. These processes, with different physical properties, have been modeled in part with reasonable accuracy. A complete description of these processes and their interactions in free surface flows is still an area of intense study.

Boussinesq-type equations have provided a theoretical framework to describe coastal wave transformation since their introduction by Peregrine (1967). The depth-integrated governing equations describe the vertical flow structure in terms of high-order derivatives of the horizontal flow velocity. To improve linear dispersion, Madsen et al. (1991) manipulated the dispersion terms to match a [2, 2] Padé expansion in terms of the dimensionless water depth. Nwogu (1993) obtained the same degree of approximation through a consistent derivation from the Euler equations with the velocity evaluated at an optimum level. Wei et al. (1995) extended Nwogu's approach to retain full nonlinearity

of the free surface boundary condition while maintaining the same order of dispersion approximation. Gobbi et al. (2000) subsequently extended the dispersion properties of the model to a $[4, 4]$ Padé approximation through a weighted average of the velocity potential. Madsen et al. (2003, 2006) extended the fully nonlinear Boussinesq formulations of Agnon et al. (1999) to include higher order dispersion over mildly and rapidly varying bathymetry with an infinite power series expansion of the velocity profile. The high-order dispersion terms, however, produce a local anomaly prior to wave breaking that might lead to numerical instability. The eddy viscosity concept (Zelt, 1991) or the roller concept (Schäffer et al., 1993; Madsen and Sørensen, 1997) is embedded in these Boussinesq-type models to account for energy dissipation due to wave breaking.

More recently Boussinesq-type models utilize conservative formulations to describe breaking waves as bores. Kim et al. (2009) derived a conservative form of Boussinesq-type equations from the Navier-Stokes equations together with a shock-capturing finite volume solution, but did not demonstrate the capability of their models in describing discontinuous flows associated with wave breaking and bore formation. Tonelli and Petti (2009) implemented the Boussinesq-type equations from Madsen and Sørensen (1992) that contain the local acceleration and flux terms in conserved variables into a finite volume model. Dutykh et al. (2011) reformulated the classical Boussinesq equation of Peregrine (1967) in conservative form and utilized a finite volume method to describe shock-related processes. Roeber et al. (2010a) re-formulated the Boussinesq-type equations of Nwogu (1993) in the conservative form of the nonlinear shallow-water equations and derived a Godunov-type finite volume scheme for the numerical solution. Since interference of dispersion on flux-dominated processes might lead to instabilities, these models have to turn off the dispersion terms in order to describe breaking waves as bores. Various moving-waterline techniques derived by Roeber et al. (2010a), Lynett et al. (2002), and Kennedy et al. (2000) allow modeling of wave runup and drawdown at the coastline. Boussinesq-type models in conservative or non-conservative formulations

have been extensively applied to study coastal processes with manageable computational requirements.

The non-hydrostatic approach provides an alternative to the Boussinesq-type equations by directly including the vertical flow structure in a multi-layer formulation. This approach decomposes the pressure into hydrostatic and non-hydrostatic components in the Navier-Stokes equations (Casulli, 1995). The continuity equation for an incompressible fluid provides a Poisson equation for the solution of the non-hydrostatic pressure. Mahadevan et al. (1996a,b) verified the well-posedness of the non-hydrostatic approach by scaling analysis and applied the resulting free-surface model to study circulations in the Gulf of Mexico. Casulli and Stelling (1998) and Stansby and Zhou (1998) demonstrated the essential contributions of the non-hydrostatic pressure and vertical flow structure even in shallow water. The dispersion characteristics can be improved by adding more layers without increasing the order of the spatial derivatives in the governing equations (Casulli, 1999; Zhou and Stansby, 1999). Stelling and Zijlema (2003) discretized the primitive non-hydrostatic governing equations on a staggered Cartesian coordinate system by the finite difference method with an edge-based compact scheme. The resulting model reproduces linear dispersion properties in deep water with just two fluid layers. Zijlema and Stelling (2005) employed a boundary-fitted coordinate system in depth integration of the governing equations in each layer to improve the resolution of the non-hydrostatic pressure near boundaries.

The non-hydrostatic approach with first-order spatial derivatives is more amenable to practical applications. Stelling and Duinmeijer (2003) proposed a momentum conserving scheme in a finite difference model to approximate breaking waves as bores or hydraulic jumps without the use of empirical energy dissipation. Zijlema and Stelling (2008) applied the depth-integrated formulation of Zijlema and Stelling (2005) with the momentum conserving scheme and a wet-dry algorithm to simulate wave breaking and runup in the surf zone. They subsequently released the serial and parallel codes,

known as SWASH (Simulating WAves till SHore), in the public domain (Zijlema et al., 2011). Yamazaki et al. (2009) applied an upwind-flux approximation scheme in a one-layer model to describe energetic wave breaking, bore propagation, and runup. Most importantly, the first-order spatial derivatives in the governing equations allow implementation of two-way nested grids to model wave transformation processes of different spatial and temporal scales (Yamazaki et al., 2011). The resulting model, known as NEOWAVE (Non-hydrostatic Evolution of Ocean WAVE), has been implemented in studies of 2009 Samoa, 2009 Mentawai, 2010 Chile, and 2011 Tohoku tsunamis (Roeber et al., 2010b; Yamazaki and Cheung, 2011; Lay et al., 2011a,b). The simplicity of the code and its computational efficiency enable modeling of basin-wide tsunami propagation and regional-scale inundation through a system of two-way nested grids.

The dispersion property of the non-hydrostatic approach is primarily determined by the number of layers over the water column. A two-layer model is sufficient to achieve good dispersion characteristic in coastal engineering applications (Zijlema and Stelling, 2005, 2008). However, implementations of the non-hydrostatic approach for wave breaking and runup have been limited to one-layer models except for the recent work of Ai and Jin (2012) with a finite volume formulation, which approximates the boundary conditions with layer-averaged velocities and requires up to ten layers to accurately describe vertical distributions of the velocity and non-hydrostatic terms. Computational requirements represent another issue that needs special consideration. A multi-layer model requires a considerable amount of computational resources in the implicit solution of the pressure Poisson equation that inhibits its application over a large region. Despite the widespread numerical implementations, analytical expressions of the linear and non-linear properties of the non-hydrostatic models have not been explored to the extent as in studies of the Boussinesq-type approach (Nwogu, 1993; Gobbi et al., 2000; Madsen et al., 2003, 2006). A systematic analysis of those properties in the non-hydrostatic model is not evident in the literature.

The goal of this dissertation is to develop an alternate formulation for non-hydrostatic free surface flows that can account for dispersion and flux-dominated processes with strongly nonlinear interactions for coastal engineering applications. The formulation begins with depth integration of the non-dimensional Euler equations with non-hydrostatic pressure. The resulting governing equations for two-layer flows, which are equivalent to those of Zijlema and Stelling (2005), are then transformed into an integrated two-layer system. This integrated system allows implementation of the momentum-conserving advection scheme for breaking wave approximation and a moving-waterline scheme for inundation calculation, while maintaining the dispersion characteristics of the original two-layer formulation for modeling of coastal processes. The pressure Poisson equation derived from the two-layer formulation requires substantial computation resources that might become an issue in practical coastal engineering applications. A parameterized non-hydrostatic pressure distribution expresses the pressure at mid flow depth in terms of the bottom pressure to reduce the computational requirements to those of the one layer model, while retaining essential dispersion characteristic through optimization of the pressure distribution. A linear pressure distribution converts this hybrid model into a one-layer model (Yamazaki et al., 2009, 2011).

The capability of the one-layer, hybrid and two-layer systems to describe fundamental linear and nonlinear wave properties is first examined. A perturbation expansion extracts the first and second order governing equations from the three systems. The corresponding analytical solutions allow a thorough examination of their linear dispersion and shoaling properties as well as nonlinear monochromatic and bichromatic interactions against solutions from first and second-order wave theories as well as the classical and extended Boussinesq equations. The theoretical analysis is supplemented by numerical solutions of the governing equations. The three systems have similar numerical procedures except for the derivation of the pressure Poisson equation. The governing equations are discretized over a staggered grid on a boundary fitted coordinate in the two-dimensional vertical plane with a finite difference scheme. The pressure correction

technique splits time integration into a hydrostatic and a non-hydrostatic step. An intermediate solution from the hydrostatic step provides the input to the pressure Poisson equation in the second step to yield non-hydrostatic pressure distribution. Numerical results are compared and validated with previous laboratory experiments for regular wave transformation over a submerged bar and a plane beach as well as solitary wave propagation on a flat bottom, a plane beach and a fringing reef.

Chapter 2

Governing Equations

This chapter summarizes the formulation of the conventional two-layer non-hydrostatic model for free surface flows and describes the derivation of the governing equations for the integrated two-layer and hybrid systems and their relation to the one-layer system. In contrast to related works in the literature, the governing equations are derived from the Euler equations in dimensionless form to highlight the contributions of the various terms to dispersion and nonlinearity.

2.1 Non-dimensional Euler Equations

Consider a two-dimensional free-surface flow in the Cartesian coordinate system (x, z) in Figure 2.1. The variables d and ζ denote water depth and surface elevation, and $h = \zeta + d$ is the flow depth. The layer interface is placed at the mid flow depth $z_\alpha = (\zeta - d)/2$, which varies with ζ over time t. Three characteristic length scales a_0, d_0, and l_0 represent the magnitude of wave amplitude, water depth, and wavelength, while the corresponding shallow-water celerity $\sqrt{gd_0}$ allows scaling of water particle velocities. These give rise to the dimensionless parameters $\epsilon = a_0/d_0$ and $\mu = d_0/l_0$, which denote nonlinearity and dispersion in the dimensionless governing equations. The following

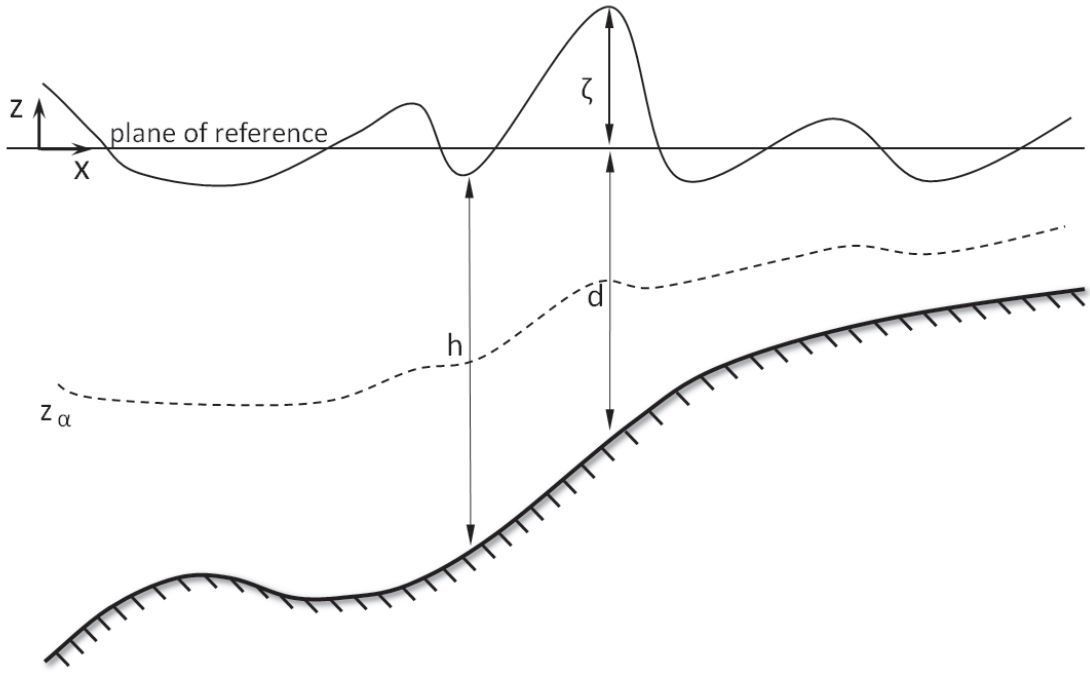

Figure 2.1. Definition sketch of a two-layer free-surface flow system.

physical variables (primed) are then converted to dimensionless quantities as

$$x = \frac{x'}{l_0} \qquad z = \frac{z'}{d_0} \qquad t = \frac{t'}{l_0/\sqrt{gd_0}} \qquad \zeta = \frac{\zeta'}{a_0} \tag{2.1.1}$$

The scaling of the velocity components (u, w) can lead to an appropriate form of governing equations for specific physical problems. For non-hydrostatic free-surface flow models in coastal engineering applications, the two components are expressed in the following dimensionless form

$$u = \frac{u'}{\epsilon\sqrt{gd_0}} \qquad w = \frac{w'}{\epsilon\mu\sqrt{gd_0}} \tag{2.1.2}$$

The nonlinear parameter ϵ scales the resulting governing equations for applications with gravity waves, while the dispersion parameter μ allows resolution of the vertical structure even in flux-dominated flows. These parameters become instrumental should truncation of high-order terms in the governing equations become necessary.

The non-hydrostatic formulation includes the pressure explicitly in the governing equations. Following Casulli (1995), the dimensional pressure is decomposed into hydro-

static and non-hydrostatic components as

$$p' = g(\zeta' - z') + q' \tag{2.1.3}$$

where q' denotes the dimensional non-hydrostatic pressure. Similarly, the scaling of the non-hydrostatic pressure will affect the form of the governing equations. A parameter n allows scaling of the non-hydrostatic pressure with respect to the hydrostatic pressure P as

$$q = \frac{q'}{nP} \tag{2.1.4}$$

When Mahadevan et al. (1996a,b) examined the well-posedness of the non-hydrostatic approach for large-scale circulation, they balanced the vertical Coriolis acceleration with the non-hydrostatic gradient by setting $n = \mu$. Marshall et al. (1997) discussed the use of this parameter in scaling of the governing equations for hydrostatic, quasi-hydrostatic, and non-hydrostatic problems and outlined a strategy for ocean models to perform efficiently and accurately in different spatial scales. In the hydrostatic and geostrophic limit, they found that $n = \mu^2/R_i$, where R_i is Richardson number. To stand out wave characteristics, factors such as Coriolis effects, surface shear stress, and viscous dissipation are not considered in this study. Vertical acceleration in the momentum equation will be fully balanced by the non-hydrostatic pressure gradient, which leads to $n = \mu^2$.

Substitution of (2.1.1), (2.1.2) and (2.1.4) into the continuity and Euler equations gives the dimensionless governing equations for non-hydrostatic free-surface flows

$$\frac{\partial u}{\partial x} + \frac{\partial w}{\partial z} = 0 \tag{2.1.5}$$

$$\frac{\partial u}{\partial t} + \epsilon\frac{\partial u^2}{\partial x} + \epsilon\frac{\partial uw}{\partial z} + \frac{\partial \zeta}{\partial x} + \mu^2\frac{\partial q}{\partial x} = 0 \tag{2.1.6}$$

$$\frac{\partial w}{\partial t} + \epsilon\frac{\partial uw}{\partial x} + \epsilon\frac{\partial w^2}{\partial z} + \frac{\partial q}{\partial z} = 0 \tag{2.1.7}$$

The kinematic boundary conditions at the free surface and seabed become

$$w_\zeta = \frac{\partial \zeta}{\partial t} + \epsilon u_\zeta \frac{\partial \zeta}{\partial x} \qquad z = \epsilon\zeta \tag{2.1.8}$$

$$w_d = -u_d \frac{\partial d}{\partial x} \qquad\qquad z = -d \tag{2.1.9}$$

The parameters ϵ and μ^2 indicate the nonlinear and dispersion terms respectively. Since $\partial u/\partial x$ and $\partial w/\partial z$ have the same order of magnitude, the dispersion parameter μ does not exist in the continuity equation (2.1.3). In the x direction, the horizontal derivative of the surface elevation has the same order of magnitude as the local acceleration, while the non-hydrostatic gradient has an order of magnitude μ^2. In the z direction, the magnitude of the local vertical acceleration and the non-hydrostatic gradient are of the same order.

Stelling and Zijlema (2003) applied the finite difference method to the dimensional form of the governing equations (2.1.5) - (2.1.7) and achieved good dispersion characteristics with just two vertical layers through the Keller-box scheme. However, the non-conservative form of the governing equations cannot fully describe discontinuous flows due to wave breaking and runup.

2.2 Conventional Two-layer Formulation

Conservative forms of governing equations enable descriptions of discontinuities in free surface flows and approximations of breaking waves as bores or hydraulic jumps. Zijlema and Stelling (2005) derived a depth-integrated form of the continuity and Euler equations (2.1.5) - (2.1.7) in a multi-layer system and converted the resulting governing equations to a conservative form with good dispersion characteristic by application of just two layers. This section provides a re-derivation of their governing equations in dimensionless form to provide a more systematic account of the nonlinear and dispersion terms.

Figure 2.1 provides the definition sketch of the two-layer flow system. Depth-integration of the continuity equation (2.1.5) in the bottom and top layers with application of Leib-

niz's rule yields

$$\frac{\partial}{\partial x}\int_{-d}^{z_\alpha} u dz - u_{z_\alpha}\frac{\partial z_\alpha}{\partial x} + w_{z_\alpha} = 0 \tag{2.2.1}$$

$$\frac{\partial}{\partial x}\int_{z_\alpha}^{\epsilon\zeta} u dz + \frac{\partial \zeta}{\partial t} + u_{z_\alpha}\frac{\partial z_\alpha}{\partial x} - w_{z_\alpha} = 0 \tag{2.2.2}$$

where u_{z_α} and w_{z_α} are the horizontal and vertical velocity components at the instantaneous location of the interface defined by $z_\alpha = (\epsilon\zeta - d)/2$. The horizontal component u_{z_α} is defined as the average from the bottom and top layers and the vertical component w_{z_α} should be distinguished from the interface vertical velocity based on a kinematic boundary condition. A relative vertical velocity $\overline{w}_{z_\alpha}$ defines the difference between w_{z_α} and the vertical velocity of the interface as

$$\overline{w}_{z_\alpha} = w_{z_\alpha} - \frac{1}{\epsilon}\frac{\partial z_\alpha}{\partial t} - u_{z_\alpha}\frac{\partial z_\alpha}{\partial x} \tag{2.2.3}$$

This variable facilitates transfer of mass and momentum across the interface that might become important for discontinuous flows. Depth integration of the horizontal momentum equation (2.1.6) at the bottom and top layers yields

$$\begin{aligned}\frac{\partial}{\partial t}\int_{-d}^{z_\alpha} u dz + \epsilon\frac{\partial}{\partial x}\int_{-d}^{z_\alpha} u^2 dz + \frac{\partial \zeta}{\partial x}(z_\alpha + d) \\ + \mu^2\left(\frac{\partial}{\partial x}\int_{-d}^{z_\alpha} q dz - q_{z_\alpha}\frac{\partial z_\alpha}{\partial x} - q_d\frac{\partial d}{\partial x}\right) + \epsilon u_{z_\alpha}\overline{w}_{z_\alpha} = 0\end{aligned} \tag{2.2.4}$$

$$\begin{aligned}\frac{\partial}{\partial t}\int_{z_\alpha}^{\epsilon\zeta} u dz + \epsilon\frac{\partial}{\partial x}\int_{z_\alpha}^{\epsilon\zeta} u^2 dz + \frac{\partial \zeta}{\partial x}(\epsilon\zeta - z_\alpha) \\ + \mu^2\left(\frac{\partial}{\partial x}\int_{z_\alpha}^{\epsilon\zeta} q dz - q_\zeta\frac{\partial \zeta}{\partial x} + q_{z_\alpha}\frac{\partial z_\alpha}{\partial x}\right) - \epsilon u_{z_\alpha}\overline{w}_{z_\alpha} = 0\end{aligned} \tag{2.2.5}$$

Depth integration of the vertical momentum equation (2.1.7) yields

$$\frac{\partial}{\partial t}\int_{-d}^{z_\alpha} w dz + \epsilon\frac{\partial}{\partial x}\int_{-d}^{z_\alpha} uw dz + q_{z_\alpha} - q_d + \epsilon w_{z_\alpha}\overline{w}_{z_\alpha} = 0 \tag{2.2.6}$$

$$\frac{\partial}{\partial t}\int_{z_\alpha}^{\epsilon\zeta} w dz + \epsilon\frac{\partial}{\partial x}\int_{z_\alpha}^{\epsilon\zeta} uw dz + q_\zeta - q_{z_\alpha} - \epsilon w_{z_\alpha}\overline{w}_{z_\alpha} = 0 \tag{2.2.7}$$

It should be pointed out that the terms $u_{z_\alpha}\overline{w}_{z_\alpha}$ and $w_{z_\alpha}\overline{w}_{z_\alpha}$ also contribute to the nonlinear properties and play an important role in momentum exchange when strong nonlinear advection occurs at discontinuities.

The governing equations (2.2.1), (2.2.2), and (2.2.4) - (2.2.7) are formulated in terms of definite integrals that can be evaluated from the piecewise linear velocity and pressure profiles. Integration of the horizontal velocity over the bottom and top layers give

$$\int_{-d}^{z_\alpha} u\,dz = h_1 u_1 \tag{2.2.8}$$

$$\int_{z_\alpha}^{\epsilon\zeta} u\,dz = h_2 u_2 \tag{2.2.9}$$

where $h_1 = z_\alpha + d$ and $h_2 = \epsilon\zeta - z_\alpha$ denote the flow depth and the subscripts 1 and 2 identify quantities for the bottom and top layers respectively. The integral of the quadratic velocity terms in (2.2.4) and (2.2.5) can be expressed as

$$\int_{-d}^{z_\alpha} u^2\,dz = \int_{-d}^{z_\alpha} (u_1 + \Delta u_1)^2\,dz = h_1 u_1^2 + \int_{-d}^{z_\alpha} \Delta u_1^2\,dz \tag{2.2.10}$$

$$\int_{z_\alpha}^{\epsilon\zeta} u^2\,dz = \int_{z_\alpha}^{\epsilon\zeta} (u_2 + \Delta u_2)^2\,dz = h_2 u_2^2 + \int_{z_\alpha}^{\epsilon\zeta} \Delta u_2^2\,dz \tag{2.2.11}$$

where Δu_1 and Δu_2 denote linear variations about the layer averaged values. Integrals of Δu_1^2 and Δu_2^2 are commonly treated as diffusion and are neglected here. Application of the trapezoidal rule gives the integrals of the non-hydrostatic pressure and vertical velocity at each layer as

$$\int_{-d}^{z_\alpha} q\,dz = \frac{h_1}{2}\left(q_{z_\alpha} + q_d\right) \tag{2.2.12}$$

$$\int_{z_\alpha}^{\epsilon\zeta} q\,dz = \frac{h_2}{2}\left(q_\zeta + q_{z_\alpha}\right) \tag{2.2.13}$$

$$\int_{-d}^{z_\alpha} w\,dz = h_1 w_1 = \frac{h_1}{2}\left(w_{z_\alpha} + w_d\right) \tag{2.2.14}$$

$$\int_{z_\alpha}^{\epsilon\zeta} w\,dz = h_2 w_2 = \frac{h_1}{2}\left(w_\zeta + w_{z_\alpha}\right) \tag{2.2.15}$$

The vertical velocity at the free surface and seabed is given by

$$w_\zeta = \frac{\partial\zeta}{\partial t} + \epsilon u_2 \frac{\partial\zeta}{\partial x} \qquad z = \epsilon\zeta \tag{2.2.16}$$

$$w_d = -u_1 \frac{\partial d}{\partial x} \qquad z = -d \tag{2.2.17}$$

and w_{z_α} is determined from the continuity equation (2.2.1) or (2.2.2).

Implementation of the above approximations gives a closed system of six governing equations with six unknowns ζ, u_1, u_2, w_{z_α}, q_{z_α} and q_d. The continuity, horizontal momentum, and vertical momentum equations for the two-layer flow system are given respectively as

$$\frac{\partial h_1 u_1}{\partial x} - \frac{1}{2}(u_1 + u_2)\frac{\partial z_\alpha}{\partial x} + w_{z_\alpha} = 0 \tag{2.2.18}$$

$$\frac{\partial h_2 u_2}{\partial x} + \frac{\partial \zeta}{\partial t} + \frac{1}{2}(u_1 + u_2)\frac{\partial z_\alpha}{\partial x} - w_{z_\alpha} = 0 \tag{2.2.19}$$

$$\begin{aligned}\frac{\partial u_1}{\partial t} + \frac{1}{h_1}(\epsilon\frac{\partial h u_1^2}{\partial x} - u_1\frac{\partial h_1}{\partial t}) + \frac{\partial \zeta}{\partial x} \\ + \frac{\mu^2}{h_1}(\frac{1}{2}\frac{\partial h_1(q_{z_\alpha} + q_d)}{\partial x} - q_{z_\alpha}\frac{\partial z_\alpha}{\partial x} - q_d\frac{\partial d}{\partial x}) + \frac{\epsilon}{h_1}u_{z_\alpha}\overline{w}_{z_\alpha} = 0\end{aligned} \tag{2.2.20}$$

$$\begin{aligned}\frac{\partial u_2}{\partial t} + \frac{1}{h_2}(\epsilon\frac{\partial h u_2^2}{\partial x} - u_2\frac{\partial h_2}{\partial t}) + \frac{\partial \zeta}{\partial x} \\ + \frac{\mu^2}{h_2}(\frac{1}{2}\frac{\partial h_2(q_\zeta + q_{z_\alpha})}{\partial x} - q_\zeta\frac{\partial \zeta}{\partial x} + q_{z_\alpha}\frac{\partial z_\alpha}{\partial x}) - \frac{\epsilon}{h_2}u_{z_\alpha}\overline{w}_{z_\alpha} = 0\end{aligned} \tag{2.2.21}$$

$$\frac{\partial w_1}{\partial t} + \frac{1}{h_1}(\epsilon\frac{\partial h_1 u_1 w_1}{\partial x} - w_1\frac{\partial h_1}{\partial t}) + q_{z_\alpha} - q_d + \frac{\epsilon}{h_1}w_{z_\alpha}\overline{w}_{z_\alpha} = 0 \tag{2.2.22}$$

$$\frac{\partial w_2}{\partial t} + \frac{1}{h_2}(\epsilon\frac{\partial h_2 u_2 w_2}{\partial x} - w_2\frac{\partial h_2}{\partial t}) + q_\zeta - q_{z_\alpha} - \frac{\epsilon}{h_2}w_{z_\alpha}\overline{w}_{z_\alpha} = 0 \tag{2.2.23}$$

Equations (2.2.18) - (2.2.23), which encompass the kinematic boundary conditions (2.2.16) and (2.2.17) and the dynamic free surface boundary condition $q_\zeta = 0$, represent the conventional formulation of two-layer non-hydrostatic free-surface flow.

2.3 Integrated Two-layer Formulation

The conventional formulation provides a direct description of the flows in each layer and resolves their interactions only at the interface. The governing equations consist of two single layer non-hydrostatic systems with interfacial motions described by the relative vertical velocity. Since the governing equations for each layer share the same structure,

it is straightforward to implement the formulation in a multi-layer system. However, this layered structure conceals the merits of the two-layer over the one-layer formulation and may encounter numerical difficulties in handling wave breaking, runup, and drawdown. To overcome these problems, a new representation of the flow structure is introduced by a linear transformation

$$u = \frac{1}{2}\, u_1 + \frac{1}{2}\, u_2 \tag{2.3.1}$$

$$\Delta u = \frac{1}{2}\, u_1 - \frac{1}{2}\, u_2 \tag{2.3.2}$$

$$w = \frac{1}{2}\, w_1 + \frac{1}{2}\, w_2 \tag{2.3.3}$$

$$\Delta w = \frac{1}{2}\, w_1 - \frac{1}{2}\, w_2 \tag{2.3.4}$$

where $(u,\, w)$ is the depth-integrated velocity and $(\Delta u,\, \Delta w)$ is the velocity gradient between the two layers. Substitution of (2.3.1) - (2.3.4) into the continuity equations (2.2.18) and (2.2.19) gives

$$\frac{\partial \zeta}{\partial t} + \frac{\partial hu}{\partial x} = 0 \tag{2.3.5}$$

$$\overline{w}_{z_\alpha} + \frac{1}{2}\, \frac{\partial h \Delta u}{\partial x} = 0 \tag{2.3.6}$$

The first continuity equation (2.3.5) is consistent with the one in the nonlinear shallow-water equations, but different from typical Boussinesq formulations. It balances the local variation of the surface elevation with the horizontal derivative of the flux without interference from dispersion. The second continuity equation (2.3.6) shows that the relative vertical velocity is proportional to the horizontal derivative of the flux gradient, which becomes zero if there is no flux exchange between the two layers.

Similarly, the transformed horizontal momentum equations, which describe evolution of u and Δu, become

$$\begin{aligned} &\frac{\partial u}{\partial t} + \frac{\epsilon}{h}\left(\frac{\partial \left(hu^2 + h\Delta u^2\right)}{\partial x} - u\frac{\partial hu}{\partial x}\right) \\ &\quad + \frac{\partial \zeta}{\partial x} + \frac{\mu^2}{h}\left(\frac{1}{2}\frac{\partial h q_{z_\alpha}}{\partial x} + \frac{1}{4}\frac{\partial h q_d}{\partial x} - q_d \frac{\partial d}{\partial x}\right) = 0 \end{aligned} \tag{2.3.7}$$

$$\frac{\partial \Delta u}{\partial t}+\frac{\epsilon}{h}\left(2\frac{\partial hu\Delta u}{\partial x}-\Delta u\frac{\partial hu}{\partial x}\right) +\frac{\mu^2}{h}\left(\frac{1}{4}\frac{\partial hq_d}{\partial x}-q_{z_\alpha}\frac{\partial\left(\epsilon\zeta-d\right)}{\partial x}-q_d\frac{\partial d}{\partial x}\right)+\frac{2\,\epsilon}{h}u_{z_\alpha}\overline{w}_{z_\alpha}=0 \tag{2.3.8}$$

With the interface defined at the mid flow depth, the second momentum equation (2.3.8) no longer contains the horizontal derivative of the surface elevation and the local variation of the flux gradient mainly reflects the balance between nonlinearity and dispersion effects. The linear transformation converts the vertical momentum equations into

$$\frac{\partial w}{\partial t}+\frac{\epsilon}{h}\left(\frac{\partial\left(huw+h\Delta u\Delta w\right)}{\partial x}-w\frac{\partial hu}{\partial x}\right)-\frac{q_d}{h}=0 \tag{2.3.9}$$

$$\frac{\partial \Delta w}{\partial t}+\frac{\epsilon}{h}\left(\frac{\partial\left(hu\Delta w+h\Delta uw\right)}{\partial x}-\Delta w\frac{\partial hu}{\partial x}\right) +2\,\frac{q_{z_\alpha}}{h}-\frac{q_d}{h}+\frac{2\,\epsilon}{h}w_{z_\alpha}\overline{w}_{z_\alpha}=0 \tag{2.3.10}$$

The vertical velocity and gradient are approximated by the trapezoidal rule as

$$w=\frac{1}{4}\left(w_\zeta+w_{z_\alpha}\right)+\frac{1}{4}\left(w_{z_\alpha}+w_d\right) \tag{2.3.11}$$

$$\Delta w=\frac{1}{4}\left(w_\zeta+w_{z_\alpha}\right)-\frac{1}{4}\left(w_{z_\alpha}+w_d\right) \tag{2.3.12}$$

where w_{z_α} is determined from the continuity equation (2.3.6) and w_ζ and w_d from the kinematic boundary conditions (2.2.16) and (2.2.17) as

$$w_\zeta=\frac{\partial\zeta}{\partial x}+(u-\Delta u)\frac{\partial\zeta}{\partial x} \tag{2.3.13}$$

$$w_d=-(u+\Delta u)\frac{\partial d}{\partial x} \tag{2.3.14}$$

The present governing equations, which are equivalent to those from the conventional formulation, provide an alternate description of the two-layer flow system.

Originated from the continuity and Euler equations, the derivation of the governing equations (2.3.5) - (2.3.10) does not involve the irrotational condition. The two-layer

flow structure is able to resolve a low level of vorticity. The non-dimensional horizontal vorticity equation reads

$$\frac{\partial u_e}{\partial z} - \mu^2 \frac{\partial w_e}{\partial x} = \Omega \tag{2.3.15}$$

where (u_e, w_e) is the fluid particle velocity and Ω the vorticity. Integration of (2.3.15) within the bottom and top layers with the corresponding boundary conditions gives

$$u_{z_\alpha} - u_d - \mu^2 \int_{-d}^{z_\alpha} \frac{\partial w_e}{\partial x} dz = \int_{-d}^{z_\alpha} \Omega \, dz \tag{2.3.16}$$

$$u_\zeta - u_{z_\alpha} - \mu^2 \int_{z_\alpha}^{\epsilon\zeta} \frac{\partial w_e}{\partial x} dz = \int_{z_\alpha}^{\epsilon\zeta} \Omega \, dz \tag{2.3.17}$$

Adding (2.3.16) and (2.3.17) together with the transformation (2.3.2) yields

$$\Delta u = -\frac{\mu^2}{2} \int_{-d}^{\epsilon\zeta} \frac{\partial w_e}{\partial x} \, dz - \frac{1}{2} \int_{-d}^{\epsilon\zeta} \Omega \, dz \tag{2.3.18}$$

which defines the horizontal velocity gradient in terms of dispersion and vorticity. The velocity gradient Δu includes effects of the vertical velocity associated with the non-hydrostatic pressure that represents the main driving mechanism for dispersion. In addition, Δu may alter the nonlinear advection terms through the two-layer flow structure to realize rotational effects associated wave breaking, runup, and drawdown. The formulation of Boussinesq equations typically involves the irrotational condition, which expresses the vertical flow structure by high-order derivatives of the horizontal velocity in the continuity equation and momentum equations to account for dispersion (Peregrine, 1967; Madsen and Sørensen, 1992; Nwogu, 1993; Wei et al., 1995; Gobbi et al., 2000; Madsen et al., 2006). To include rotational effects, Veeramony and Svendsen (2000) implemented a roller concept based on the solution of the vorticity transport equations without considering viscosity to model wave breaking in the surf zone. Kim et al. (2009) re-derived a set of Boussinesq equations from the Navier Stokes equations to capture rotational flows around coastal structures.

The integrated two-layer system (2.3.5) - (2.3.10) maintains the same linear dispersion characteristics as the conventional two-layer formulation (Zijlema and Stelling,

2005), but provides two sets of governing equations to describe dispersion and flux-dominated processes. In deep water, the dispersion-dominated governing equations (2.3.6), (2.3.8) and (2.3.10) alter the depth-integrated velocity to describe short-period dispersive waves. As waves propagate into shallow water, the flux-dominated governing equations (2.3.5), (2.3.7) and (2.3.9) describe breaking and broken waves as bores through momentum conservation and wave runup and drawdown as sheet flows. The dispersion-dominated system remains in the doldrums complementing shock-related hydraulic processes without creating numerical instabilities. The two sets of governing equations are coupled through Δu and Δw in contrast to the conventional two-layer formulation, in which the interactions only take place at the interface. In addition, the nonlinear interfacial advection terms $u_{z_\alpha}\overline{w}_{z_\alpha}$ and $w_{z_\alpha}\overline{w}_{z_\alpha}$, which only exist in momentum equations (2.3.8) and (2.3.10), are responsible for momentum exchange between the two layers. They only contribute to nonlinear wave properties and play a fundamental role in determining the wave profile and flow structure when interfacial activities are dominant.

This integrated two-layer system provides a general approach to describe wave transformation from deep to shallow water as well as the coastal processes for practical application, but contains six unknowns ζ, u, Δu, $w_{h/2}$, $q_{h/2}$ and q_d in the six governing equations. The numerical solution involves a pressure Poisson equation, which contains a non-symmetric 9-band sparse matrix for one-dimensional problems or a non-symmetric 15-band sparse matrix for two-dimensional problems. The computational requirements might become an issue for application over a large region.

2.4 One-layer Formulation

For weakly dispersive waves, the depth-integrated velocity gradient (Δu, Δw) and interfacial advection diminish. The non-hydrostatic pressure and the velocity have a linear

distribution over the water column. The governing equations of the integrated two-layer formulation (2.3.5) - (2.3.10) reduces to those of a one-layer system in terms of the depth-averaged velocity (u, w) and non-hydrostatic pressure q_d at the bottom as

$$\frac{\partial \zeta}{\partial t}+\frac{\partial hu}{\partial x}=0 \tag{2.4.1}$$

$$\frac{\partial u}{\partial t}+\frac{\epsilon}{h}\left(\frac{\partial hu^2}{\partial x}-u\frac{\partial hu}{\partial x}\right)+\frac{\partial \zeta}{\partial x}+\frac{\mu^2}{2}\frac{\partial q_d}{\partial x}+\frac{\mu^2 q_d}{2h}\frac{\partial\left(\zeta-d\right)}{\partial x}=0 \tag{2.4.2}$$

$$\frac{\partial w}{\partial t}+\frac{\epsilon}{h}\left(\frac{\partial huw}{\partial x}-w\frac{\partial hu}{\partial x}\right)-\frac{q_d}{h}=0 \tag{2.4.3}$$

The depth-averaged vertical velocity is approximated by

$$w=\frac{1}{2}w_\zeta+\frac{1}{2}w_d \tag{2.4.4}$$

in which the vertical velocity at the free surface and bottom are given by

$$w_\zeta=\frac{\partial \zeta}{\partial t}+\epsilon u\frac{\partial \zeta}{\partial x} \tag{2.4.5}$$

$$w_d=-u\frac{\partial d}{\partial x} \tag{2.4.6}$$

The one-layer system, which has three variables ζ, u, and q_d in the three governing equations, is closed by the kinematic boundary conditions at the free surface and bottom in (2.4.5) and (2.4.6).

In the numerical solution, the pressure Poisson equation involves a tridiagonal and a 5-band matrix in one and two-dimensional problems. In addition, the rank of the matrix is reduced by one half in comparison to the two-layer system. Yamazaki et al. (2009, 2011) developed the numerical model, NEOWAVE, based on this one-layer formulation. The simplicity of the code and its computational efficiency enable modeling of basin-wide tsunami propagation and regional-scale inundation through a system of two-way nested grids (Roeber et al., 2010b; Yamazaki and Cheung, 2011; Lay et al., 2011a). However, the dispersion properties of the one-layer structure are not sufficient to model transformation of short period waves from deep to shallow water in most coastal engineering applications.

2.5 Hybrid Formulation

The integrated two-layer system reduces to a one-layer system without the gradient terms. The corresponding non-hydrostatic pressure has a linear distribution equivalent to $q_{z_\alpha} = 0.5\, q_d$. The piecewise linear distribution of the non-hydrostatic pressure is amenable to highly dispersive waves and discontinuous flows. In lieu of a two-layer system, some features can be retained through the non-hydrostatic pressure in the form

$$q_{z_\alpha} = \alpha\, q_d \tag{2.5.1}$$

where α is a free parameter to optimize the wave characteristics over a range of water depth parameters analogous to the approach introduced by Nwogu (1993) for the Boussinesq equations. Since the non-hydrostatic pressure at the free surface q_ζ is zero, the relation (2.5.1) with α ranging from 0.5 to 1.0 is equivalent to a predefined piecewise linear distribution of the non-hydrostatic pressure. When $\alpha = 0.5$, the pressure has a linear distribution over the water column as in a one-layer model.

The pressure relation (2.5.1) provides an alternate formulation for depth-integrated non-hydrostatic flows. Substitution of this relation into the governing equations (2.3.5) - (2.3.10) yields a hybrid system that retains the simplicity and efficiency of a one-layer model and adequate dispersion properties of a two-layer model. The governing equations for flux-dominated flows read

$$\frac{\partial \zeta}{\partial t} + \frac{\partial hu}{\partial x} = 0 \tag{2.5.2}$$

$$\begin{aligned} &\frac{\partial u}{\partial t} + \frac{\epsilon}{h}\left(\frac{\partial \left(hu^2 + h\Delta u^2\right)}{\partial x} - u\frac{\partial hu}{\partial x}\right) + \frac{\partial \zeta}{\partial x} \\ &\quad + \mu^2\left(\frac{\alpha}{2} + \frac{1}{4}\right)\left(\frac{\partial q_d}{\partial x} + \frac{q_d}{h}\frac{\partial h}{\partial x}\right) - \mu^2 q_d \frac{\partial d}{\partial x} = 0 \end{aligned} \tag{2.5.3}$$

$$\frac{\partial w}{\partial t} + \frac{\epsilon}{h}\left(\frac{\partial \left(huw + h\Delta u\Delta w\right)}{\partial x} - w\frac{\partial hu}{\partial x}\right) - \frac{q_d}{h} = 0 \tag{2.5.4}$$

The governing equations for dispersion-dominated system become

$$\frac{\partial \zeta}{\partial t} - \frac{\partial h\Delta u}{\partial x} + u\,\frac{\partial\left(\zeta - d\right)}{\partial x} - 2\,w_{z_\alpha} = 0 \tag{2.5.5}$$

$$\begin{aligned}\frac{\partial \Delta u}{\partial t} + \frac{\epsilon}{h}\left(2\,\frac{\partial hu\Delta u}{\partial x} - \Delta u\frac{\partial hu}{\partial x}\right) + \frac{\mu^2}{4}\frac{\partial q_d}{\partial x} \\ +\mu^2\left(\frac{1}{4} - \alpha\right)\frac{q_d}{h}\frac{\partial h}{\partial x} + \mu^2\left(2\alpha - 1\right)\frac{q_d}{h}\frac{\partial d}{\partial x} + \frac{2\,\epsilon}{h}u_{z_\alpha}\overline{w}_{z_\alpha} = 0\end{aligned} \tag{2.5.6}$$

$$\begin{aligned}\frac{\partial \Delta w}{\partial t} + \frac{\epsilon}{h}\left(\frac{\partial\left(hu\Delta w + h\Delta uw\right)}{\partial x} - \Delta w\frac{\partial hu}{\partial x}\right) \\ + \frac{\left(2\alpha - 1\right)q_d}{h} + \frac{2\,\epsilon}{h}w_{z_\alpha}\overline{w}_{z_\alpha} = 0\end{aligned} \tag{2.5.7}$$

Equations (2.3.11) - (2.3.14) are still employed to connect the vertical velocity with the horizontal fluid motion in the two layers.

The governing equations (2.5.2) - (2.5.7) have the same structure as the two-layer flow system, but with the unknown pressure q_{z_α} at the interface replaced by the free parameter α. The introduction of α allows tuning of wave dispersion due to the non-hydrostatic pressure, but does not alter the dispersion characteristics associated with the bottom slope as shown in the horizontal momentum equation (2.5.3). On the other hand, α modifies the flow and bottom terms without affecting the pressure gradient in the momentum equation (2.5.6). The removal of the interface non-hydrostatic pressure q_{z_α} reduces the pressure Poisson equation from a two-layer system to a one-layer system. The model still retains a two-layer flow structure through the solution of the velocity gradient $(\Delta u, \Delta w)$ subject to the predefined piecewise linear distribution of the non-hydrostatic pressure. However, this approximation lowers the order of dispersion from the two-layer system. The optimal value for free parameter α is determined by varying it from 0.5 to 1.0 to best fit the exact linear dispersion relation over a specific range of water depth parameters.

Chapter 3

Wave Properties

Waves slow down and shoal as they propagate from deep to shallow water. In addition, nonlinear wave-wave interactions play an important role as the wave height increases in the near-shore region. Researchers have utilized the linear dispersion relation, the linear shoaling gradient, and the quadratic transfer function as analytical tools for evaluation of model performance. The linear dispersion relation measures the capability of wave models in describing the celerity as a function of wave period and water depth, while the linear shoaling gradient quantifies the effects of bottom slope on wave transformation. The transfer functions for super and sub-harmonics describe the nonlinear wave-wave interaction across the frequency spectrum. In this chapter, the integrated two-layer, hybrid, and one-layer systems are converted into the Boussinesq form in terms of high-order derivatives for derivation of the linear and nonlinear wave properties. The first and second-order governing equations in terms of ϵ are extracted through the perturbation expansions

$$\zeta = \zeta_1 + \epsilon\zeta_2 + \epsilon^2\zeta_3 + ... \tag{3.1}$$

$$u = u_1 + \epsilon u_2 + \epsilon^2 u_3 + ... \tag{3.2}$$

$$\Delta u = \Delta u_1 + \epsilon\Delta u_2 + \epsilon^2\Delta u_3 + ... \tag{3.3}$$

where subscripts 1, 2, and 3 represent the first, second, and third-order solutions respectively. Fourier analysis is conducted to derive the linear dispersion relation, the linear shoaling gradient, and the quadratic transfer function for comparison with solutions from the classical and extended Boussinesq equations of Peregrine (1967) and Nwogu (1993).

3.1 Linear Properties

3.1.1 Linear governing equations

For the integrated two-layer system, the non-hydrostatic pressure q_{z_α} and q_d can be explicitly expressed through the vertical momentum equations (2.3.9) and (2.3.10) by invoking the interface continuity equation (2.3.6), the vertical velocity approximations (2.3.11) and (2.3.12), and the kinematic boundary conditions (2.3.13) and (2.3.14). Substitution of the resulting expressions for q_{z_α} and q_d into (2.3.7) and (2.3.8) gives rise to the horizontal momentum equations in terms of the physical variables $(\zeta, u, \Delta u)$. The governing equations in the Boussinesq form are expressed in terms of high-order derivatives of the horizontal velocity for derivation of the wave properties. Implementation of the perturbation expansion (3.1) - (3.3) and retaining terms up to the first order, the linearized governing equations in dimensional form read

$$\frac{\partial \zeta_1}{\partial t} + d\,\frac{\partial u_1}{\partial x} + u_1\,\frac{\partial d}{\partial x} = 0 \tag{3.1.1}$$

$$\begin{aligned}\frac{\partial u_1}{\partial t} + g\frac{\partial \zeta_1}{\partial x} - \frac{5}{16}\,d^2\frac{\partial^3 u_1}{\partial x^2 \partial t} - \frac{1}{8}\,d^2\frac{\partial^3 \Delta u_1}{\partial x^2 \partial t} \\ - \frac{15}{16}\,d\frac{\partial^2 u_1}{\partial x \partial t}\frac{\partial d}{\partial x} - \frac{5}{16}\,d\frac{\partial^2 \Delta u_1}{\partial x \partial t}\frac{\partial d}{\partial x} = 0\end{aligned} \tag{3.1.2}$$

$$\begin{aligned}\frac{\partial \Delta u_1}{\partial t} - \frac{1}{8}\,d^2\frac{\partial^3 u_1}{\partial x^2 \partial t} - \frac{1}{16}\,d^2\frac{\partial^3 \Delta u_1}{\partial x^2 \partial t} \\ - \frac{1}{2}\,d\frac{\partial^2 u_1}{\partial x \partial t}\frac{\partial d}{\partial x} - \frac{3}{16}\,d\frac{\partial^2 \Delta u_1}{\partial x \partial t}\frac{\partial d}{\partial x} = 0\end{aligned} \tag{3.1.3}$$

In contrast to the Boussineq equations, the continuity equation (3.1.1) does not contain dispersion terms to ensure mass conservation. The momentum equations (3.1.2) and (3.1.3) include the classical frequency dispersion terms and and dispersion due to the bottom slope. The equation structure allows derivation of the linear shoaling gradient and dispersion relation accounting for high-order effects from the velocity gradient and its coupling with the horizontal velocity.

The linearized governing equations for the one-layer system can be derived similarly from (2.4.1) - (2.4.3) with the aid of (2.4.4) - (2.4.6) to remove the vertical velocity and non-hydrostatic pressure terms. In the absence of Δu, the governing equations include a continuity and a momentum equation

$$\frac{\partial \zeta_1}{\partial t} + d\,\frac{\partial u_1}{\partial x} + u_1\,\frac{\partial d}{\partial x} = 0 \tag{3.1.4}$$

$$\frac{\partial u_1}{\partial t} + g\frac{\partial \zeta_1}{\partial x} - \frac{1}{4}\,d^2\frac{\partial^3 u_1}{\partial x^2 \partial t} - \frac{3}{4}\,d\frac{\partial^2 u_1}{\partial x \partial t}\frac{\partial d}{\partial x} = 0 \tag{3.1.5}$$

Although the one-layer system retains similar dispersion terms without considering Δu, the governing equations cannot be simplified directly from (3.1.1) - (3.1.3) because of the fundamental difference in the assumed flow structure. The dispersion terms in (3.1.5), which result from a linear distribution of the non-hydrostatic pressure, also have different coefficients comparing to the corresponding terms in (3.1.2). In relation to the classical Boussinesq equations (Peregrine, 1967), the frequency dispersion term has a coefficient of $1/4$ instead of $1/3$ that results in different applicable ranges of the models (Yamazaki, 2010).

The hybrid system contains most of the essential features in the two-layer system including a piecewise linear distribution of the non-hydrostatic pressure. In the derivation of the linear governing equations, the non-hydrostatic pressure q_d is expressed in terms of the physical variables $(\zeta, u, \Delta u)$ through the vertical momentum equation (2.5.4) and the interface continuity equation (2.5.5) using (2.3.11) - (2.3.12). Substitution of q_d into (2.5.3) and (2.5.6) gives the horizontal momentum equations. The linearized governing

equations for the hybrid system become

$$\frac{\partial \zeta_1}{\partial t} + d\frac{\partial u_1}{\partial x} + u_1 \frac{\partial d}{\partial x} = 0 \tag{3.1.6}$$

$$\begin{aligned}\frac{\partial u_1}{\partial t} + g\frac{\partial \zeta_1}{\partial x} - \frac{1}{8}(2\alpha+1)\, d^2 \frac{\partial^3 u_1}{\partial x^2 \partial t} - \frac{1}{16}(2\alpha+1)\, d^2 \frac{\partial^3 \Delta u_1}{\partial x^2 \partial t} \\ - \frac{1}{8}(10\alpha+1)\, d\frac{\partial d}{\partial x}\frac{\partial^2 u_1}{\partial x \partial t} - \frac{1}{16}(10\alpha+1)\, d\frac{\partial d}{\partial x}\frac{\partial^2 \Delta u_1}{\partial x \partial t} = 0\end{aligned} \tag{3.1.7}$$

$$\begin{aligned}\frac{\partial \Delta u_1}{\partial t} - \frac{1}{8}d^2 \frac{\partial^3 u_1}{\partial x^2 \partial t} - \frac{1}{16}d^2 \frac{\partial^3 \Delta u_1}{\partial x^2 \partial t} \\ - \frac{1}{8}(4\alpha+1)\, d\frac{\partial d}{\partial x}\frac{\partial^2 u_1}{\partial x \partial t} - \frac{1}{16}(4\alpha+1)\, d\frac{\partial d}{\partial x}\frac{\partial^2 \Delta u_1}{\partial x \partial t} = 0\end{aligned} \tag{3.1.8}$$

The governing equations have the same form as the two-layer system. The coefficients of the dispersion terms contain the free parameter α, which can be adjusted to provide desirable performance over a range of water depth parameters. A single parameter, however, cannot reproduce all the coefficients or the dispersion properties of the two-layer system. For α = 0.5 and in the absence of Δu, the governing equations reduce to those of the one-layer system.

3.1.2 Linear dispersion

Linear dispersion relates the wave period and water depth to the celerity over a flat bottom. This section compares the dispersion relations from the linearized governing equations of the one-layer, two-layer, and hybrid systems with the exact relation given by Airy wave theory as

$$c^2 = \frac{gd\, tanh\,(kd)}{kd} \tag{3.1.9}$$

where c is celerity, k is wave number, and kd is the water depth parameter. To derive the dispersion relations, a system of small amplitude periodic waves over a flat bottom is considered

$$\zeta_1(x,t) = a_1\, \mathrm{e}^{i(kx-\omega t)} \tag{3.1.10}$$

$$u_1(x,t) = u_1 \, \mathrm{e}^{i(kx-\omega t)} \tag{3.1.11}$$

$$\Delta u_1(x,t) = \Delta u_1 \, \mathrm{e}^{i(kx-\omega t)} \tag{3.1.12}$$

where $i = \sqrt{-1}$ and ω is angular frequency. Substitution of (3.1.10) and (3.1.11) into the linearized governing equations of the one-layer system gives the dispersion relation

$$c_1^2 = \frac{g\,d}{1 + \frac{1}{4}k^2d^2} \tag{3.1.13}$$

which contains a second-order polynominal in terms of kd. In comparison, the linear dispersion relation of the classical Boussinesq equations is

$$c_B^2 = \frac{g\,d}{1 + \frac{1}{3}k^2d^2} \tag{3.1.14}$$

which has the same polynominal with a different coefficient carried over from the governing equations. Both provide basic approximations to the exact linear dispersion relation for small values of kd.

Equation (3.1.12) accounts for the piecewise linear distribution of the horizontal velocity distribution over the water column in the two-layer and hybrid systems. Substitution of (3.1.10) - (3.1.12) into the linearized governing equations of the two-layer system gives the dispersion relation

$$c_2^2 = \frac{gd\left(1 + \frac{1}{16}k^2d^2\right)}{1 + \frac{3}{8}k^2d^2 + \frac{1}{256}k^4d^4} \tag{3.1.15}$$

which contains a second-order and a fourth-order polynominal in the numerator and denominator respectively. This forms a $[2,4]$ Pad$\acute{e}$ approximation in terms of kd and provides good agreement to the exact linear dispersion. On the other hand, the linear dispersion relation of the hybrid system gives a $[2,2]$ Pad$\acute{e}$ approximation as

$$c_\alpha^2 = \frac{gd\left(1 + \frac{1}{16}k^2d^2\right)}{1 + \left(\frac{3}{16} + \frac{1}{4}\alpha\right)k^2d^2} \tag{3.1.16}$$

The fourth-order term k^4d^4 in the denominator is reduced to the product of a second-order term k^2d^2 and the free parameter α. The linear dispersion relation of the Boussinesq-type equations of Nwogu (1993) has the same form, but contains the free parameter in

both the numerator and denominator resulting from modulation of the dispersion terms in the momentum as well as the continuity equation.

Coastal wave transformation occurs when the water depth parameter kd is less than 3. Therefore, the free parameter α in (3.1.16) is optimized with respect to the exact linear dispersion relation by minimizing the absolute error of the normalized celerity over $0 < kd \leq 3$ as

$$error\,(\alpha) = \int_{\sigma}^{3} \left(\frac{c_\alpha}{c_0} - \frac{c_{exact}}{c_0} \right)^2 d\,(kd) \tag{3.1.17}$$

where

$$c_0 = \sqrt{gd} \tag{3.1.18}$$

is the shallow-water celerity and σ is set equal to 0.01 to avoid singularity in the integration. An α of 0.85442 gives a minimum error of 1.5×10^{-5} and c_α becomes

$$c^2_{\alpha=0.85442} = \frac{gd\left(1 + \frac{1}{16}k^2d^2\right)}{1 + \frac{2}{5}k^2d^2} \tag{3.1.19}$$

which has the same form and very similar coefficients as the linear dispersion relation derived by Nwogu (1993)

$$c^2_N = \frac{gd(1 + 0.06\,k^2d^2)}{1 + 0.393\,k^2d^2} \tag{3.1.20}$$

Despite the differences in formulation and approximation, both approaches lead to the same linear dispersion relation through an optimization scheme.

The one-layer, hybrid, and two-layer systems represent a systematic improvement of the dispersion properties through increasing degrees of freedom in describing the vertical flow structure. Figure 3.1 compares the normalized celerity obtained from these systems with those from Airy wave theory and the classical Boussinesq equations. The one-layer system shows a major improvement over the classical Boussinesq equations in terms of dispersion properties through a coefficient of 1/4 instead of 1/3. The two-layer system reproduces the linear dispersion characteristics of Airy wave theory over the range of kd

considered. A separate analysis has shown that the error is less than 5% in relation to the exact solution for kd = 11. The hybrid system, which has errors of less than 1% and 5% for kd = 3.0 and 4.3 respectively, allows modeling of coastal wave transformation from deep to shallow water.

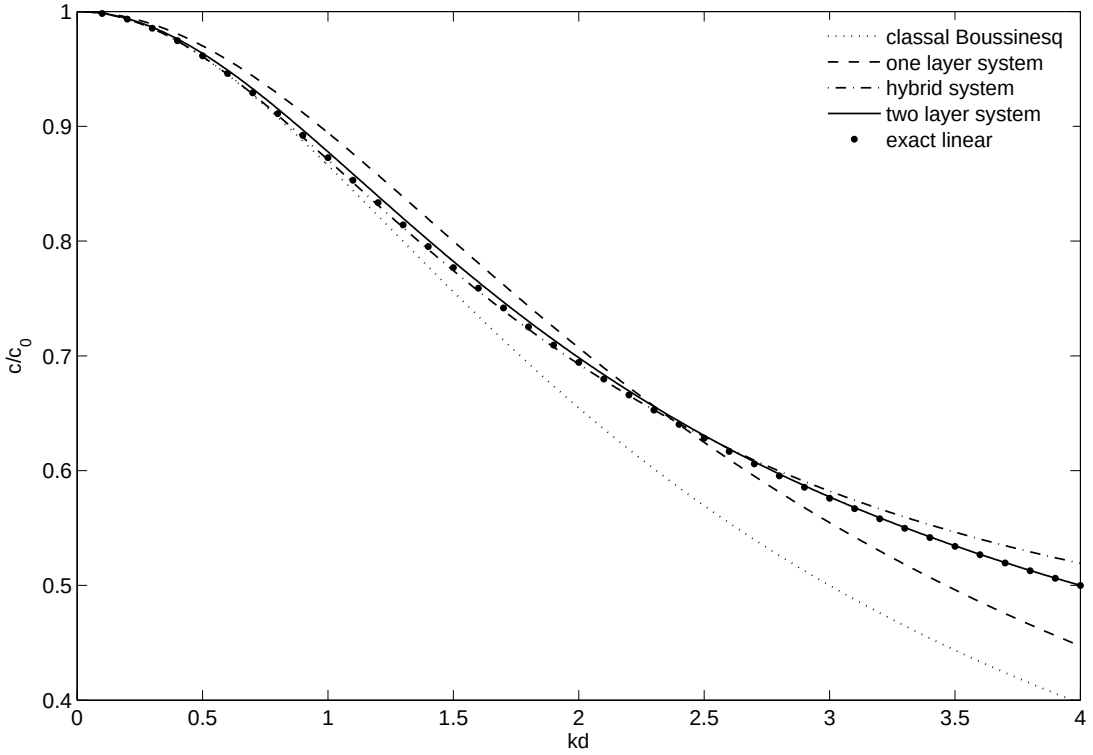

Figure 3.1. Comparison of linear dispersion relations.

3.1.3 Linear shoaling

The group velocity, closely related to dispersion, describes the shoaling process through conservation of energy flux. In addition, Madsen and Sørensen (1992) introduced the linear shoaling gradient γ to measure the effect of bottom slope on wave transformation through the relation

$$\frac{1}{A}\frac{\partial A}{\partial x} = -\frac{\gamma}{d}\frac{\partial d}{\partial x} \tag{3.1.21}$$

where A denotes wave amplitude. They utilized Airy wave theory in combination with conservation of energy flux to derive the expression

$$\gamma = \frac{kd\,tanh\,(kd)\,(1 - kd\,tanh\,(kd))\,(1 - tanh^2\,(kd))}{(tanh\,(kd) + kd\,(1 - tanh^2\,(kd)))^2} \tag{3.1.22}$$

The shoaling gradient represents the ratio of the relative amplitude gradient and bottom slope. For example, a positive γ on an ascending slope (i.e., $\partial d/\partial x < 0$) indicates increasing wave amplitude or vice verse.

Following the procedures given by Schäffer and Madsen (1995), the solution of wave shoaling on a gentle slope is expressed as

$$\zeta_1\,(x,t) = A\,(x)\,\mathrm{e}^{i\left(\omega t - \int k(x)dx\right)} \tag{3.1.23}$$

$$u_1\,(x,t) = (u_r\,(x) + i u_i\,(x))\,\mathrm{e}^{i\left(\omega t - \int k(x)dx\right)} \tag{3.1.24}$$

$$\Delta\,u_1\,(x,t) = (\Delta\,u_r\,(x) + i\Delta\,u_i\,(x))\,\mathrm{e}^{i\left(\omega t - \int k(x)dx\right)} \tag{3.1.25}$$

where the subscripts r and i indicate the real and imaginary parts of the respective variables. Substitution of (3.1.23) - (3.1.25) into the linearized governing equations and collection of the real part without the gradient terms and the imaginary part with first-order derivatives only yield a set of equations from which the shoaling gradient can be determined. The results for the one-layer, two-layer, and hybrid systems read

$$\gamma_1 = \frac{1 - \frac{3}{4}k^2d^2}{4} \tag{3.1.26}$$

$$\gamma_2 = \frac{1 - \frac{11}{16}\,k^2d^2 - \frac{1}{128}\,k^4d^4 + \frac{19}{2048}\,k^6d^6 + \frac{33}{65536}\,k^8d^8 + \frac{5}{1048576}\,k^{10}d^{10}}{4 + k^2d^2 + \frac{7}{32}\,k^4d^4 + \frac{5}{256}\,k^6d^6 + \frac{25}{16384}\,k^8d^8} \tag{3.1.27}$$

$$\begin{aligned}\gamma_\alpha = \{\,1 &+ \left(\frac{3}{8} - \frac{7\alpha}{4}\right)k^2d^2 + \left(\frac{11}{128} - \frac{3}{16}\alpha + \frac{\alpha^2}{8}\right)k^4d^4 \\ &+ \left(\frac{21}{2048} - \frac{3\alpha}{1024} + \frac{\alpha^2}{256}\right)k^6d^6 \\ &+ \left(\frac{9}{65536} - \frac{3\alpha}{8192} + \frac{3\alpha^2}{4096} + \frac{\alpha^3}{512}\right)k^8d^8\,\} \\ \{\,4 &+ k^2d^2 + \left(\frac{5}{32} + \frac{\alpha}{8}\right)k^4d^4 + \left(\frac{3}{256} + \frac{\alpha}{64}\right)k^6d^6 \\ &+ \left(\frac{9}{16384} + \frac{3\alpha}{2048} + \frac{\alpha^2}{1024}\right)k^8d^8\,\}^{-1}\end{aligned} \tag{3.1.28}$$

The shoaling gradients in these three systems are expressed as rational functions in kd. Their values converge to $1/4$ as $kd \to 0$ as in the exact solution (3.1.21). In the one-layer and two-layer systems, the polynominals in the numerator are two orders higher than those in the denominator. This leads to divergence of the shoaling gradients as $kd \to \infty$, whereas the exact solution converges to zero. In the hybrid system, the numerator and denominator have the same order of polynominals and thus the shoaling gradient converges to a finite value at large kd depending on α.

The free parameter in the hybrid system defines the shoaling properties in coastal wave transformation. Its value can be optimized for a range of kd through minimization of the absolute error defined by

$$error\,(\alpha) = \int_0^{kd} (\gamma_\alpha - \gamma)^2\, d\,(kd) \tag{3.1.29}$$

Table 3.1 shows the optimized values of α and the errors in the shoaling gradient for different ranges of kd. The shoaling gradient is optimized over $0 \leq kd \leq 3$ with an error of 1.20×10^{-2} for $\alpha = 0.70359$. However, the dispersion relation (3.1.16) is optimized for $\alpha = 0.85442$, which results in a larger error of 1.98×10^{-2} in the shoaling gradient. Figure 3.2 compares the shoaling gradient over the range of α considered. The results show good agreement with the exact shoaling gradient for $kd < 0.5$, when shoaling begins to affect the wave height according to Airy wave theory. Although discrepancies appear for larger values of kd, their effects on the local shoaling process are secondary. Figure 3.3 compares the exact shoaling gradients with those from the one-layer, two-layer, hybrid system with $\alpha = 0.85442$, and the Boussinesq model of

Table 3.1. The optimized free parameter α for different range of kd

kd	α	error
[0 , 1]	0.63853	3.38×10^{-6}
[0 , 2]	0.65844	1.59×10^{-4}
[0 , 3]	0.70359	1.20×10^{-2}

Nwogu (1993) presented by Beji and Nadaoka (1996). The shoaling gradient for the one-layer system decreases monotonically and grossly underestimates the solution for large values of kd. The two-layer system reproduces the exact solution up to $kd = 1.7$, but overestimates the shoaling gradient for larger values of kd. The shoaling gradients of the hybrid system and Nwogu (1993) follow the same trend as that of the two-layer system, but shows noticeable discrepancies with the exact solution for large values of kd.

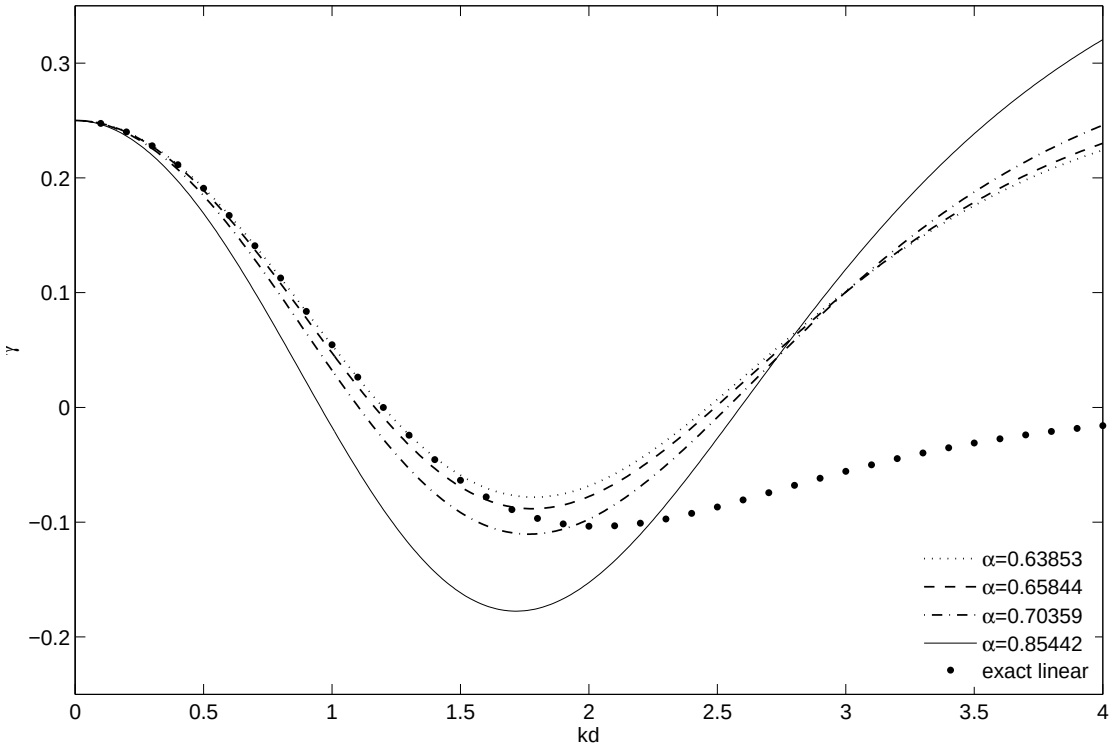

Figure 3.2. Comparison of linear shoaling gradient from the hybrid model over applicable ranges of kd in Table 3.1.

The comparisons show that a single value of α cannot optimize the dispersion relation and shoaling gradient in the hybrid system at the same time. It is obvious that $\alpha = 0.70359$ gives the best fit to the exact shoaling gradient within $0 \leq kd \leq 3$. The dispersion relation, on the other hand, performs better with $\alpha = 0.85442$, which leads to a larger error in the shoaling gradient. Dispersion defines the group velocity, which is the

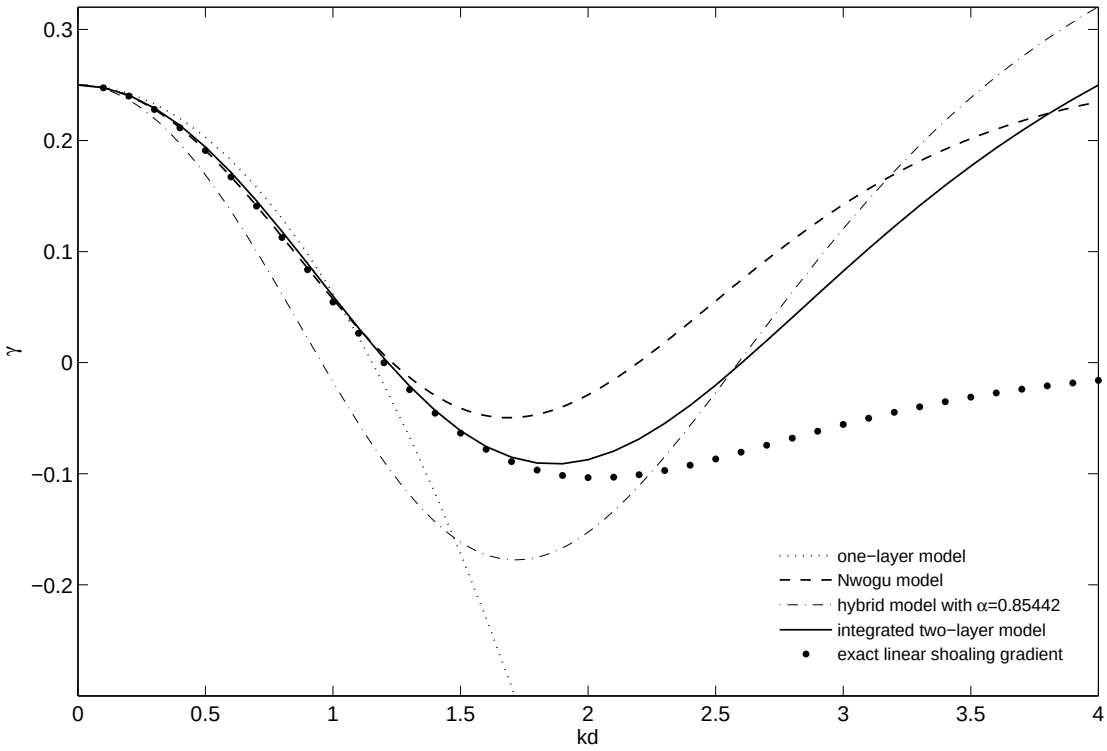

Figure 3.3. Comparison of linear shoaling gradient from different models.

primary factor in the shoaling process through conservation of energy flux. The shoaling gradient, which is derived in part from the dispersion relation to account for the effects of a gentle bottom slope, might not be a good indicator of shoaling properties (Chen and Liu, 1995). Throughout this dissertation, $\alpha = 0.85442$ is applied in the hybrid model to capture the more important dispersion properties in coastal wave transformation. The selection of this value will be validated with laboratory data in the case studies.

3.2 Nonlinear Properties

Linear dispersion and shoaling define basic coastal wave processes. The free-surface boundary condition is nonlinear in terms of wave amplitude leading to further modifi-

cations of the free surface and velocity profiles. Nonlinearity transfers energy to high and low frequency components in the generation of forced short and long waves. This section summarizes the development of the second-order governing equations for the one-layer, hybrid, and two-layer models from which the quadratic transfer function for wave amplitude can be derived and compared with the solution from the Boussinesq equations of Nwogu (1993).

3.2.1 Second-Order Interaction of Monochromatic Waves

The second-order governing equations account for the nonlinear interactions to provide a correction to the linear solution. The non-homogeneous equations have the same structure as the linear governing equations, but with addition of nonlinear forcing terms on the right-hand side. Nwogu (1993) derived the second-order governing equations from his extended Boussinesq formulation as

$$\frac{\partial \zeta_2}{\partial t} + d\frac{\partial u_2}{\partial x} + \left(\alpha + \frac{1}{3}\right) d^3 \frac{\partial^3 u_2}{\partial x^3} = -\zeta_1 \frac{\partial u_1}{\partial x} - u_1 \frac{\partial \zeta_1}{\partial x} \tag{3.2.1}$$

$$\frac{\partial u_2}{\partial t} + g\frac{\partial \zeta_2}{\partial x} + \alpha\, d^2 \frac{\partial^3 u_2}{\partial x^2 \partial t} = -u_1 \frac{\partial u_1}{\partial x} \tag{3.2.2}$$

where α is a free parameter adjusting the elevation of the horizontal velocity and the subsequent dispersion properties. The first-order spatial derivatives of $\zeta_1 u_1$ and $\frac{1}{2}u_1^2$ serve as weak nonlinear forcing without association of α. The second-order solution from (3.2.1) and (3.2.2) provides a reference for comparison with the results from the non-hydrostatic approach.

Substitution of the perturbation expansions (3.1) - (3.3) in the Boussinesq form of the two-layer, hybrid, and one-layer systems and collection of terms with leading order of ϵ provide the corresponding second-order governing equations. The evolution of Δu results in a third governing equation in the two-layer and hybrid systems and new

nonlinear terms in comparison to the Boussinesq approach. For the two-layer system, the second-order governing equations read

$$\frac{\partial \zeta_2}{\partial t} + d\frac{\partial u_2}{\partial x} = -\frac{\partial \zeta_1}{\partial x}u_1 - \zeta_1\frac{\partial u_1}{\partial x} \tag{3.2.3}$$

$$\begin{aligned}
&\frac{\partial u_2}{\partial t} + g\frac{\partial \zeta_2}{\partial x} - \frac{5}{16}d^2\frac{\partial^3 u_2}{\partial x^2\partial t} - \frac{1}{8}d^2\frac{\partial^3 \Delta u_2}{\partial x^2\partial t} \\
&\qquad = -u_1\frac{\partial u_1}{\partial x} - 2\,\Delta u_1\frac{\partial \Delta u_1}{\partial x} - \frac{\zeta_1}{d}\frac{\partial \zeta_1}{\partial x} - \frac{\zeta_1}{d}\frac{\partial u_1}{\partial t} \\
&\qquad\quad - \frac{9}{16}\,d^2\Delta u_1\frac{\partial^3 u_1}{\partial x^3} - \frac{1}{16}\,d^2\Delta u_1\frac{\partial^3 \Delta u_1}{\partial x^3} \\
&\qquad\quad + \frac{1}{16}\,d^2\frac{\partial \Delta u_1}{\partial x}\frac{\partial^2 \Delta u_1}{\partial x^2} - \frac{13}{16}\,d^2\frac{\partial \Delta u_1}{\partial x}\frac{\partial^2 u_1}{\partial x^2} \\
&\qquad\quad + \frac{3}{8}\,d\zeta_1\frac{\partial^3 \Delta u_1}{\partial x^2\partial t} + \frac{3}{4}\,d\zeta_1\frac{\partial^3 u_1}{\partial x^2\partial t} \\
&\qquad\quad + \frac{1}{2}\,d^2u_1\frac{\partial^3 u_1}{\partial x^3} + \frac{1}{8}\,d^2u_1\frac{\partial^3 \Delta u_1}{\partial x^3} \\
&\qquad\quad + \frac{9}{16}\,d\frac{\partial \zeta_1}{\partial x}\frac{\partial^2 u_1}{\partial x\partial t} + \frac{11}{16}\,d\frac{\partial \zeta_1}{\partial x}\frac{\partial^2 \Delta u_1}{\partial x\partial t} \\
&\qquad\quad + \frac{5}{16}\,d\frac{\partial^2 \zeta_1}{\partial x^2}\frac{\partial \Delta u_1}{\partial t} - \frac{3}{16}\,d\frac{\partial^2 \zeta_1}{\partial x^2}\frac{\partial u_1}{\partial t} \\
&\qquad\quad - \frac{1}{8}\,d^2\frac{\partial u_1}{\partial x}\frac{\partial^2 \Delta u_1}{\partial x^2} + \frac{1}{4}\,d^2\frac{\partial u_1}{\partial x}\frac{\partial^2 u_1}{\partial x^2}
\end{aligned} \tag{3.2.4}$$

$$\begin{aligned}
&\frac{\partial \Delta u_2}{\partial t} - \frac{1}{8}d^2\frac{\partial^3 u_2}{\partial x^2\partial t} - \frac{1}{16}d^2\frac{\partial^3 \Delta u_2}{\partial x^2\partial t} \\
&\qquad = +\frac{\partial \Delta u_1}{\partial t}\frac{\zeta_1}{d} + \Delta u_1\frac{\partial u_1}{\partial x} + u_1\frac{\partial \Delta u_1}{\partial x} \\
&\qquad\quad - \frac{1}{16}\,d^2u_1\frac{\partial^3 \Delta u_1}{\partial x^3} - \frac{3}{16}\,d^2u_1\frac{\partial^3 u_1}{\partial x^3} + \frac{3}{16}\,d^2\Delta u_1\frac{\partial^3 u_1}{\partial x^3} \\
&\qquad\quad + \frac{5}{16}\,d^2\frac{\partial^2 u_1}{\partial x^2}\frac{\partial \Delta u_1}{\partial x} - \frac{1}{16}\,d^2\frac{\partial u_1}{\partial x}\frac{\partial^2 u_1}{\partial x^2} + \frac{1}{16}\,d^2\frac{\partial u_1}{\partial x}\frac{\partial^2 \Delta u_1}{\partial x^2} \\
&\qquad\quad - \frac{5}{16}\,d\zeta_1\frac{\partial^3 u_1}{\partial x^2\partial t} - \frac{3}{16}\,d\zeta_1\frac{\partial^3 \Delta u_1}{\partial x^2\partial t} \\
&\qquad\quad - \frac{3}{16}\,d\frac{\partial \zeta_1}{\partial x}\frac{\partial^2 \Delta u_1}{\partial x\partial t} + \frac{1}{8}\,d\frac{\partial \zeta_1}{\partial x}\frac{\partial^2 u_1}{\partial x\partial t} \\
&\qquad\quad + \frac{1}{16}\,d\frac{\partial^2 \zeta_1}{\partial x^2}\frac{\partial u_1}{\partial t} - \frac{1}{8}\,d\frac{\partial^2 \zeta_1}{\partial x^2}\frac{\partial \Delta u_1}{\partial t}
\end{aligned} \tag{3.2.5}$$

The continuity equation (3.2.3) does not contain dispersion terms, but has the same forcing term as the Boussinesq approach of Nwogu (1993) in (3.2.1). The momentum equations (3.2.4) and (3.2.5) contain additional forcing terms that involve the surface elevation ζ_1 and its first and second-order spatial derivatives $\partial\zeta_1/\partial x$ and $\partial^2\zeta_1/\partial x^2$. These

two equations couple not only in the homogeneous part but also the nonlinear forcing part to include effects of vorticity through the velocity gradient that are not considered in the nonlinear forcing of Nwogu (1993).

The second order governing equations of the hybrid system maintain the structure of the two-layer system as

$$\frac{\partial \zeta_2}{\partial t} + d\frac{\partial u_2}{\partial x} = -\frac{\partial \zeta_1}{\partial x}u_1 - \zeta_1\frac{\partial u_1}{\partial x} \tag{3.2.6}$$

$$\begin{aligned}
&\frac{\partial u_2}{\partial t} + g\frac{\partial \zeta_2}{\partial x} - \frac{1}{8}d^2(2\alpha+1)\frac{\partial^3 u_2}{\partial x^2\partial t} - \frac{1}{16}d^2(2\alpha+1)\frac{\partial^3 \Delta u_2}{\partial x^2\partial t} \\
&\qquad = -\frac{\zeta_1}{d}\frac{\partial u_1}{\partial t} - u_1\frac{\partial u_1}{\partial x} - 2\Delta u_1\frac{\partial \Delta u_1}{\partial x} - \frac{\zeta_1}{d}\frac{\partial \zeta_1}{\partial x} \\
&\qquad + \frac{1}{8}d(2\alpha+1)\frac{\partial^2 \zeta_1}{\partial x^2}\frac{\partial \Delta u_1}{\partial t} - \frac{5}{16}d^2(2\alpha+1)\frac{\partial^2 u_1}{\partial x^2}\frac{\partial \Delta u_1}{\partial x} \\
&\qquad - \frac{1}{8}d^2(2\alpha+1)\frac{\partial u_1}{\partial x}\frac{\partial^2 u_1}{\partial x^2} - \frac{1}{16}d^2(2\alpha+1)\frac{\partial u_1}{\partial x}\frac{\partial^2 \Delta u_1}{\partial x^2} \\
&\qquad + \frac{5}{16}d(2\alpha+1)\frac{\partial \zeta_1}{\partial x}\frac{\partial^2 \Delta u_1}{\partial x\partial t} + \frac{3}{8}d(2\alpha+1)\frac{\partial \zeta_1}{\partial x}\frac{\partial^2 u_1}{\partial x\partial t} \\
&\qquad + \frac{3}{16}d(2\alpha+1)\zeta_1\frac{\partial^3 \Delta u_1}{\partial x^2\partial t} + \frac{1}{16}d^2(2\alpha+1)u_1\frac{\partial^3 \Delta u_1}{\partial x^3} \\
&\qquad - \frac{3}{16}d^2(2\alpha+1)\Delta u_1\frac{\partial^3 u_1}{\partial x^3} + \frac{1}{8}d^2(2\alpha+1)u_1\frac{\partial^3 u_1}{\partial x^3} \\
&\qquad + \frac{3}{8}d(2\alpha+1)\zeta_1\frac{\partial^3 u_1}{\partial x^2\partial t}
\end{aligned} \tag{3.2.7}$$

$$\begin{aligned}
&\frac{\partial \Delta u_2}{\partial t} - \frac{1}{8}d^2\frac{\partial^3 u_2}{\partial x^2\partial t} - \frac{1}{16}d^2\frac{\partial^3 \Delta u_2}{\partial x^2\partial t} = \frac{1}{8}d\frac{\partial^2 \zeta_1}{\partial x^2}\frac{\partial \Delta u_1}{\partial t} - \frac{\zeta_1}{d}\frac{\partial \Delta u_1}{\partial t} \\
&\qquad - 2u_1\frac{\partial \Delta u_1}{\partial x} - \Delta u_1\frac{\partial u_1}{\partial x} - \frac{3}{16}d^2\Delta u_1\frac{\partial^3 u_1}{\partial x^3} + \frac{1}{8}d^2u_1\frac{\partial^3 u_1}{\partial x^3} \\
&\qquad - \frac{1}{8}d^2\frac{\partial^2 u_1}{\partial x^2}\frac{\partial u_1}{\partial x} - \frac{1}{16}d^2\frac{\partial^2 \Delta u_1}{\partial x^2}\frac{\partial u_1}{\partial x} - \frac{5}{16}d^2\frac{\partial^2 u_1}{\partial x^2}\frac{\partial \Delta u_1}{\partial x} \\
&\qquad - \frac{1}{16}d(4\alpha-5)\frac{\partial \zeta_1}{\partial x}\frac{\partial^2 \Delta u_1}{\partial x\partial t} - \frac{1}{8}d(4\alpha-3)\frac{\partial \zeta_1}{\partial x}\frac{\partial^2 u_1}{\partial x\partial t} \\
&\qquad + \frac{3}{16}d\zeta_1\frac{\partial^3 \Delta u_1}{\partial x^2\partial t} + \frac{1}{16}d^2u_1\frac{\partial^3 \Delta u_1}{\partial x^3} + \frac{3}{8}d\zeta_1\frac{\partial^3 u_1}{\partial x^2\partial t}
\end{aligned} \tag{3.2.8}$$

However, the coefficients of all high-order derivatives in the momentum equation (3.2.7) and two high-order derivatives in (3.2.8) contain the free parameter α. This demonstrates that the free parameter modulates not only the dispersion but also the nonlinearity and

vorticity of the hybrid system. The second-order governing equations for the one-layer system reduce to

$$\frac{\partial \zeta_2}{\partial t} + d\frac{\partial u_2}{\partial x} = -\frac{\partial \zeta_1}{\partial x}u_1 - \zeta_1\frac{\partial u_1}{\partial x} \tag{3.2.9}$$

$$\begin{aligned}\frac{\partial u_2}{\partial t} + g\frac{\partial \zeta_2}{\partial x} - \frac{1}{4}d^2\frac{\partial^3 u_2}{\partial x^2 \partial t} = -u_1\frac{\partial u_1}{\partial x} - \frac{1}{4}d^2\frac{\partial u_1}{\partial x}\frac{\partial^2 u_1}{\partial x^2} + \frac{1}{4}d^2 u_1\frac{\partial^3 u_1}{\partial x^3} \\ +\frac{3}{4}d\frac{\partial \zeta_1}{\partial x}\frac{\partial^2 u_1}{\partial x \partial t} + \frac{1}{2}d\zeta_1\frac{\partial^3 u_1}{\partial x^2 \partial t}\end{aligned} \tag{3.2.10}$$

which contain the basic nonlinear forcing from the non-hydrostatic formulation. The absence of the velocity gradient implies a low-order approximation of dispersion and the lack of vorticity in the velocity field of the one-layer model. All three systems contain the same continuity equation meaning that the vertical flow structure associated with the non-hydrostatic pressure influences the nonlinearity through the momentum equations only.

The second-order solution depends on the nonlinear forcing terms associated with the vertical flow structure in the three systems. Computation of the second-order harmonics due to interactions of first-order waves allows comparison with the classical solution and evaluation of model performance in terms of nonlinearity. The first-order solution of monochromatic waves can be written as

$$\zeta_1(x,t) = a_1\, cos\,(kx - \omega t) \tag{3.2.11}$$

$$u_1(x,t) = b_1\, cos\,(kx - \omega t) \tag{3.2.12}$$

$$\Delta u_1(x,t) = c_1\, cos\,(kx - \omega t) \tag{3.2.13}$$

where a_1, b_1, and c_1 are amplitude. The linear solution produces self-interacting second-order harmonics in the form

$$\zeta_2(x,t) = a_2\, cos\,(2kx - 2\omega t) \tag{3.2.14}$$

$$u_2(x,t) = b_2\, cos\,(2kx - 2\omega t) \tag{3.2.15}$$

$$\Delta u_2(x,t) = c_2\, cos\,(2kx - 2\omega t) \tag{3.2.16}$$

where a_2, b_2 and c_2 are amplitude that varies with the water depth parameter kd. The second-order Stokes solution reads

$$a_{2S} = \frac{1}{4} a_1^2 k \left(3\, coth^3(kd) - coth(kd)\right) \tag{3.2.17}$$

which is used to compare with the solutions from the two-layer, hybrid, and one-layer models as well as the Boussinesq equations of Nwogu (1993).

Substitution of the first-order solution (3.2.11) - (3.2.13) into the linearized governing equations (3.1.1) - (3.1.3) of the two-layer system gives the expressions of b_1 and c_1 in terms of a_1. The linear dispersion relation (3.1.15) provides an expression for the angular frequency ω in terms of kd. These three expressions consolidate the variables of the first and second-order solutions (3.2.11) - (3.2.16) for substitution into the second-order governing equations (3.2.3) - (3.2.5) to give

$$a_{2T} = \frac{1}{4} a_1^2 k \frac{49152 + 33792k^2d^2 + 9280k^4d^4 + 796k^6d^6 + 15k^8d^8}{3k^3d^3\left(5120 + 640k^2d^2 + 36k^4d^4 + k^6d^6\right)} \tag{3.2.18}$$

The amplitude of the second-order harmonic comprises 6th and 8th-order polynominals in the denominator and numerator. A similar procedure provides a_2 for the hybrid and one-layer systems as

$$\begin{aligned} a_{2H} = \frac{1}{4} a_1^2 k (3072 + (1536 + 768\alpha)k^2d^2 + (420 + 432\alpha - 256\alpha^2)k^4d^4 \\ +(27 + 24\alpha - 16\alpha^2)k^6d^6)\left(24k^3d^3(16 + k^2d^2)(1 + 2\alpha)\right)^{-1} \end{aligned} \tag{3.2.19}$$

$$a_{2O} = \frac{1}{4} a_1^2 k \frac{4 + k^2d^2}{k^3d^3} \tag{3.2.20}$$

The power of the polynominals reduces to 2 and 6 in the denominator and numerator in the hybrid system and to 2 and 0 in the one-layer system. In comparison, the solution from the second-order Boussinesq equations of Nwogu (1993) has a power of 2 and 4 in the denominator and numerator

$$a_{2N} = \frac{1}{4} a_1^2 k \, \frac{9 - 42\alpha\, k^2d^2 - 6k^2d^2 + 24\alpha^2\, k^4d^4 + 8\alpha\, k^4d^4}{k^3d^3\left(3 - 3\alpha\, k^2d^2 - k^2d^2\right)} \tag{3.2.21}$$

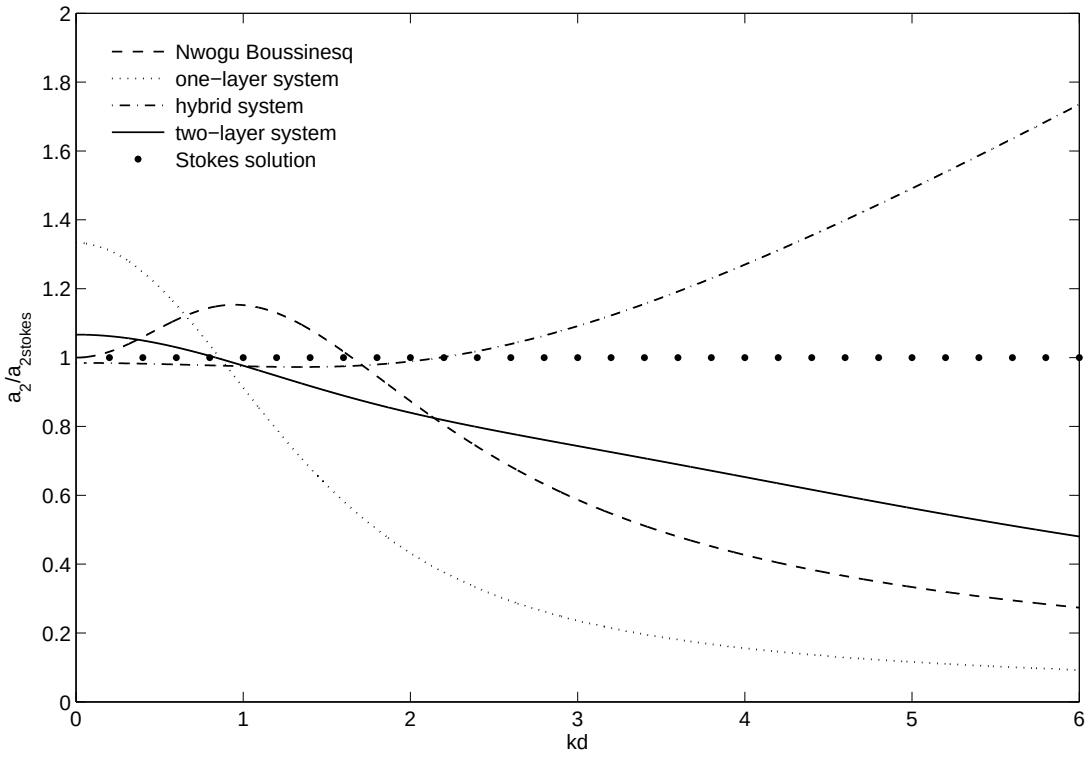

Figure 3.4. Relative amplitude of self-interacting super-harmonics from different models.

Despite being expressed by polynomials of different order, all four solutions have a common coefficient of $a_1^2 k/(kd)^3$ in contrast to $a_1^2 k$ in the second-order Stokes solution.

Figure 3.4 compares the normalized second-order harmonics from the two-layer, hybrid, and one-layer models with those from the Boussinesq approach of Nwogu (1993) and Stokes wave theory. The results from the hybrid model is based on the selected value of $\alpha = 0.85442$ that optimizes the dispersion relation. When normalized by the second-order Stokes solution, only the Boussinesq approach exactly reproduces the amplitude at $kd = 0$. Derived under a weakly nonlinear assumption, this approach overestimates the amplitude in $0 \leq kd \leq 1.65$ for up to 15.3% and gives underestimations for deeper water with a relative amplitude of 0.5871 at $kd = 3$. The solutions from the non-hydrostatic approach exhibit different characteristics with kd. The two-layer model gives a relative

amplitude of 1.07 at $kd = 0$ and shows an overall downward trend, dropping below 1 at $kd = 0.8$ and resulting in value of 0.7432 at $kd = 3$. The one-layer model begins with 1.333 at $kd = 0$ and follows the same trend, but with larger errors. This implies the one and two-layer models may produce a slightly higher surface elevation through the nonlinear forcing over time for relative long waves. The hybrid model gives the best overall agreement with the second-order Stokes theory. It starts with a relative amplitude of 0.9844 at $kd = 0$ and produces a maximum value of 1.044 within its applicable range of $kd \leq 3$.

3.2.2 Second-Order Interaction of Bichromatic Waves

Nonlinear surface waves with different frequencies interact with each other to generate super-harmonics at sum of the frequencies and sub-harmonics at difference of the frequencies by which wave energy is transferred from the peak to the sidebands of the spectrum. The second-order interaction between two first-order wave components plays a fundamental role in this process. This section summarizes the derivation of the second-order bichromatic solutions from the two-layer, hybrid, one-layer, and the extended Boussinesq models for comparison with the second-order Stokes solution.

Consider wave propagation over water of constant depth for derivation of analytical solutions. A wave group consisting of two wave frequencies ω_m and ω_n with the corresponding wave numbers k_m and k_n at the first order can be written as

$$\zeta_1(x,t) = a_m\, cos(k_m x - \omega_m t) + a_n\, cos(k_n x - \omega_n t) \tag{3.2.22}$$

$$u_1(x,t) = \frac{\omega_m}{k'_{um}d} a_m\, cos(k_m x - \omega_m t) + \frac{\omega_n}{k'_{un}d} a_n\, cos(k_n x - \omega_n t) \tag{3.2.23}$$

$$\Delta u_1(x,t) = \frac{\omega_m}{k'_{\Delta um}d} a_m\, cos(k_m x - \omega_m t) + \frac{\omega_n}{k'_{\Delta un}d} a_n\, cos(k_n x - \omega_n t) \tag{3.2.24}$$

where a is wave amplitude and k'_{um}, k'_{un}, $k'_{\Delta um}$, and $k'_{\Delta un}$ are coefficients determined from the first-order governing equations. The first subscript of k' denotes the affiliation to either u or Δu, and the second subscript corresponds to wave component of either m or n. For example, substitution of (3.2.22) - (3.2.24) into the linear governing equations (3.1.1) - (3.1.3) of the two-layer system gives

$$k'_{um} = k_m \tag{3.2.25}$$

$$k'_{un} = k_n \tag{3.2.26}$$

$$k'_{\Delta um} = -k_m \frac{16 + k_m^2 d^2}{2k_m^2 d^2} \tag{3.2.27}$$

$$k'_{\Delta un} = -k_n \frac{16 + k_n^2 d^2}{2k_n^2 d^2} \tag{3.2.28}$$

A similar procedure can be applied to the one-layer and hybrid systems to determine the corresponding coefficients.

To abbreviate the expressions of the second-order solutions, let $\theta_m = k_m x - \omega_m t$ and $\theta_n = k_n x - \omega_n t$. Self and cross-interactions of the bichromatic waves in the form of (3.2.22) - (3.2.24) force the development of four second-order components, which include three super-harmonics $2\theta_m$, $2\theta_n$, and $(\theta_m + \theta_n)$ and one sub-harmonics $(\theta_m - \theta_n)$. The resulting second-order solution can be written as

$$\begin{aligned} \zeta_2(x,t) = a_m a_n \, G_\zeta^{m+n} \, cos(\theta_m + \theta_n) + \frac{1}{2} \, a_m^2 \, G_\zeta^{2m} cos(\, 2\theta_m \,) \\ + a_m a_n \, H_\zeta^{m-n} \, cos(\theta_m - \theta_n) + \frac{1}{2} \, a_n^2 \, G_\zeta^{2n} \; cos(\, 2\theta_n \,) \end{aligned} \tag{3.2.29}$$

$$\begin{aligned} u_2(x,t) = a_m a_n \, G_u^{m+n} cos(\theta_m + \theta_n) + \frac{1}{2} \, a_m^2 \, G_u^{2m} cos(\, 2\theta_m \,) \\ + a_m a_n H_u^{m-n} cos(\theta_m - \theta_n) + \frac{1}{2} \, a_n^2 \, G_u^{2n} \; cos(\, 2\theta_n \,) \end{aligned} \tag{3.2.30}$$

$$\begin{aligned} \Delta u_2(x,t) = a_m a_n G_{\Delta u}^{m+n} cos(\theta_m + \theta_n) + \frac{1}{2} \, a_m^2 \, G_{\Delta u}^{2m} cos(\, 2\theta_m \,) \\ + a_m a_n H_{\Delta u}^{m-n} cos(\theta_m - \theta_n) + \frac{1}{2} \, a_n^2 \, G_{\Delta u}^{2n} \; cos(\, 2\theta_n \,) \end{aligned} \tag{3.2.31}$$

where G and H are the super and sub-harmonic transfer functions for the respective subscripted variables and superscripted wave components. Substitution of the first and second-order bichromatic systems (3.2.22) - (3.2.24) and (3.2.29) - (3.2.31) into the second-order governing equations (3.2.3) - (3.2.5) of the two-layer system yields six equations for the six unknown quadratic transfer functions. The transfer functions of the self-interacting super-harmonics $2\theta_m$ and $2\theta_n$ has been discussed in section 3.2.1. The transfer functions of the cross-interacting super-harmonics $(\theta_m + \theta_n)$ and sub-harmonics $(\theta_m - \theta_n)$ are examined here in relation to the solutions from Nwogu (1993) and the second-order Stokes theory.

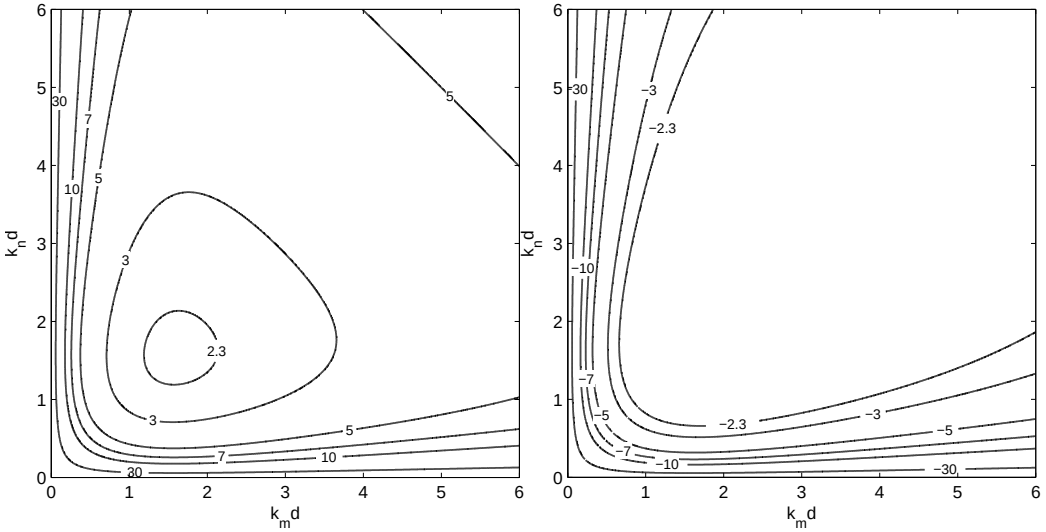

Figure 3.5. Amplitude of super-harmonics (left) and sub-harmonics (right) from second-order Stokes theory.

Published transfer functions of super and sub-harmonics are derived from the Laplace equation with the second-order free surface boundary conditions based on Stokes wave theory (Ottesen-Hansen, 1978; Dean and Sharma, 1981; Sand and Mansard, 1986). These solutions are expressed as functions of $\omega\sqrt{d/\left(4\pi^2 g\right)}$. In this study, the transfer functions are re-derived as functions of kd as shown in figure 3.5. Since $k_m d$ and $k_n d$ are interchangeable, both contour plots are symmetric about the diagonal $k_m d = k_n d$, which

correspond to the self-interacting solution. It is well known that the super-harmonic transfer function has a minimum in the intermediate-wave range and increases for longer and shorter waves. The super-harmonics modify the first-order wave profile by elevating the crest and flattening the trough. The absolute value of the sub-harmonic transfer function increases from short to long waves and converges to the setdown when $k_m d$ approaching $k_n d$. These low frequency waves are also called wave-group induced setdown, which is closely related with many coastal wave phenomena such as low-frequency drift motions of ships in harbors, surf beats, and coastal sediment transport.

Figure 3.6 plots the transfer functions from the three non-hydrostatic models and the Boussinesq model of Nwogu (1993). The results are normalized by the second-order Stokes solution and each panel shows contour lines of the relative amplitude with equal intervals. Based on the upper limit of long waves at $kd = 0.3$ and the lower limit of short waves at $kd = 3.0$, the two-dimensional plots in terms of kd are divided into 9 symmetric segments for discussion. The diagonal segments correspond to interactions between two long waves, two intermediate waves, and two short waves at first order. The relative amplitude along the diagonal from each model follows closely with the results of a_2/a_{2S} in figure 3.4. In the segment for long-wave interactions, the Boussinesq and hybrid models produce nearly the same transfer function as the second-order Stokes wave theory, whereas the one and two-layer models give slightly higher relative amplitude of 1.2846 to 1.3333 and 1.0569 to 1.0667. The capability to describe the super-harmonics of intermediate waves varies among the four models. The formulation of Nwogu (1993) shows considerable errors with the relative amplitude ranging from 0.5872 to 1.1534, while the two-layer model has a smaller range from 0.7432 to 1.0569. The one-layer model gives a relative amplitude of 1.2846 toward the long-wave limit, but with a value as low as 0.2360 at the short-wave limit, which outside its applicable range. The hybrid model has the best performance among the four with a relative amplitude range of 0.9726 to 1.2152. A coastal wave transformation model needs to describe deep-water input wave conditions at $kd \geq 3$. The one-layer model, two-layer model and the Boussinesq model

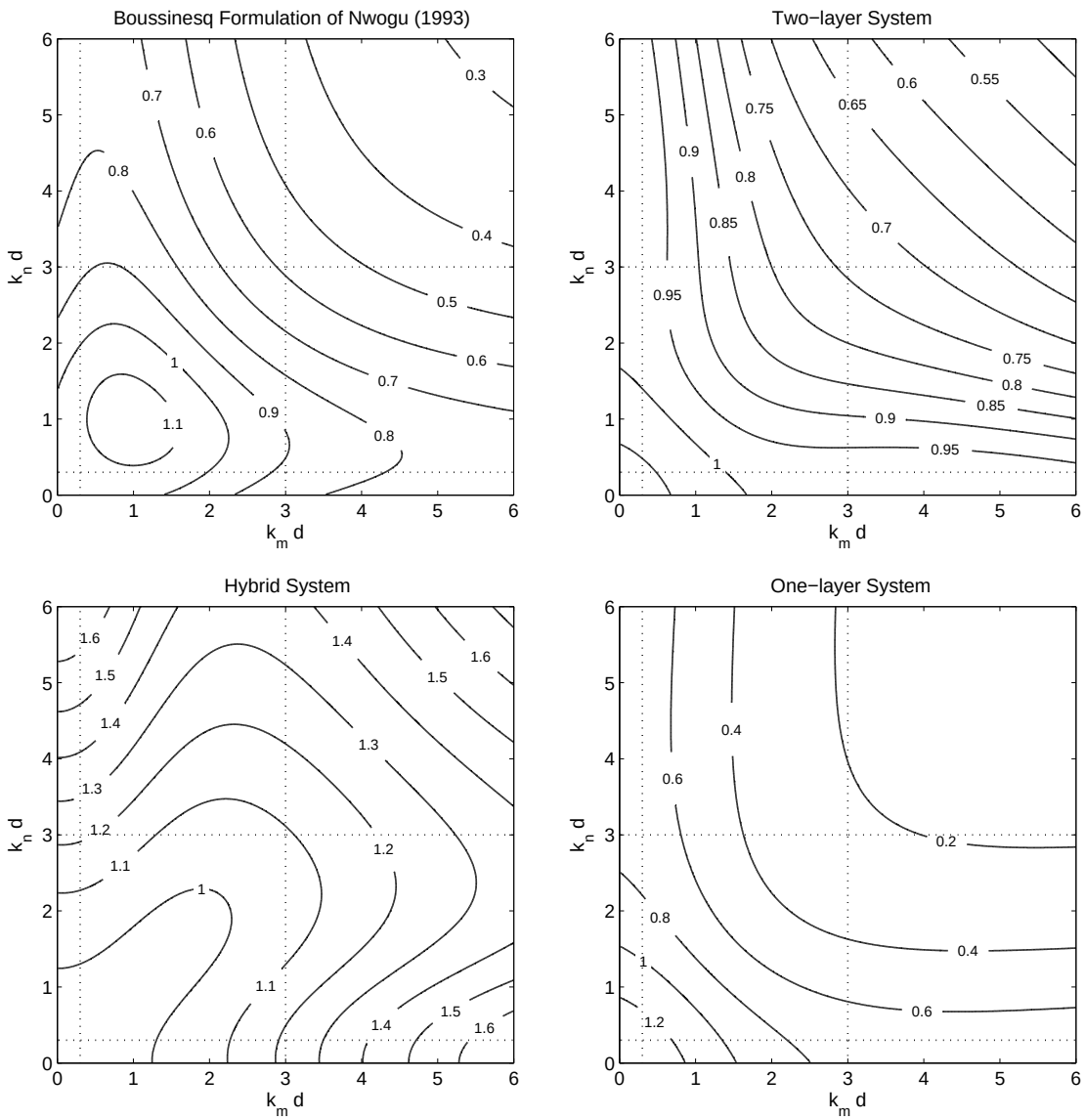

Figure 3.6. Relative amplitude of super-harmonics from Boussinesq (upper left), two-layer (upper right), hybrid (lower left), and one-layer (lower right) models.

of Nwogu (1993), which greatly underestimate the super-harmonics with relative amplitude of 0.2737, 0.7432, and 0.5872 at $kd = 3$, might not fully describe the nonlinearity of the input wave conditions at deep water. The hybrid model slightly overestimates the super-harmonics with a relative amplitude of 1.0913.

The transfer function in figure 3.6 also illustrate the model capability to account for second-order interactions between long and intermediate waves, long and short waves, and intermediate and short waves. Nonlinear interactions between long and immediate

waves might be important when surf beat develops from wave breaking in the surf zone. The one-layer model has the largest range of relative amplitude from 0.7127 to 1.3155, because it is not fully applicable over the entire range of intermediate waves. The two-layer model has the smallest relative amplitude from 0.9753 to 1.0631 despite a larger error for second-order self interactions. Although the hybrid model and the Bossinesq model of Nwogu (1993) have very similar dispersion relations, they exhibit distinct nonlinear properties especially for long and intermediate wave interactions. The relative amplitude of the hybrid model varies from 0.9824 to 1.2227, while the Boussinesq model varies from 0.8363 to 1.0833. Overall, the hybrid model has the most favorable nonlinear properties to describe the super-harmonics for wave transformation from deep to shallow water. The model has the lowest relative error over a wide band along the diagonal extending to the upper limit of the intermediate range. This is important for definition of the input deep water wave conditions and steepening of wave profiles prior to wave breaking. It has low errors for cross interactions between long waves and the immediate waves in the surf zone.

Sub-harmonic interactions are equally important in coastal processes related to infra-gravity waves and resonance. Figure 3.7 plots the normalized transfer functions from the three non-hydrostatic models and the Boussinesq model of Nwogu (1993). For long-wave interactions, the Boussinesq and hybrid models produce very good agreement with the second-order Stokes solution, while the one and two-layer models gives higher relative amplitude of 1.333 and 1.07. In the intermediate range, the Boussinesq model underestimates the transfer function with relative amplitude from 0.9818 to 0.3833 at the short-wave limit. The one-layer and two-layer models have a similar downward trend with relative amplitude of 1.3134 and 1.0627 at the long-wave limit to 0.2095 and 0.7819 at the short-wave limit. The hybrid model, however, shows a different pattern. It gives underestimations down to 0.6872 toward the short-wave limit along the diagonal and higher values with a maximum relative amplitude of 1.2061 in the off-diagonal directions. For short-wave interactions, the hybrid model maintains the small

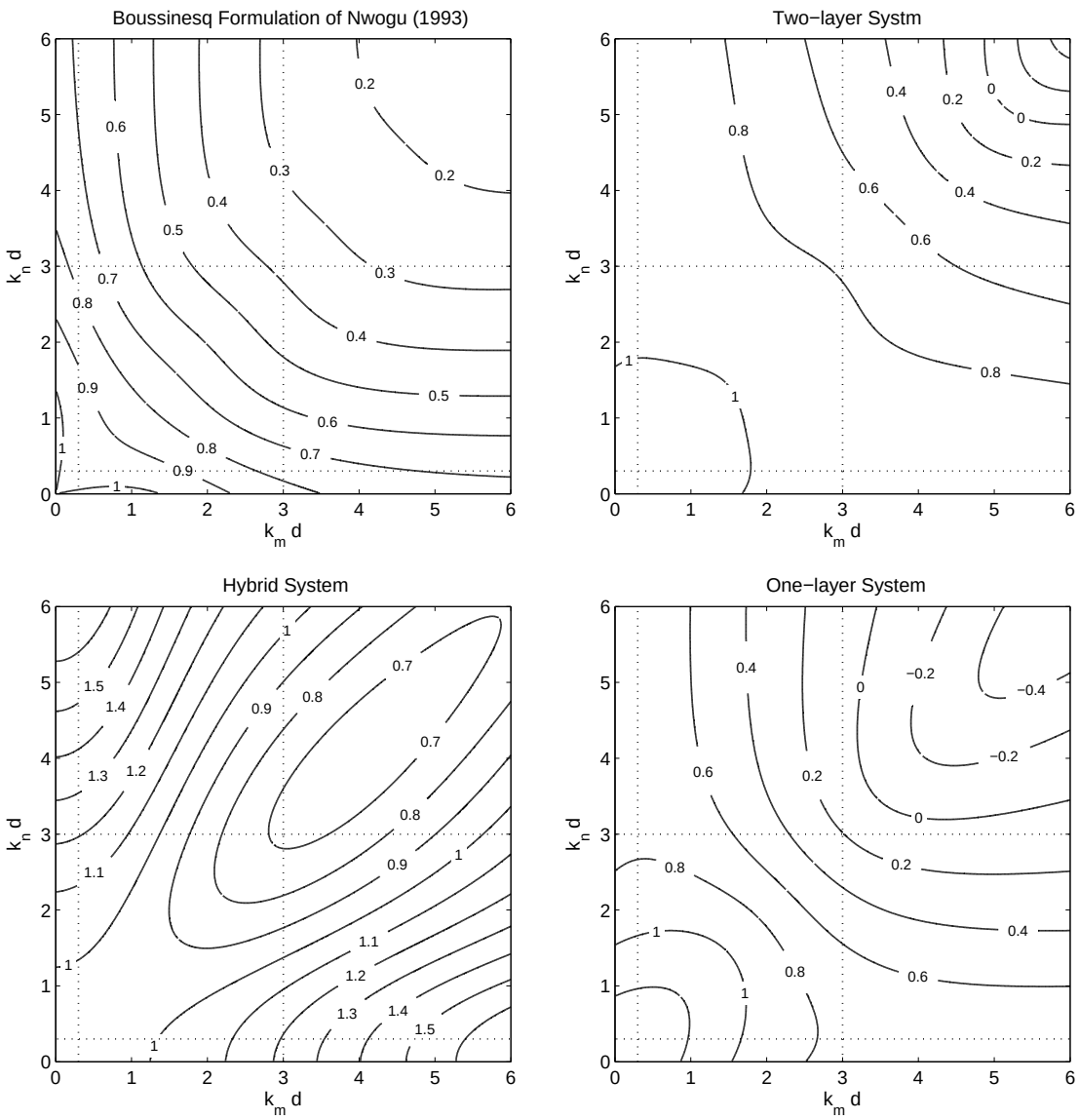

Figure 3.7. Relative amplitude of sub-harmonics from Boussinesq (upper left), two-layer (upper right), hybrid (lower left), and one-layer (lower right) models.)

level of error, while the other three models deteriorate rapidly with kd. Cross interactions between short, intermediate, and long waves are not as important for generation of sub-harmonics because of the large difference in frequency. The Boussinesq, two-layer, and hybrid models can reasonably handle interactions between long and intermediate waves especially for small values of kd in the range. It should be re-iterated that the one-layer model is not applicable toward the upper limit of the intermediate range.

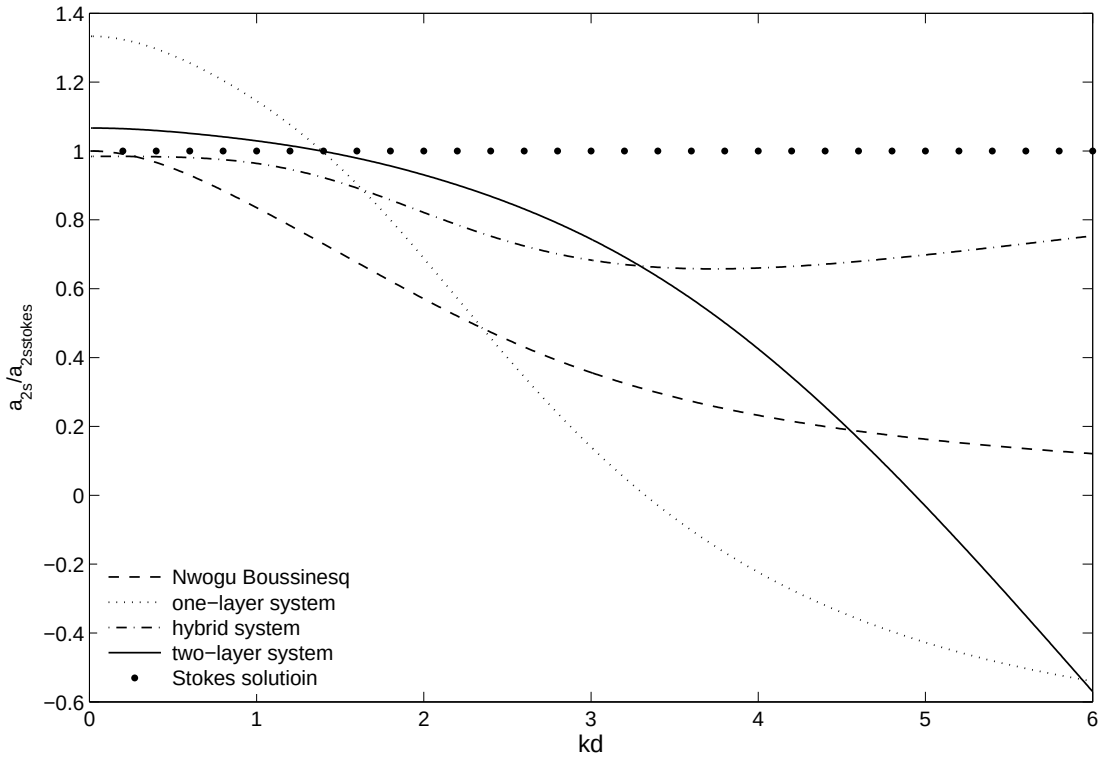

Figure 3.8. Ratio of approximate sub-harmonic transfer coefficients to Stokes solution for self-interaction.

The sub-harmonics convert to steady setdown of the water level at the limiting condition of $k_m d \rightarrow k_n d$. Figure 3.8 compares the four solutions along the diagonal of the sub-harmonic transfer functions. The second-order solution from the Boussinesq model of Nwogu (1993) agrees with the Stokes solution at the long-wave limit and gradually deteriorates with kd. The one and two-layer model overestimate the Stokes solution for $kd < 1.4$ and producing larger errors than the Boussinesq model at large values of kd. The hybrid model closely approximates the Stokes solution for $kd < 1$ and maintains a much smaller error than the Boussinesq model for large values of kd. Similar to the super-harmonic results, the hybrid model provides the best performance in reproducing sub-harmonic interactions.

Chapter 4

Numerical Formulation

This chapter describes the numerical implementation of the governing equations for the integrated two-layer, hybrid, and one-layer system. The numerical formulation for the two-layer system is addressed first and then adapted for the hybrid model through the predefined non-hydrostatic pressure distribution. Assigning a value of 0.5 for the free parameter gives rise to the one-layer model.

4.1 Integrated two-layer system

The governing equations of the two-layer free-surface flow provide separate descriptions of the flux and dispersion-dominated processes. Equations (2.3.5), (2.3.7) and (2.3.9) describe the flux-dominated processes including discontinuous flows, and equation (2.3.6), (2.3.8) and (2.3.10) provide corrections to highly dispersive waves and rotational flows. The six governing equations are re-organized into a quasi-linear form for the implementation of the momentum-conserving advection scheme of Stelling and Duinmeijer (2003) and the θ-method for time integration. The governing equations for the flux-dominated flows are

$$\frac{\partial \zeta}{\partial t} + \frac{\partial hu}{\partial x} = 0 \tag{4.1.1}$$

$$\frac{\partial u}{\partial t} + g\frac{\partial \zeta}{\partial x} + \frac{1}{2}\frac{\partial q_{z_\alpha}}{\partial x} + \frac{1}{4}\frac{\partial q_d}{\partial x} = S_u \tag{4.1.2}$$

$$\frac{\partial w}{\partial t} - \frac{q_d}{\zeta + d} = S_w \tag{4.1.3}$$

and the remaining governing equations are

$$w_{z_\alpha} - u_{z_\alpha}\frac{\partial z_\alpha}{\partial x} - \frac{\partial z_\alpha}{\partial t} + \frac{1}{2}\frac{\partial h\Delta u}{\partial x} = 0 \tag{4.1.4}$$

$$\frac{\partial \Delta u}{\partial t} + \frac{1}{4}\frac{\partial q_d}{\partial x} = S_{\Delta u} \tag{4.1.5}$$

$$\frac{\partial \Delta w}{\partial t} + \frac{2\, q_{z_\alpha}}{\zeta + d} - \frac{q_d}{\zeta + d} = S_{\Delta w} \tag{4.1.6}$$

in which the source terms are given by

$$\begin{aligned} S_u = -\frac{1}{h}\left(\frac{\partial hu^2 + h\Delta u^2}{\partial x} - u\frac{\partial hu}{\partial x}\right) \\ - \frac{q_{z_\alpha}}{2h}\frac{\partial h}{\partial x} - \frac{q_d}{4h}\frac{\partial h}{\partial x} + \frac{q_d}{h}\frac{\partial d}{\partial x} \end{aligned} \tag{4.1.7}$$

$$S_w = -\frac{1}{h}\left(\frac{\partial huw + h\Delta u\Delta w}{\partial x} - w\frac{\partial hu}{\partial x}\right) \tag{4.1.8}$$

$$\begin{aligned} S_{\Delta u} = -\frac{1}{h}\left(2\,\frac{\partial hu\Delta u}{\partial x} - \Delta u\,\frac{\partial hu}{\partial x}\right) - \frac{q_d}{4h}\frac{\partial h}{\partial x} \\ + \frac{q_{z_\alpha}}{h}\frac{\partial\,(\zeta - d)}{\partial x} + \frac{q_d}{h}\frac{\partial d}{\partial x} - \frac{2u_{z_\alpha}\overline{w}_{z_\alpha}}{h} \end{aligned} \tag{4.1.9}$$

$$S_{\Delta w} = -\frac{1}{h}\left(\frac{\partial hu\Delta w + h\Delta uw}{\partial x} - \Delta w\,\frac{\partial hu}{\partial x}\right) - \frac{2w_{z_\alpha}\overline{w}_{z_\alpha}}{h} \tag{4.1.10}$$

The horizontal and vertical advection terms, in the forms as shown in (4.1.7) - (4.1.10), allow approximation of breaking waves as bores or hydraulic jumps and ensure momentum conservation across the discontinuities. The interfacial advection terms are only involved in (4.1.9) and (4.1.10) for description of mass and momentum exchange across the interface.

4.1.1 Time-integration equations

The governing equations are discretized with a finite difference scheme in the horizontal direction and a finite volume scheme over the water column. Figure 4.1 shows the staggered grid and flow variables. The non-hydrostatic pressure and vertical velocity are defined at the cell center x_i and the horizontal velocity at the cell interfaces $x_{i-1/2}$ and $x_{i+1/2}$. The θ-method is implemented to integrate the governing equations (4.1.1) - (4.1.6), which gives

$$\begin{aligned}\frac{\zeta_i^{n+1}-\zeta_i^n}{\Delta t}+\frac{1}{\Delta x}\{&+\theta\left((hu)_{i+1/2}^{n+1}-(hu)_{i-1/2}^{n+1}\right)\\&+(1-\theta)\left((hu)_{i+1/2}^{n}-(hu)_{i-1/2}^{n}\right)\}=0\end{aligned}\tag{4.1.11}$$

$$\begin{aligned}\frac{u_{i+1/2}^{n+1}-u_{i+1/2}^{n}}{\Delta t}&+\frac{g}{\Delta x}\left\{\theta\left(\zeta_{i+1}^{n+1}-\zeta_i^{n+1}\right)+(1-\theta)\left(\zeta_{i+1}^{n}-\zeta_i^{n}\right)\right\}\\&+\frac{1}{2\Delta x}\left\{\theta\left(q_{z_{\alpha_{i+1}}}^{n+1}-q_{z_{\alpha_i}}^{n+1}\right)+(1-\theta)\left(q_{z_{\alpha_{i+1}}}^{n}-q_{z_{\alpha_i}}^{n}\right)\right\}\\&+\frac{1}{4\Delta x}\left\{\theta\left(q_{d_{i+1}}^{n+1}-q_{d_i}^{n+1}\right)+(1-\theta)\left(q_{d_{i+1}}^{n}-q_{d_i}^{n}\right)\right\}=S_{u_{i+1/2}^n}\end{aligned}\tag{4.1.12}$$

$$\frac{w_i^{n+1}-w_i^n}{\Delta t}-\left\{\frac{\theta\, q_{d_i}^{n+1}}{h_i^{n+1}}+\frac{(1-\theta)\, q_{d_i}^{n}}{h_i^{n}}\right\}=S_{w_i^n}\tag{4.1.13}$$

$$\begin{aligned}w_{z_\alpha,i}^n=&\frac{u_i^n}{2\,\Delta x}\left(\zeta_{i+1/2}^n-d_{i+1/2}-\zeta_{i-1/2}^n+d_{i-1/2}\right)\\&-\frac{1}{2\,\Delta x}\left((hu)_{i+1/2}^n+(h\Delta u)_{i+1/2}^n-(hu)_{i-1/2}^n-(h\Delta u)_{i-1/2}^n\right)\end{aligned}\tag{4.1.14}$$

$$\begin{aligned}\frac{\Delta u_{i+1/2}^{n+1}-\Delta u_{i+1/2}^{n}}{\Delta t}+\frac{1}{4\Delta x}\{&+\theta\left(q_{d_{i+1}}^{n+1}-q_{d_i}^{n+1}\right)\\&+(1-\theta)\left(q_{d_{i+1}}^{n}-q_{d_i}^{n}\right)\}=S_{\Delta u_{i+1/2}^n}\end{aligned}\tag{4.1.15}$$

$$\begin{aligned}\frac{\Delta w_i^{n+1}-\Delta w_i^{n}}{\Delta t}&+2\left\{\frac{\theta\, q_{z_{\alpha i}}^{n+1}}{h_i^{n+1}}+\frac{(1-\theta)\, q_{z_{\alpha_i}}^{n}}{h_i^{n}}\right\}\\&-\left\{\frac{\theta\, q_{d_i}^{n+1}}{h_i^{n+1}}+\frac{(1-\theta)\, q_{d_i}^{n}}{h_i^{n}}\right\}=S_{\Delta w_i^n}\end{aligned}\tag{4.1.16}$$

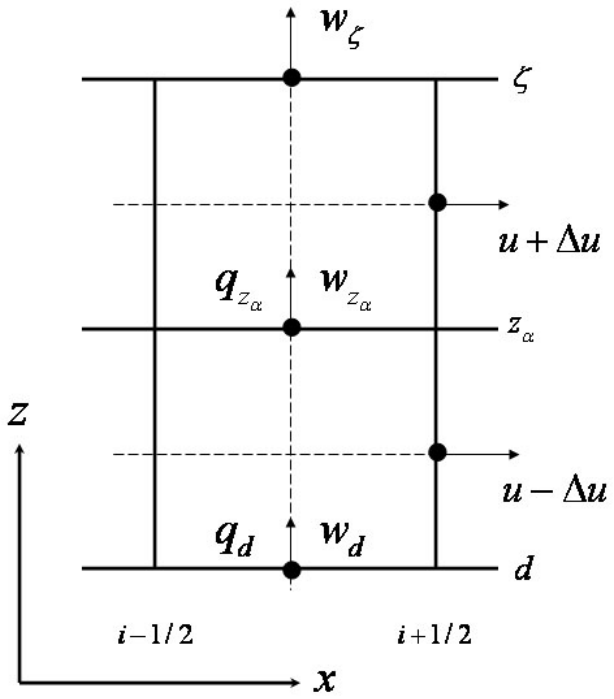

Figure 4.1. Staggered grid and flow parameters.

A central difference scheme is applied to the first-order spatial derivatives in the source terms except for the horizontal advection speeds, which are treated with a second-order upwind scheme according to Zijlema and Stelling (2008)

$$u_i = \begin{cases} 1.5\,u_{i-1} - 0.5\,u_{i-2} & \text{if } (hu)_i \geq 0 \\ 1.5\,u_{i+1} - 0.5\,u_{i+2} & \text{if } (hu)_i < 0 \end{cases} \tag{4.1.17}$$

The vertical advection speed at the cell interface, $w_{i+1/2}$, $\Delta w_{i+1/2}$, are evaluated by taking average of the values at adjacent cell centers.

Equations (4.1.11) - (4.1.16) involve eight unknowns in the non-hydrostatic flow system. Implementation of a finite volume scheme to the continuity equation (2.1.5) over the two layers provides the remaining two equations to ensure conservation of mass and to close the system. Integration of the flow variables along the boundaries of the grid cells in the top and bottom layers and implementation of the linear transformation from (2.3.1) to

(2.3.4) give

$$h^{n+1}_{i+1/2}u^{n+1}_{i+1/2} - h^{n+1}_{i-1/2}u^{n+1}_{i-1/2} + w^{n+1}_{i,\zeta}\Delta x - w^{n+1}_{i,d}\Delta x = 0 \tag{4.1.18}$$

$$-h^{n+1}_{i+1/2}\Delta u^{n+1}_{i+1/2} + h^{n+1}_{i-1/2}\Delta u^{n+1}_{i-1/2} + w^{n+1}_{i,\zeta}\Delta x - 2\,w^{n+1}_{i,z_\alpha}\Delta x + w^{n+1}_{i,d}\Delta x = 0 \tag{4.1.19}$$

The numerical procedure, which is also known as the pressure correction technique, includes a hydrostatic and a non-hydrostatic step (Zijlema and Stelling, 2005). An intermediate solution of the surface elevation and horizontal velocity is obtained from (4.1.11), (4.1.12) and (4.1.15) and the vertical velocity from (4.1.13), (4.1.14) and (4.1.16). Implementation of (4.1.18) and (4.1.19) over all grid cells forms a Poisson-type equation from which the non-hydrostatic pressure is determined. Equations (4.1.11) - (4.1.16) then update the solution to the next time step.

4.1.2 Numerical procedures

This section provides a detailed description of the numerical procedures for the hydrostatic and non-hydrostatic steps of the solution. In the hydrostatic step, the θ-terms are initially ignored in (4.1.11), (4.1.12) and (4.1.15) to evaluate an intermediate solution of the horizontal velocity and free surface elevation:

$$\frac{\zeta^{**}_i - \zeta^n_i}{\Delta t} + \frac{(hu)^n_{i+1/2} - (hu)^n_{i-1/2}}{\Delta x} = 0 \tag{4.1.20}$$

$$\frac{u^{**}_{i+1/2} - u^n_{i+1/2}}{\Delta t} + g\,\frac{\zeta^n_{i+1} - \zeta^n_i}{\Delta x} + \frac{1}{2}\frac{q^n_{z_{\alpha_{i+1}}} - q^n_{z_{\alpha_i}}}{\Delta x} + \frac{1}{4}\frac{q^n_{d_{i+1}} - q^n_{d_i}}{\Delta x} = S^n_{u_{i+1/2}} \tag{4.1.21}$$

$$\frac{\Delta u^{**}_{i+1/2} - \Delta u^n_{i+1/2}}{\Delta t} + \frac{1}{4}\,\frac{q^n_{d_{i+1}} - q^n_{d_i}}{\Delta x} = S_{\Delta u^n_{i+1/2}} \tag{4.1.22}$$

where the double-asterisk denotes the intermediate solution. The surface elevation and horizontal velocity are then refined with the corresponding θ-terms in (4.1.11) and (4.1.12) as

$$\begin{aligned}\frac{\zeta^*_i - \zeta^{**}_i}{\Delta t} + \theta\,\big(&\frac{h^*_{i+1/2}u^*_{i+1/2} - h^*_{i-1/2}u^*_{i-1/2}}{\Delta x} \\ &- \frac{h^n_{i+1/2}u^n_{i+1/2} - h^n_{i-1/2}u^n_{i-1/2}}{\Delta x}\big) = 0\end{aligned} \tag{4.1.23}$$

$$\frac{u^*_{i+1/2} - u^{**}_{i+1/2}}{\Delta t} + g\,\theta\,\frac{\zeta^*_{i+1} - \zeta^{**}_{i+1} - (\zeta^*_i - \zeta^{**}_i)}{\Delta x} = 0 \tag{4.1.24}$$

where the asterisk denotes the refined intermediate solution. Inserting (4.1.24) into (4.1.23) and denoting $\Delta\zeta_i = \zeta^*_i - \zeta^{**}_i$ give rise to a tridiagonal matrix in the form

$$\begin{aligned} -\frac{g\theta^2\Delta t^2}{\Delta x^2}h^*_{i+1/2}\Delta\,\zeta_{i+1} - \frac{g\theta^2\Delta t^2}{\Delta x^2}h^*_{i-1/2}\Delta\,\zeta_{i-1} \\ + \left(1 + \frac{g\theta^2\Delta t^2}{\Delta x^2}h^*_{i+1/2} + \frac{g\theta^2\Delta t^2}{\Delta x^2}h^*_{i-1/2}\right)\Delta\,\zeta_i \\ = + \frac{\theta\,\Delta t}{\Delta x}\left(h^n_{i+1/2}u^n_{i+1/2} - h^n_{i-1/2}u^n_{i-1/2}\right) \\ - \frac{\theta\,\Delta t}{\Delta x}\left(h^*_{i+1/2}u^{**}_{i+1/2} - h^*_{i-1/2}u^{**}_{i-1/2}\right) \end{aligned} \tag{4.1.25}$$

Once $\Delta\zeta$ is obtained from (4.1.25), u^* can be calculated from (4.1.24). The procedure repeats until convergency at $|u^{*(1)} - u^{*(0)}| \leq 0.00001$.

The non-hydrostatic step begins with an intermediate solution of the vertical velocity from (4.1.13) and (4.1.16) with the θ-terms ignored:

$$\frac{w^*_i - w^n_i}{\Delta t} - \frac{q^n_{d_i}}{h^n_i} = S^n_{w,i} \tag{4.1.26}$$

$$\frac{\Delta w^*_i - \Delta w^n_i}{\Delta t} + \frac{2\,q^n_{z_{\alpha_i}}}{h^n_i} - \frac{q^n_{d_i}}{h^n_i} = S^n_{\Delta w,i} \tag{4.1.27}$$

The momentum equations, which contain the terms not used in the hydrostatic step and the initial computation of the vertical velocity, read

$$\begin{aligned} \frac{u^{n+1}_{i+1/2} - u^*_{i+1/2}}{\Delta t} + \frac{1}{4}\,\frac{\theta}{\Delta x}\left\{q^{n+1}_{d_{i+1}} - q^{n+1}_{d_i} - q^n_{d_{i+1}} + q^n_{d_i}\right\} \\ + \frac{1}{2}\,\frac{\theta}{\Delta x}\left\{q^{n+1}_{z_{\alpha_{i+1}}} - q^{n+1}_{z_{\alpha_i}} - q^n_{z_{\alpha_{i+1}}} + q^n_{z_{\alpha_i}}\right\} = 0 \end{aligned} \tag{4.1.28}$$

$$\frac{w^{n+1}_i - w^*_i}{\Delta t} - \theta\left\{\frac{\Delta q_{d_i}}{h^{n+1}_i} + \left(\frac{1}{h^{n+1}_i} - \frac{1}{h^n_i}\right)q^n_{d_i}\right\} = 0 \tag{4.1.29}$$

$$\frac{\Delta u^{n+1}_{i+1/2} - \Delta u^*_{i+1/2}}{\Delta t} + \frac{1}{4}\,\frac{\theta}{\Delta x}\left\{q^{n+1}_{d_{i+1}} - q^{n+1}_{d_i} - q^n_{d_{i+1}} + q^n_{d_i}\right\} = 0 \tag{4.1.30}$$

$$\frac{\Delta w_i^{n+1} - \Delta w_i^*}{\Delta t} + 2\,\theta \left\{ \frac{\Delta q_{z_{\alpha_i}}}{h_i^{n+1}} + \left(\frac{1}{h_i^{n+1}} - \frac{1}{h_i^n} \right) q_{z_{\alpha_i}}^n \right\} - \theta \left\{ + \frac{\Delta q_{d_i}}{h_i^{n+1}} + \left(\frac{1}{h_i^{n+1}} - \frac{1}{h_i^n} \right) q_{d_i}^n \right\} = 0 \tag{4.1.31}$$

where $\Delta u^* = \Delta u^{**}$, $q_d^{n+1} = q_d^n + \Delta q_d$, and $q_{z_\alpha}^{n+1} = q_{z_\alpha}^n + \Delta q_{z_\alpha}$. Substituting (4.1.28) - (4.1.31) into (4.1.18) and (4.1.19) gives a system of simultaneous equations for Δq_d and Δq_{z_α} in the form

$$A_1\, \Delta q_d + B_1\, \Delta q_{z_\alpha} = G_1 \tag{4.1.32}$$

$$A_2\, \Delta q_d + B_2\, \Delta q_{z_\alpha} = G_2 \tag{4.1.33}$$

The non-symmetric, tridiagonal matrices A_1, A_2, B_1, and B_2 are defined by

$$a_{1l} = -\frac{1}{4}\frac{\theta\,\Delta t}{\Delta x} h_{i-1/2}^{n+1} \tag{4.1.34}$$

$$a_{1c} = +\frac{1}{4}\frac{\theta\,\Delta t}{\Delta x} h_{i+1/2}^{n+1} + \frac{1}{4}\frac{\theta\,\Delta t}{\Delta x} h_{i-1/2}^{n+1} - \frac{4\,\theta\,\Delta x\,\Delta t}{h_i^{n+1}} \tag{4.1.35}$$

$$a_{1r} = -\frac{1}{4}\frac{\theta\,\Delta t}{\Delta x} h_{i+1/2}^{n+1} \tag{4.1.36}$$

$$b_{1l} = -\frac{1}{2}\frac{\theta\,\Delta t}{\Delta x} h_{i-1/2}^{n+1} \tag{4.1.37}$$

$$b_{1c} = +\frac{1}{2}\frac{\theta\,\Delta t}{\Delta x} h_{i+1/2}^{n+1} + \frac{1}{2}\frac{\theta\,\Delta t}{\Delta x} h_{i-1/2}^{n+1} + \frac{8\,\theta\,\Delta x\,\Delta t}{h_i^{n+1}} \tag{4.1.38}$$

$$b_{1r} = -\frac{1}{2}\frac{\theta\,\Delta t}{\Delta x} h_{i+1/2}^{n+1} \tag{4.1.39}$$

$$a_{2l} = +\frac{1}{4}\frac{\theta\,\Delta t}{\Delta x} h_{i-1/2}^{n+1} - \theta\,\Delta t \left(\frac{\partial d}{\partial x} \right)_i \tag{4.1.40}$$

$$a_{2c} = -\frac{1}{4}\frac{\theta\,\Delta t}{\Delta x} h_{i+1/2}^{n+1} - \frac{1}{4}\frac{\theta\,\Delta t}{\Delta x} h_{i-1/2}^{n+1} - \frac{12\,\theta\,\Delta x\,\Delta t}{h_i^{n+1}} \tag{4.1.41}$$

$$a_{2r} = +\frac{1}{4}\frac{\theta\,\Delta t}{\Delta x} h_{i+1/2}^{n+1} + \theta\,\Delta t \left(\frac{\partial d}{\partial x} \right)_i \tag{4.1.42}$$

$$b_{2l} = -\,\theta\,\Delta t\left(\frac{\partial d}{\partial x}\right)_i \tag{4.1.43}$$

$$b_{2c} = +\,16\,\frac{\theta\,\Delta x\,\Delta t}{h_i^{n+1}} \tag{4.1.44}$$

$$b_{2r} = -\,\theta\,\Delta t\left(\frac{\partial d}{\partial x}\right)_i \tag{4.1.45}$$

where the subscript c denotes the diagonal and l and r denote the elements to the left and right. The forcing vectors G_1 and G_2 from the non-hydrostatic source terms are defined by

$$\begin{aligned} G_1 = &-h_{i+1/2}^{n+1}u_{i+1/2}^{*} + h_{i-1/2}^{n+1}u_{i-1/2}^{*} \\ &+4\,\Delta x\left\{\Delta w_i^{*} - 2\,\theta\,\Delta t\left(\frac{1}{h_i^{n+1}} - \frac{1}{h_i^{n}}\right)q_{z_{\alpha_i}}^{n} + \theta\,\Delta t\left(\frac{1}{h_i^{n+1}} - \frac{1}{h_i^{n}}\right)q_{d_i}^{n}\right\} \end{aligned} \tag{4.1.46}$$

$$\begin{aligned} G_2 = &+h_{i+1/2}^{n+1}\Delta u_{i+1/2}^{*} - h_{i-1/2}^{n+1}\Delta u_{i-1/2}^{*} \\ &+4\,\Delta x\left\{w_i^{*} + \theta\,\Delta t\left(\frac{1}{h_i^{n+1}} - \frac{1}{h_i^{n}}\right)q_{d_i}^{n}\right\} \\ &+4\,\Delta x\left\{2\,\Delta w_i^{*} - 4\,\theta\,\Delta t\left(\frac{1}{h_i^{n+1}} - \frac{1}{h_i^{n}}\right)q_{z_{\alpha_i}}^{n}\right\} \\ &+4\,\Delta x\left\{\frac{1}{2}\left(\frac{\partial d}{\partial x}\right)_i\left(u_{i+1/2}^{*} + u_{i-1/2}^{*} + \Delta u_{i+1/2}^{*} + \Delta u_{i-1/2}^{*}\right)\right\} \end{aligned} \tag{4.1.47}$$

Equations (4.1.32) and (4.1.33) give rise to a Poisson-type system with a non-symmetric, 9-band sparse matrix from which the non-hydrostatic pressure can be obtained by a linear equation solver. The horizontal and vertical velocities are then updated from (4.1.28) - (4.1.31) to complete the solution.

For inundation and runup calculations, special numerical treatments are necessary to describe the moving waterline in the swash zone. The moving-waterline scheme of Yamazaki et al. (2009) is utilized to keep track of the wet-dry boundary through extrapolation of the numerical solution from the wet region onto the beach. The non-hydrostatic pressure is set to be zero at the wet cells along the wet-dry boundary to conform with the solution scheme of the non-hydrostatic model. In the implementation, a thin layer

of water, usually $0.0001\,m$ thick, is overlaid on the dry cells to improve numerical stability. As long as the time step Δt is small enough to guarantee the waterline movement is smaller than Δx, wave runup could be computed without any difficulties.

4.2 Hybrid system

The numerical procedures for the hybrid system follow closely the two-layer formulation. The governing equations (2.5.2) - (2.5.7) are re-organized into a quasi-linear form, which is discretized over a staggered grid on a boundary-fitted coordinate with a finite difference scheme. Implementation of the θ-method splits the time integration into the hydrostatic and non-hydrostatic steps. The hydrostatic step provides an intermediate solution from the nonlinear shallow-water equations with the non-hydrostatic pressure from the previous time step. Substitution of the intermediate solution from the hydrostatic step into the cell-integrated continuity equation forms the pressure Poisson equation. The velocity components are then updated through the computed non-hydrostatic pressure at the bottom for next time step as in the two-layer model. The development of the pressure Poisson equation, which is distinct from the formulation of the two-layer system, is presented here.

The discretization of the six governing equations (2.5.2) - (2.5.7) reduces the number of unknowns to seven together with a predetermined free parameter. Implementation of a finite volume scheme to the continuity equation (2.1.5) and integration along the boundaries of the grid cells in the top and bottom layers gives

$$h_i^{n+1} u_{i+\frac{1}{2}}^{n+1} - h_i^{n+1} u_{i-\frac{1}{2}}^{n+1} - 4\Delta x \Delta w_i^{n+1} = 0 \tag{4.2.1}$$

The horizontal and vertical velocity components at the new time step is given by integration of the intermediate solution from the hydrostatic step as well as the non-hydrostatic

pressure terms through (2.5.3) and (2.5.7) as

$$u_{i-\frac{1}{2}}^{n+1} = u_{i-\frac{1}{2}}^{*} - \left(\frac{\alpha}{2} + \frac{1}{4}\right)\frac{\Delta t}{\Delta x}\left(\Delta q_{d_i} - \Delta q_{d_{i-1}}\right) \tag{4.2.2}$$

$$u_{i+\frac{1}{2}}^{n+1} = u_{i+\frac{1}{2}}^{*} - \left(\frac{\alpha}{2} + \frac{1}{4}\right)\frac{\Delta t}{\Delta x}\left(\Delta q_{d_{i+1}} - \Delta q_{d_i}\right) \tag{4.2.3}$$

$$\Delta w_i^{n+1} = \Delta w_i^{*} - \frac{(2\alpha - 1)\,\Delta t}{h_i^{n+1}}\Delta q_{d_i} - \Delta t\,(2\alpha - 1)\left(\frac{1}{h_i^{n+1}} - \frac{1}{h_i^{n}}\right) q_{d_i}^{n} \tag{4.2.4}$$

where the asterisk $(*)$ indicates intermediate solutions from the hydrostatic step and $\Delta q_d = q_d^{n+1} - q_d^n$ is the non-hydrostatic pressure correction. The numerical formulation retains the piecewise linear distribution of the variables in the vertical direction through the parameter α, but only involves the non-hydrostatic pressure at the bottom.

Equations (4.2.2) - (4.2.4) connect the non-hydrostatic solution with the intermediate solution and the non-hydrostatic pressure correction. After the hydrostatic solution is determined from time integration, substitution of these equations into (4.2.1) gives the pressure Poisson equation in terms of $\Delta\, q_d$ as

$$A\,\Delta\, q_d = \, G \tag{4.2.5}$$

where the coefficients are given by

$$a_l = -\left(\frac{\alpha}{2} + \frac{1}{4}\right)\frac{\Delta t}{\Delta x} h_i^{n+1} \tag{4.2.6}$$

$$a_c = +\left(\alpha + \frac{1}{2}\right)\frac{\Delta t}{\Delta x} h_i^{n+1} + \frac{4\,(2\alpha - 1)\,\Delta t \Delta x}{h_i^{n+1}} \tag{4.2.7}$$

$$a_r = -\left(\frac{\alpha}{2} + \frac{1}{4}\right)\frac{\Delta t}{\Delta x} h_i^{n+1} \tag{4.2.8}$$

and the forcing vector from the non-hydrostatic source terms is

$$\begin{aligned} G = &+ h_i^{n+1} u_{i-\frac{1}{2}}^{*} - h_i^{n+1} u_{i+\frac{1}{2}}^{*} \\ &+ 4\Delta x\left(\Delta w_i^{n} - \Delta t\,(2\alpha - 1)\left(\frac{1}{h_i^{n+1}} - \frac{1}{h_i^{n}}\right) q_{d_i}^{n}\right) \end{aligned} \tag{4.2.9}$$

The pressure Poisson equation (4.2.5) contains a non-symmetric tridiagonal matrix versus a non-symmetric, 9-band sparse matrix in the two-layer system. Since only the non-hydrostatic pressure at the bottom is involved, the matrix A has half of the rank in comparison to a two-layer model. The reductions in bandwidth and rank substantially lower the computational requirements of the hybrid model.

4.3 One-layer system

The numerical discretization and time integration for the one-layer model are a special case of the hybrid model when $\alpha = 0.5$ and the dispersion-dominated governing equations are disabled. Examination of the diagonal component (4.2.7) of the pressure Poisson equation reveals that the matrix becomes ill-posed for $\alpha = 0.5$. The numerical formulation in the discretized continuity equation (4.2.1) is based on the vertical velocity gradient Δw, which vanishes in a one-layer system when $\alpha = 0.5$. For completeness, the pressure Poisson equation for a one-layer system is derived here.

Similar to the two-layer and hybrid models, the pressure Poisson equation is derived from cell-integration of the continuity equation (2.1.5) as

$$h_i^{n+1} u_{i+\frac{1}{2}}^{n+1} - h_i^{n+1} u_{i-\frac{1}{2}}^{n+1} - 2\Delta x \left(w_{d_i}^{n+1} - w_i^{n+1} \right) = 0 \tag{4.3.1}$$

The horizontal velocity is given by (2.5.3) through (4.2.3) and (4.2.4). The depth-integrated vertical velocity is given by (2.4.3) and the bottom velocity by (2.4.6) as

$$w_i^{n+1} = w_i^* + \frac{\Delta t}{h_i^{n+1}} \Delta q_i + \Delta t \left(\frac{1}{h_i^{n+1}} - \frac{1}{h_i^n} \right) q_{d_i}^n \tag{4.3.2}$$

$$w_{d_i}^{n+1} = -\frac{1}{2\Delta x} \left(u_{i-\frac{1}{2}}^{n+1} + u_{i+\frac{1}{2}}^{n+1} \right) \left(d_{i+\frac{1}{2}} - d_{i-\frac{1}{2}} \right) \tag{4.3.3}$$

Equation (4.3.1) gives a system of simultaneous equations in the form of (4.2.6) with the coefficients and forcing defined by

$$a_l = -\frac{1}{2} \frac{\Delta t}{\Delta x} h_i^{n+1} + \frac{1}{2} \frac{\Delta t}{\Delta x} \left(d_{i+\frac{1}{2}} - d_{i-\frac{1}{2}} \right) \tag{4.3.4}$$

$$a_c = + \frac{\Delta t}{\Delta x} h_i^{n+1} + \frac{2\Delta t \Delta x}{h_i^{n+1}} \tag{4.3.5}$$

$$a_r = - \frac{1}{2} \frac{\Delta t}{\Delta x} h_i^{n+1} - \frac{1}{2} \frac{\Delta t}{\Delta x} \left(d_{i+\frac{1}{2}} - d_{i-\frac{1}{2}} \right) \tag{4.3.6}$$

$$\begin{aligned} G = & + h_i^{n+1} u_{i-\frac{1}{2}}^* - h_i^{n+1} u_{i+\frac{1}{2}}^* \\ & - 2\Delta x \{ w_i^n + \Delta t \left(\frac{1}{h_i^{n+1}} - \frac{1}{h_i^n} \right) q_{d_i}^n \\ & + \frac{1}{2\Delta x} \left(u_{i-\frac{1}{2}}^n + u_{i+\frac{1}{2}}^n \right) \left(d_{i+\frac{1}{2}} - d_{i-\frac{1}{2}} \right) \} \end{aligned} \tag{4.3.7}$$

The matrix in this linear system is also non-symmetric tridiagonal as in the hybrid system and Yamazaki et al. (2009).

Chapter 5

Results and Discussion

The non-hydrostatic formulation provides a series of models to study coastal processes over a spectrum of ocean waves from tsunamis to wind seas. The one-layer model caters to weakly-dispersive long waves such as tsunamis and provides a baseline for comparison with the two-layer and hybrid models. The two-layer model maintains strong dispersion characteristics for propagation of wind waves and utilizes a momentum conserving scheme to describe the flux-dominated breaking process in runup calculations. The hybrid system provides better performance than one-layer models in dispersion and shoaling properties and requires less computational resources than a two-layer system. This chapter examines the performance of the three models through a series of numerical experiments involving long and short waves. Modeling of solitary wave propagation in a channel of constant water depth allows examination of the balance between dispersion and nonlinearity as well as assessment of model convergency with respect to temporal and spatial resolution. The laboratory experiment of Beji and Battjes (1993) for transformation of small amplitude waves over a submerged bar provide a test case to examine the dispersion characteristics in a weakly nonlinear setting, while the laboratory data from Nwogu (1993) on wave transformation over a plane beach allow examination of the dispersion, shoaling, and nonlinear properties. Wave breaking and runup are assessed through laboratory data from Synolakis (1987) for solitary wave transformation

on a plane beach. Finally, the shock-capturing capability is validated through the laboratory data of Roeber (2010) on wave transformation over fringing reefs. Each of the test cases utilizes $\theta = 1$ in the numerical procedures of the hydrostatic and non-hydrostatic steps to guarantee convergency and the same spatial and temporal resolution for direct comparison of the results.

5.1 Solitary wave propagation in a channel

A standard test for the dispersion characteristics of non-hydrostatic and Boussinesq-type models is the propagation of solitary waves in a frictionless channel of constant depth. Due to the balance between nonlinearity and dispersion, the computed solitary wave should maintain its profile when traveling over water with uniform depth. Since a solitary wave involves mass flux, it provides a suitable test for nearshore wave models.

In the numerical experiment, a $2500\,m$ long and $10\,m$ deep channel is considered with the initial conditions corresponding to a solitary wave of $2\,m$ high at $100\,m$ from the left boundary. A reflecting boundary condition is implemented at the two ends of the channel. The solitary wave solution provides the horizontal velocity and surface elevation as

$$u = \frac{c\,\zeta}{\zeta + d} \tag{5.1.1}$$

$$\zeta = \frac{4a\,exp\left(-\sqrt{\frac{3a}{d^2(a+d)}}\,(x - ct)\right)}{\left(1 + exp\left(-\sqrt{\frac{3a}{d^2(a+d)}}\,(x - ct)\right)\right)^2} \tag{5.1.2}$$

where $a = 2\,m$, $d = 10\,m$, and $c = \sqrt{g\,(a+d)}$. The vertical velocity and gradient are inferred from the solitary wave solution provided by Stelling and Zijlema (2003) as

$$w = \frac{1}{2}\,(-\zeta + d)\,\frac{\partial u}{\partial x} \tag{5.1.3}$$

$$\Delta w = \frac{1}{4}\,(\zeta + d)\,\frac{\partial u}{\partial x} \tag{5.1.4}$$

A grid size of $\Delta x = 3\,m$ and a time step of $\Delta t = 0.05\,s$ achieve a Courant number of $\Delta t\sqrt{gd}/\Delta x = 0.1651$.

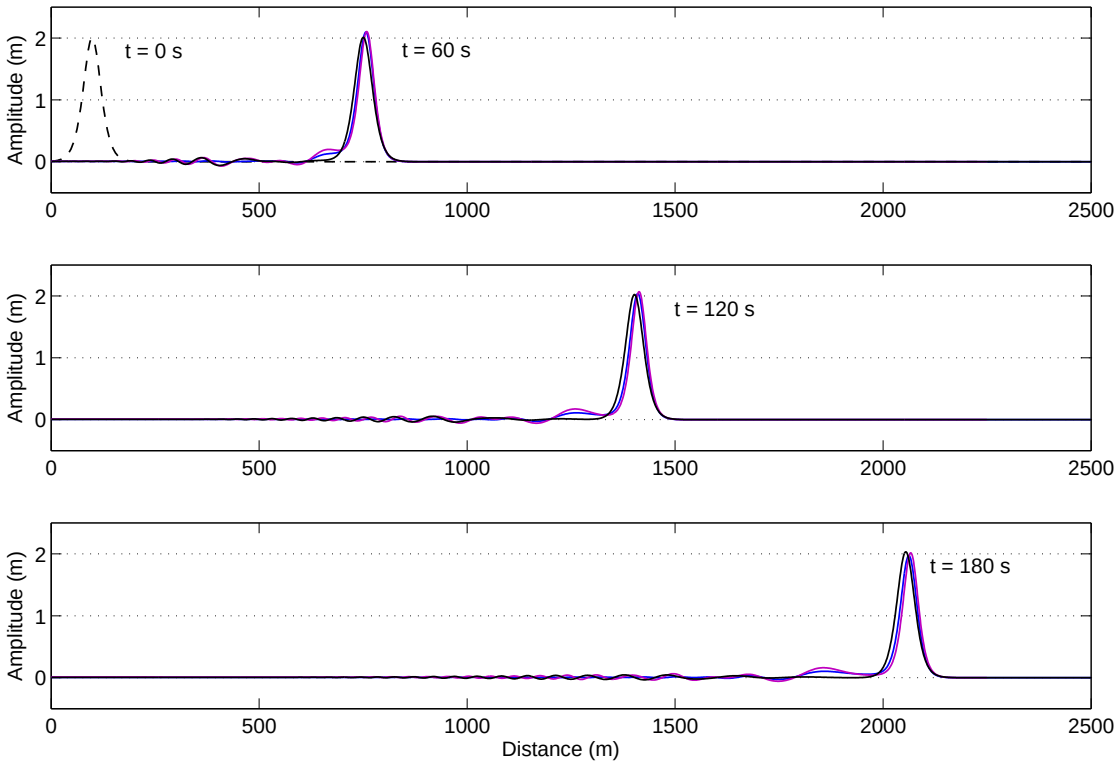

Figure 5.1. Solitary wave profile along a channel with constant water depth. Integrated two-layer model (black line), hybrid model (blue line), and one-layer model (purple line).

Figure 5.1 shows the wave profiles at $60\,s$, $120\,s$, and $180\,s$. The incompatibility between the initial analytical and the subsequent numerical solutions results in development of trailing waves at the beginning for all three models. The two-layer model, which maintains the waveform and height through the remaining computation, demonstrates a good balance between dispersion and nonlinearity in the governing equations. For the one-layer and hybrid models, a low-frequency component begin to separate from the leading solitary wave causing an initial increase of the wave amplitude at $t = 60\,s$. This small-amplitude component propagates at a lower speed and gradually lags behind the leading solitary wave decreasing its amplitude over time. This indicates an imbalance

between dispersion and nonlinearity in the governing equations that are further modified by the numerical schemes.

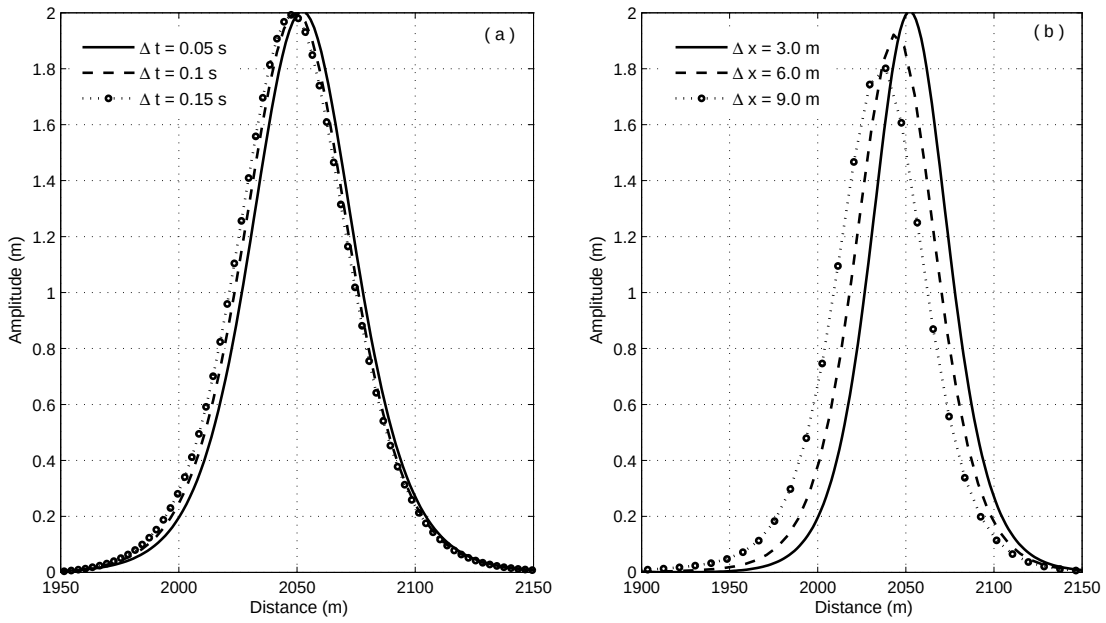

Figure 5.2. Solitary wave profiles at $t = 180\,s$ with different temporal and spatial resolution (a) $\Delta x = 3\,m$ (b) $\Delta t = 0.05\,s$.

The two-layer model is less susceptible to numerical artifacts arising from dispersion and nonlinearity and provides a platform for testing of the accuracy and stability of the numerical scheme. Figure 5.2 compares the wave profiles at $t = 180\,s$ with different temporal and spatial resolution. The profile computed with $\Delta t = 0.05\,s$ and $\Delta x = 3.0\,m$ is nearly identical to the analytical solution and provides a reference for comparison. In Figure 5.2 (a), the spatial resolution $\Delta x = 3.0\,m$ is fixed and the time step varies from $\Delta t = 0.05$ to $0.15\,s$ resulting in Courant numbers between 0.1651 and 0.4952. The results show reduction of the amplitude and celerity at high Courant numbers because of accumulation of truncation errors due to the increased number of iterations at each time step. Figure 5.2 (b) shows the wave profiles computed with Δx = 3, 6, and $9\,m$ at $\Delta t = 0.05\,s$. The Courant number remains low in these cases. However, a large grid size coupled with an explicit scheme for the advection terms may result in

significant numerical dissipation in the present model. Further testing showed that the model remains stable for a Courant number up to 0.79.

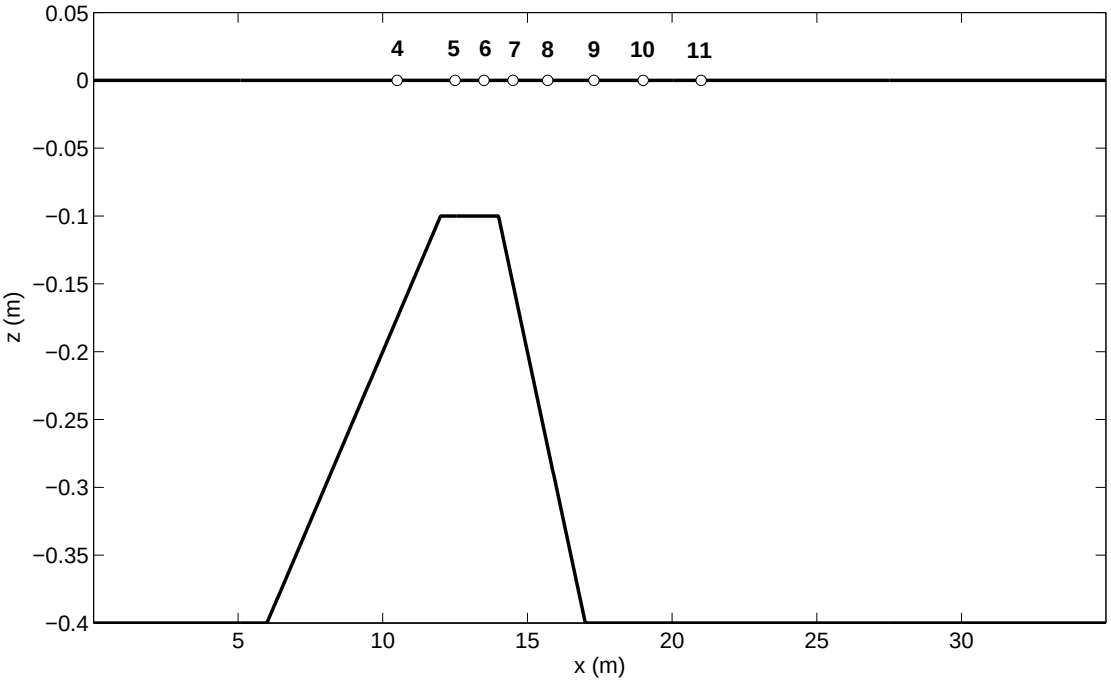

Figure 5.3. Sketch of submerged bar experiment. Circles indicate wave gauge locations.

5.2 Sinusoidal wave propagation over a bar

The laboratory experiments of Beji and Battjes (1993) and Luth et al. (1994) on wave propagation over a submerged bar provide a good illustration of coastal wave processes. Their work provides a useful dataset for validation of numerical wave models especially in their capability to describe dispersive waves (Stelling and Zijlema, 2003; Yamazaki et al., 2009; Roeber et al., 2010a). Figure 5.3 shows the numerical model setup. The flume is $35\,m$ long and $0.4\,m$ deep. A $0.3\,m$ high trapezoidal bar is located at $6\,m$ from the wave maker. The bar has a $2\,m$ crest with a 1:20 front slope and a 1:10 back slope. Regular sinusoidal waves are generated from the left boundary and a $10\,m$ sponge layer

and a radiation condition at the right boundary mimic the gravel beach in the laboratory experiment. Test case with wave amplitude and period of $0.01\,m$ and $2.02\,s$ corresponding to $kd = 0.67$ is selected. The small wave amplitude results in a weakly nonlinear problem that stands out the dispersion and shoaling properties in the comparison among the integrated two-layer, hybrid and one-layer models. With the origin defined at the wave maker, all three models utilize a grid size of $\Delta x = 0.05\,m$ in the $35\,m$ long computational domain. The use of the time step $\Delta t = 0.01\,s$ gives a Courant number of $Cr = 0.3962$. The surface roughness is small and unimportant in this experiment.

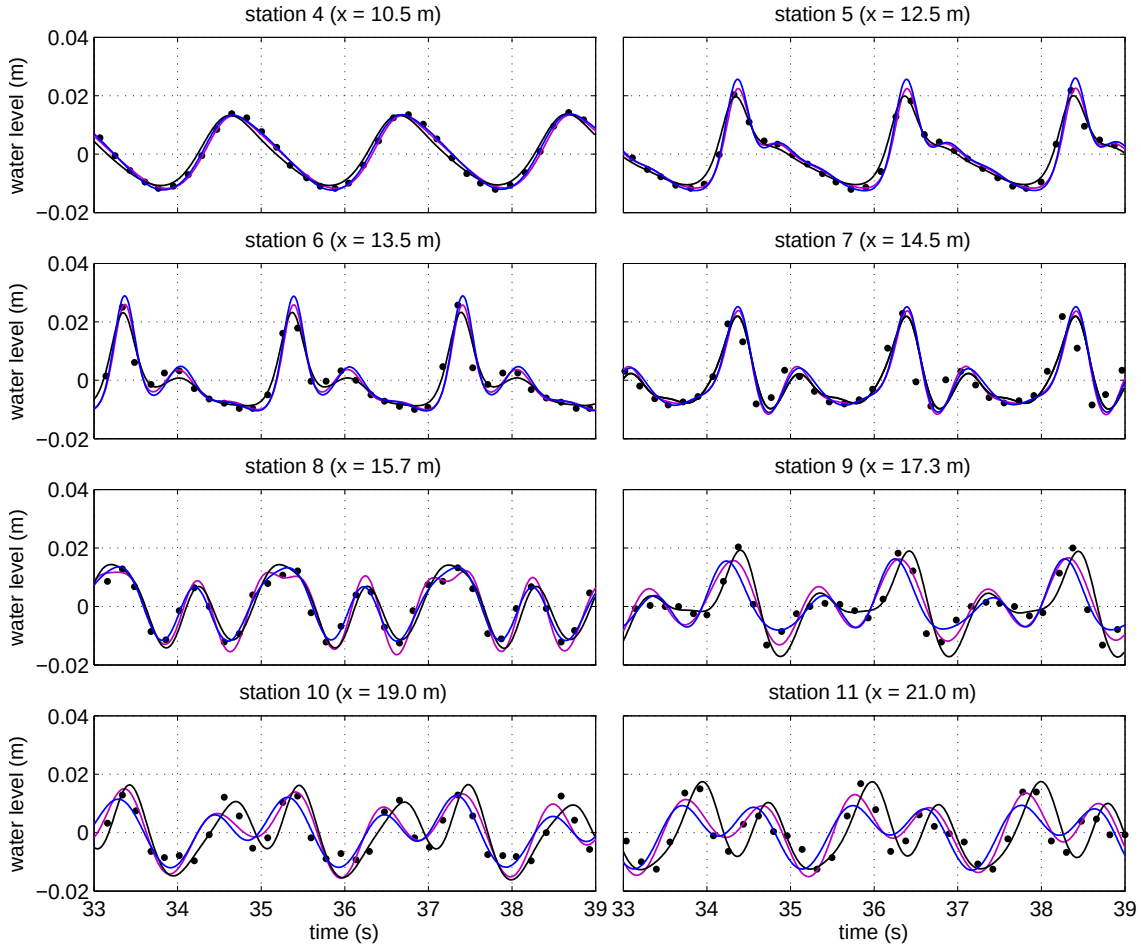

Figure 5.4. Comparison of computed and recorded free surface elevations over and behind a submerged bar. Integrated two-layer model (black line), hybrid model (blue line), one-layer model (purple line), and laboratory data (dots).

Figure 5.4 plots the recorded and computed surface profiles at eight stations over and behind the bar. The incident sinusoidal waves shoal over the front slope and the profile

becomes asymmetric at station 4. The comparison indicates very good agreement on the surface elevations from all three models up to station 7 on the back slope just behind the crest. The results from the one-layer model begin to deviate at station 8 when higher harmonics are released from the waves propagating down the slope. The results at stations 9 to 11, which are located behind the bar, show greater discrepancies among the three models. Although the one-layer and hybrid models are outside the applicable range of the dominant third-order harmonics at $0.67\,s$ with $kd = 3.6$, their results provide close approximations of the measurements. However, the dispersion properties become dependent on the numerical scheme when models are implemented beyond their applicable range (Yamazaki et al., 2009). The two-layer model, which reproduces the exact linear dispersion relation with an error of less than 5% up to $kd = 11$, provide good agreement with the recorded waveforms.

5.3 Regular wave shoaling on a plane beach

The laboratory experiment of Nwogu (1993) on wave propagation over a plane slope allows examination of model capabilities in describing wave dispersion, shoaling, and nonlinearity simultaneously. The experiments were conducted in a basin of $20\,m$ long, $30\,m$ wide, and $3\,m$ high at the National Research Council of Canada in Ottawa. Waves generated at a water depth of $0.56\,m$ propagate normally toward a 1:25 plane slope. A test case with regular incident waves of $0.033\,m$ amplitude and $1.5\,s$ period is considered. This gives rise to $kd = 1.0$ at the wave maker and decreasing values toward the beach for demonstration of the shoaling process. All three models utilize a grid size of $\Delta x = 0.025\,m$ and a time step of $\Delta t = 0.0025\,s$ to achieve the Courant number $Cr = 0.2344$. The surface roughness becomes important for wave processes on the

beach. A Manning coefficient of $n = 0.012$ accounts for the smooth concrete beach in the laboratory experiment.

Figure 5.5 compares the measured and computed surface profiles at $0.24\,m$ and $0.14\,m$ water depth corresponding to $kd = 0.7$ and 0.5. The hybrid model shows good agree-

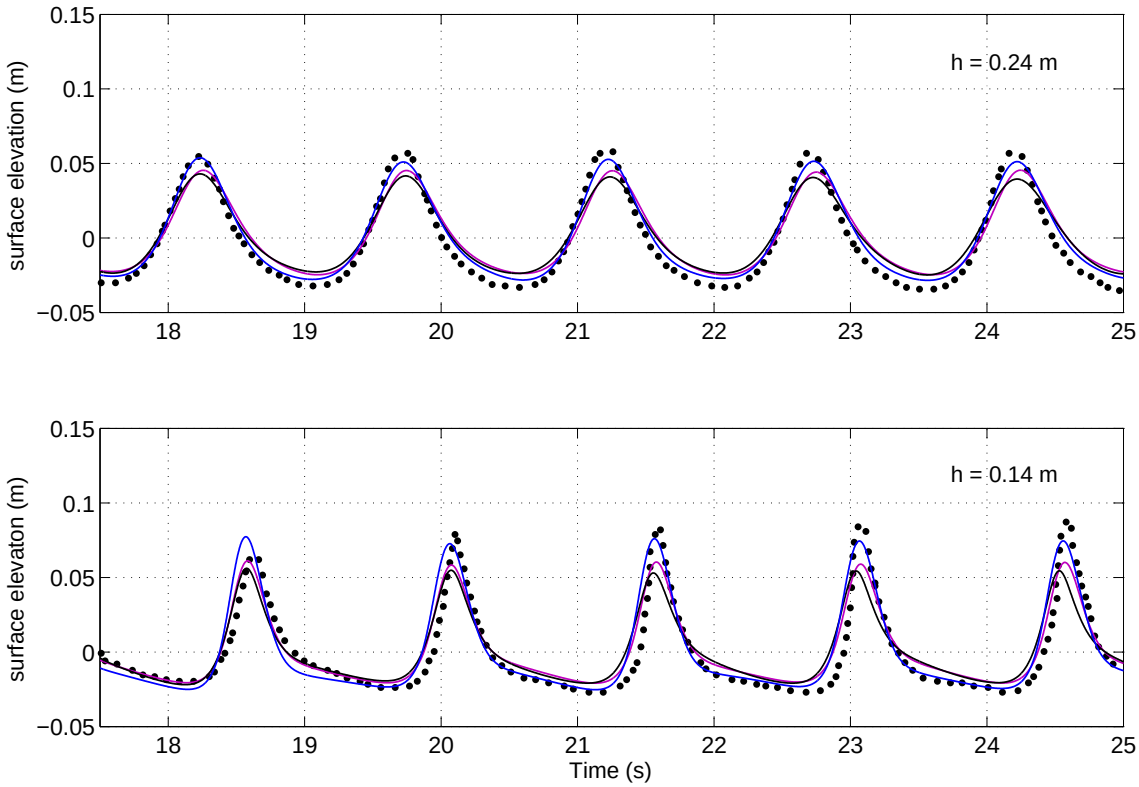

Figure 5.5. Comparison of computed and recorded surface elevation in the plane beach experiment. Integrated two-layer model (black line), hybrid model (blue line), one-layer model (purple line), and experiment data(dots).

ment with the laboratory data, whereas the one and two-layer models underestimate the wave height at both locations despite having better agreement with the exact linear shoaling gradient in the range of kd considered. At $h = 0.24\,m$, the hybrid model gives good predictions of the crest but slightly underestimates the trough. The one and two-layer models, however, underestimate both the crest and trough elevations. Since all three models capture the phase correctly, nonlinearity instead of dispersion is an issue in this case. A major source of nonlinearity derives from the kinematic free surface bound-

ary condition, which is approximated differently through the layer-averaged velocity in these models (see equations 2.3.13 and 2.4.5).

The hybrid model provides the best agreement with the laboratory data at $h = 0.14\,m$. The one and two-layer models reproduce the non-symmetric wave profile, but further underestimate the wave height due to increasing importance of nonlinearity at shallower water. The numerical results reinforce the findings from the second-order analysis in Section 3.2 that the hybrid model has better nonlinear properties associated with the layer-averaged velocity resulting from the predefined non-hydrostatic pressure distribution. However, the waves were observed to break around $h = 0.14\,m$ in the laboratory experiment. Apart from nonlinearity, dissipation due to wave breaking and the surf zone processes also affects the results. Although all three models describe wave breaking through the momentum-conserving advection scheme, the implementation in each model depends on the flow variables involved and results in different dissipation rates and incipient times.

5.4 Solitary wave transformation on a plane beach

The two-layer, hybrid, and one-layer formulations allow direct implementation of a momentum conserving scheme to describe breaking waves and a moving-waterline scheme to track flooding and drying of the beach. The laboratory experiment of solitary wave transformation on a plane beach from Synolakis (1987) provides a good dataset to validate these three models for wave breaking and runup calculations. A test case with a 1:19.85 beach slope and a wave height to depth ratio of $A/h = 0.3$ are considered here. A Manning coefficient of $n = 0.01$ approximates the surface roughness of the plexiglass flume and beach. Following Titov and Synolakis (1995), the initial solitary wave is placed one half wavelength from the toe of the beach in the numerical experiment.

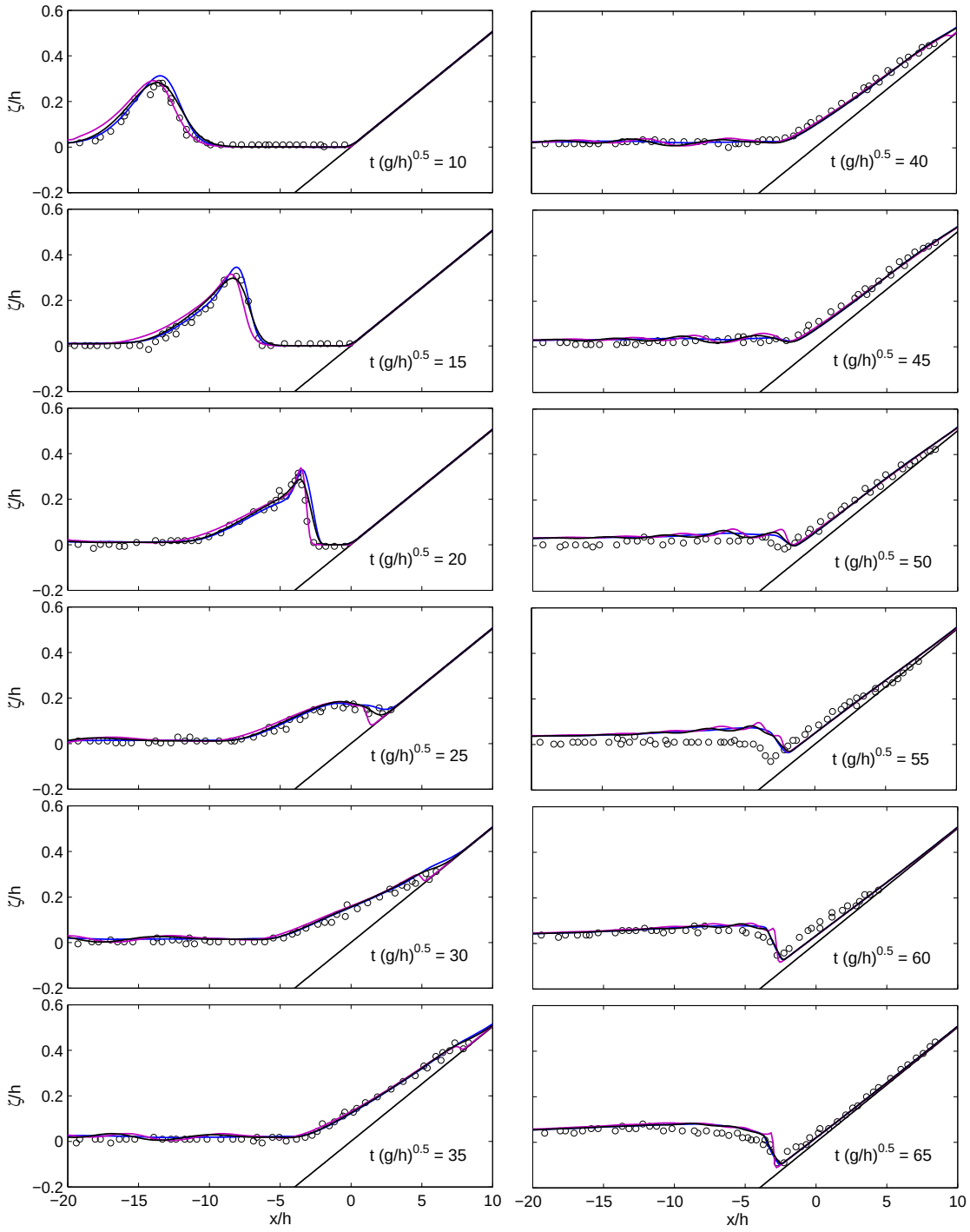

Figure 5.6. Comparison of computed and recorded surface profiles in the experiment of solitary wave runup on a 1:19.85 plane beach with $A/h = 0.3$. Integrated two-layer model (black line), hybrid model (blue line), one-layer model (purple line), and laboratory data (circles).

Figure 5.6 shows comparisons between the measured and computed waveforms over the slope. The solitary wave begins to transform as it enters shoaling water starting from $x/h = -20$ and develops into a plunging breaker around $t\,(g/h)^{0.5} = 20$ just before reaching the waterline. All three models reproduce the breaking process as a collapsing bore through momentum conservation without artificial dissipation mechanisms. The two-layer model generates a slightly lower bore compared with the hybrid and one-layer model. The flow transitions into a flux or advection-dominated process over the beach at $t\,(g/h)^{0.5} = 25$. The one-layer model yields a surge with a steep wave front that persists through the runup process. In contrast, the two-layer and hybrid models produce a surge with a gradual decrease of flow depth to the waterline. The resulting surge reaches a maximum elevation of $\zeta/h = 0.55$ around $t\,(g/h)^{0.5} = 40$. The drawdown process of the flow begins to generate a hydraulic jump around $t\,(g/h)^{0.5} = 50$. The one-layer model develops a steeper wave front compared to the laboratory measurements as well as the hybrid and two-layer model results. All three models describe the runup and drawdown processes reasonably well, but could not fully describe the hydraulic jump at $t\,(g/h)^{0.5} = 55$ probably due to the three-dimensional flow structure in the laboratory experiment. The computed results recover toward the end of the test demonstrating the resilience of these models.

The vertical flow exchange in a two-layer system is essential to maintain the correct speed and prevent a bore-like feature at the moving waterline. This can be demonstrated by turning off the interfacial advection terms $u_{z_\alpha}\overline{w}_{z_\alpha}$ and $w_{z_\alpha}\overline{w}_{z_\alpha}$ to eliminate vertical flow exchange in the two-layer model. Figure 5.7 compares the computed waveforms with and without the interfacial advection terms with the laboratory measurements. The two solutions produce the same results as the solitary wave shoals over the slope just before wave breaking around $t\,(g/h)^{0.5} = 20$. After wave breaking, a surge develops on the beach at about $t\,(g/h)^{0.5} = 25$. The solution with interfacial advection shows a smooth transition to the waterline. Without it, a bore-like feature develops immediately behind the waterline. The wave front maintains its distinctive feature and travels further

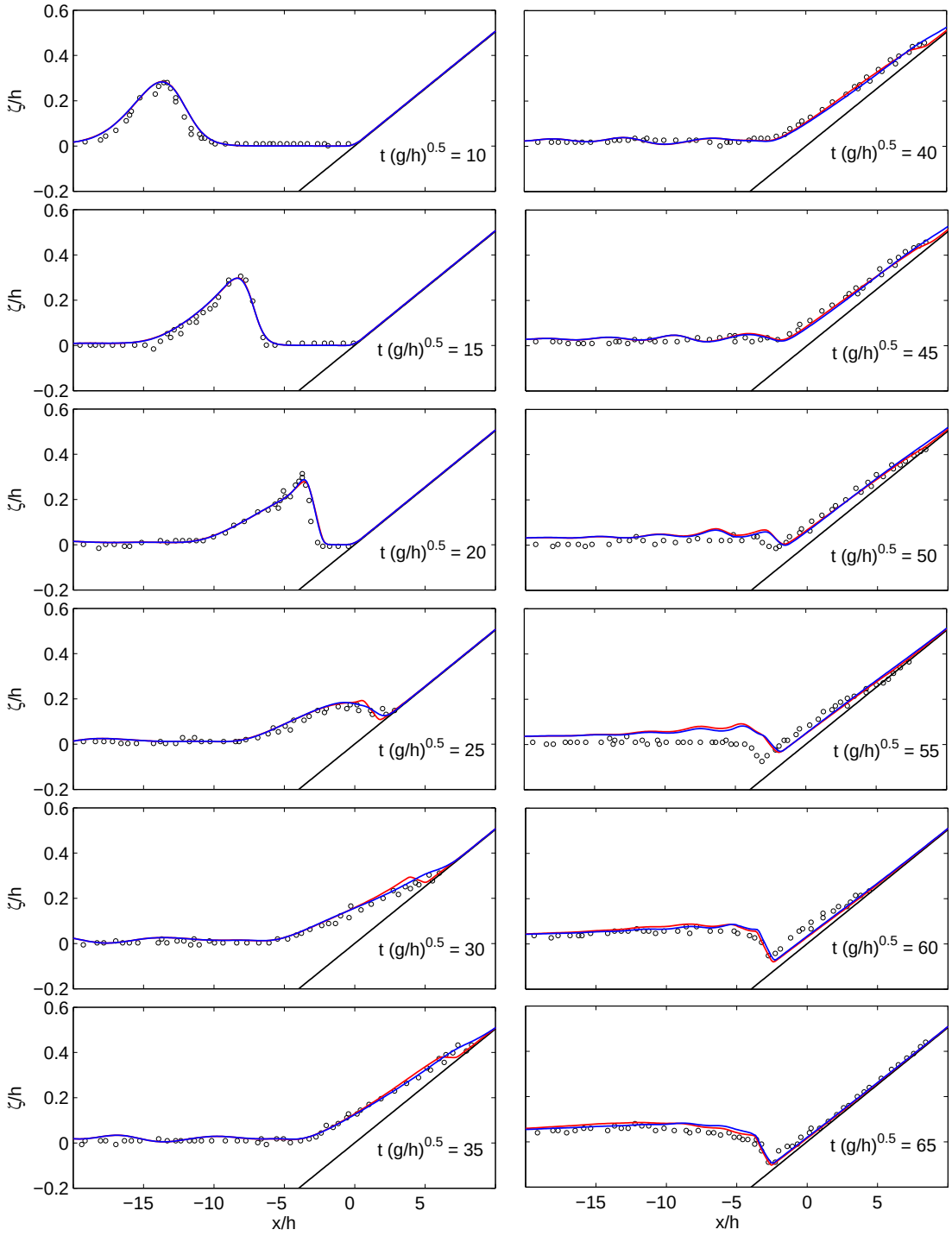

Figure 5.7. Surface profiles of solitary wave transformation on a plane beach from the integrated two-layer model with (blue line) and without (red line) interfacial advection. Circles denote laboratory measurements.

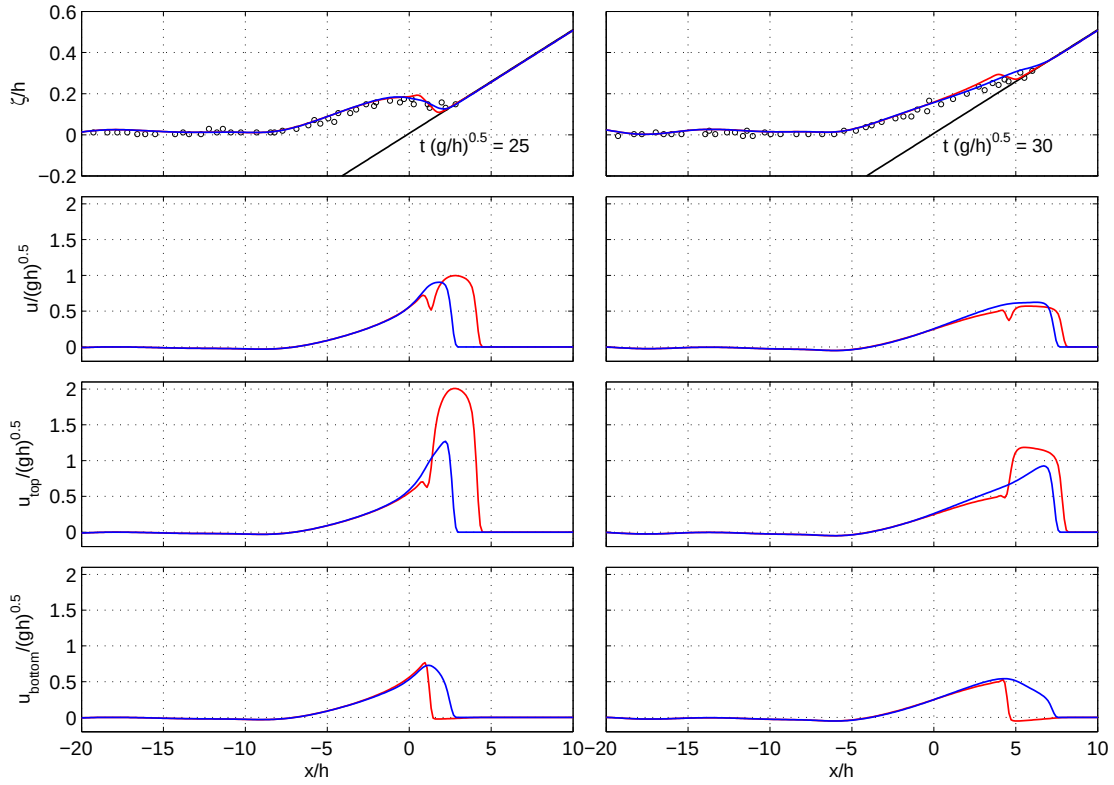

Figure 5.8. Surface and horizontal velocity profiles from the integrated two-layer model with (blue line) and without (red line) interfacial advection when $t(g/h)^{0.5}$ = 25 and 30.

onshore until the flow recedes at around $t\,(g/h)^{0.5} = 42$. Only minor discrepancies exist between the two numerical solutions when the flow draws down the beach.

To understand the difference in the two solutions, the horizontal velocity profiles at $t(g/h)^{0.5} = 25$ and 30 are examined in figure 5.8. When the bore collapses onto the shoreline, the velocity of the top layer u_{top} is higher than that of the bottom layer u_{bottom}. The two layers exchange momentum and mass through interfacial advection. The faster top layer transports water into the bottom layer at the wave front to advance the sheet flow at the correct speed on the initially dry bed. This transportation also induces an upward return flow from the bottom layer to balance the momentum and mass fluxes. This exchange between the two layers results in a rotational flow that mimics a vortex

at the wave front. It is in this way that the two layers of flow function coherently and act as a whole. The results show the flow velocity in each layer smoothly approaches zero at the waterline. When interfacial advection is disabled, the two layers lose the ability to describe interfacial activities and start to behave separately at the wave front. The top layer over takes the bottom layer to generate a bore-like feature in surface elevation and produces a sharp increase of the flow velocity beyond the wave front into a sheet flow. The flow in bottom layer terminates with a rapid decrease of the velocity at the wave front. This leads to a local discontinuity of the depth-integrated velocity at the bore-like feature. The comparison indicates that without interfacial advection, the transport of the fluid is not continuous and an unrealistic flow structure may occur at the waterline.

5.5 Solitary wave propagation over a fringing reef

Roeber (2010) conducted two series of laboratory experiments on solitary wave transformation over idealized fringing reefs at the O.H. Hinsdale Wave Research Laboratory of Oregon State University. The configuration consists of a steep fore reef, a reef crest, and a reef flat commonly seen in tropical coastal environments. The experiments provided a valuable dataset for validating shock-capturing capabilities of dispersive wave models (Roeber et al., 2010a). The selected tests for the present study were conducted in the Large Wave Flume of $104\,m$ long, $3.66\,m$ wide, and $4.57\,m$ high. The setup includes a fore reef with a 1:12 slope beginning at $25.9\,m$ from the wave maker followed by a $0.2\,m$ wide reef crest and a reef flat. The water depth of $2.56\,m$, which is at the level of the reef crest, submerges the flat by $0.2\,m$ to form a shallow lagoon. The submerged reef does not involve flows over initially dry surface and avoid problems with the lack of interfacial advection in the one-layer model to provide a consistent comparison of the dispersion and nonlinear properties in the three models. This condition accentuates

the shock-related hydraulic processes involving bores and hydraulic jumps for model evaluation.

The solitary wave heights of $A = 0.256\,m$ and $0.768\,m$ are considered. These result in dimensionless wave heights of $A/d = 0.1$ and 0.3 to examine the model capability in handling dispersion and shoaling in varying degrees of nonlinearity. All three models use a grid size of $\Delta x = 0.1\,m$ and a time step of $\Delta t = 0.005\,s$ for a Courant number of $Cr = 0.2476$. A Manning coefficient of $n = 0.012$ defines the surface roughness of the concrete reef system in the laboratory experiment. Figure 5.9 shows the computed and measured surface elevations along the flume for $A/d = 0.1$. The small amplitude solitary wave steepens over the reef and overtops the reef crest without breaking. The surge transitions from subcritical to supercritical over the back slope of the crest and generates a hydraulic jump in the lagoon. The influx of water in turn produces a bore propagating in the downstream direction. All three models give very good agreement with the laboratory data. The results from the hybrid and two-layer models are nearly identical. The one-layer model gives rise to a minor discrepancy near the bore and hydraulic jump due insufficient resolution of the non-hydrostatic pressure at the discontinuities.

The comparison in figure 5.10 shows more discernible discrepancies between the three solutions for the larger wave height of $A/d = 0.3$. While all three models produce the same incident solitary wave profile in front of the reef, slight deviations emerge as the wave shoals over the slope because of the varying capability to account for non-hydrostatic and nonlinear effects. Consistent with the results from non-dispersive or weakly dispersive models (Yamazaki et al., 2009; Wei et al., 2006), the profile from the one-layer model steepens and collapses earlier as the wave begins to break over the reef crest around $t\sqrt{g/h} = 87.46$. These models approximate the breaking process as a collapsing bore albeit with a slight offset in timing and give the same predictions over the fore reef, when the surface slope decreases and nonlinearity abates after wave breaking. This results in similar hydraulic jumps over the back slope of the reef crest.

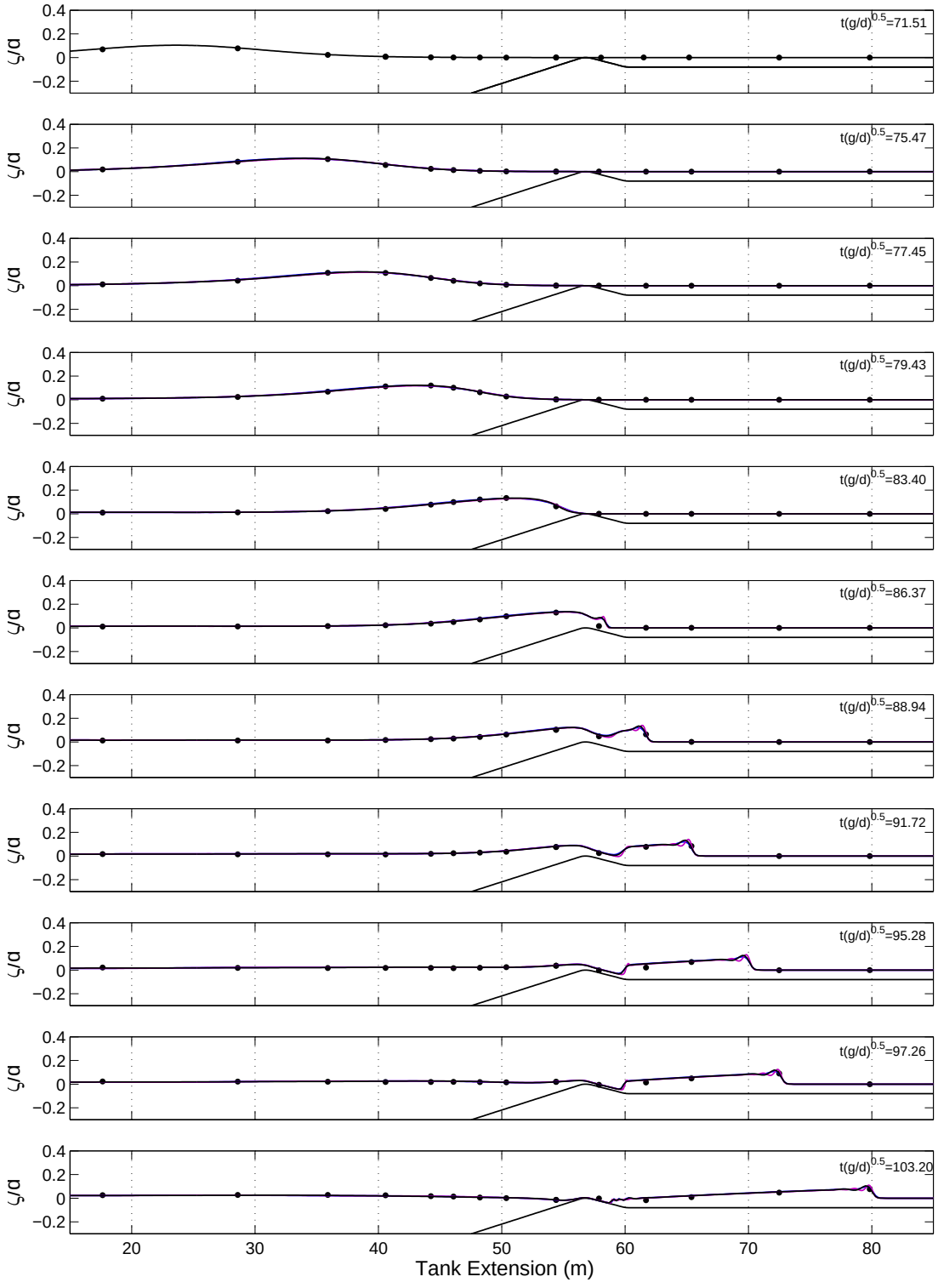

Figure 5.9. Comparison of computed and recorded surface profiles in the reef experiment with $A/h = 0.1$. Integrated two-layer model (black line), hybrid model (blue line), one-layer model (purple line), and measured data (dots).

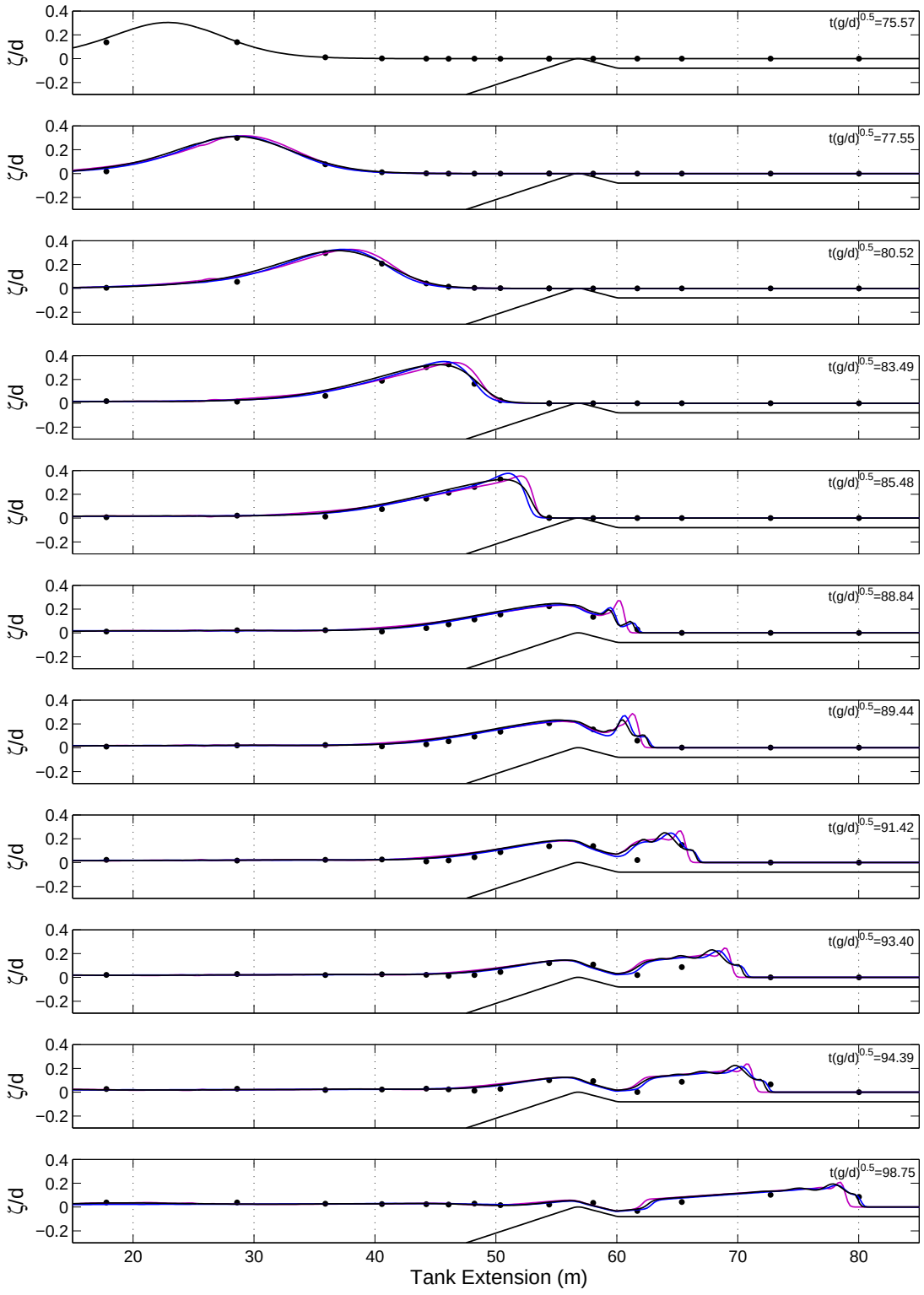

Figure 5.10. Comparison of computed and recorded surface profiles in the reef experiment with $A/h = 0.3$. Integrated two-layer model (black line), hybrid model (blue line), one-layer model (purple line), and measured data (dots).

As the bore begins to develop and propagate into the lagoon, the discrepancy in the celerity becomes significant over time.

The flow over the reef flat is flux dominated, but the vertical flow structure is important near discontinuities. The one-layer flow structure impedes the advection across the discontinuity and distorts the strength and phase of the shock. The effects, which might not be noticeable in the hydraulic jump immediately behind the reef crest, are cumulative for the propagating bore and become more pronounced with higher nonlinearity. The hybrid and two-layer models allow both horizontal and vertical advection across the discontinuity to more appropriately describe the flow structure as well as the bore formation and propagation as in the laboratory experiment. Shock-capturing capabilities and adequate resolution of vertical flow structures are necessary to describe flow discontinuities.

Roeber (2010) also conducted a series experiments of the solitary wave propagation in the same setup but with a smaller water depth of $2.5\,m$. This exposes the crest by $0.06\,m$ and submerges the flat by $0.14\,m$. The exposed reef involves intermittent wet-dry conditions that require the interfacial advection to facilitate vertical flow exchange and to maintain correct speed and wave profile for the sheet flow across it. Figure 5.11 compares the measured wave profile and the two-layer model results with and without interfacial advection. The two numerical solutions remain identical through the wave breaking process until the wave reaches the reef crest at $t(g/d)^{0.5} = 68.74$. Without interfacial advection, the higher momentum in the top layer causes the wave front to surge forward and generate a bore in the lagoon. The subsequent overtopping of the solitary wave over the crest generates a second bore. The two bores are fully developed by $t(g/d)^{0.5} = 73.10$ and travel down the lagoon. In contrast, interfacial advection allows transfer of the excess momentum to the bottom layer and maintain the sheet flow across the crest. This produces a single bore in the lagoon as observed in the laboratory experiment Roeber (2010). The comparison indicates that interfacial

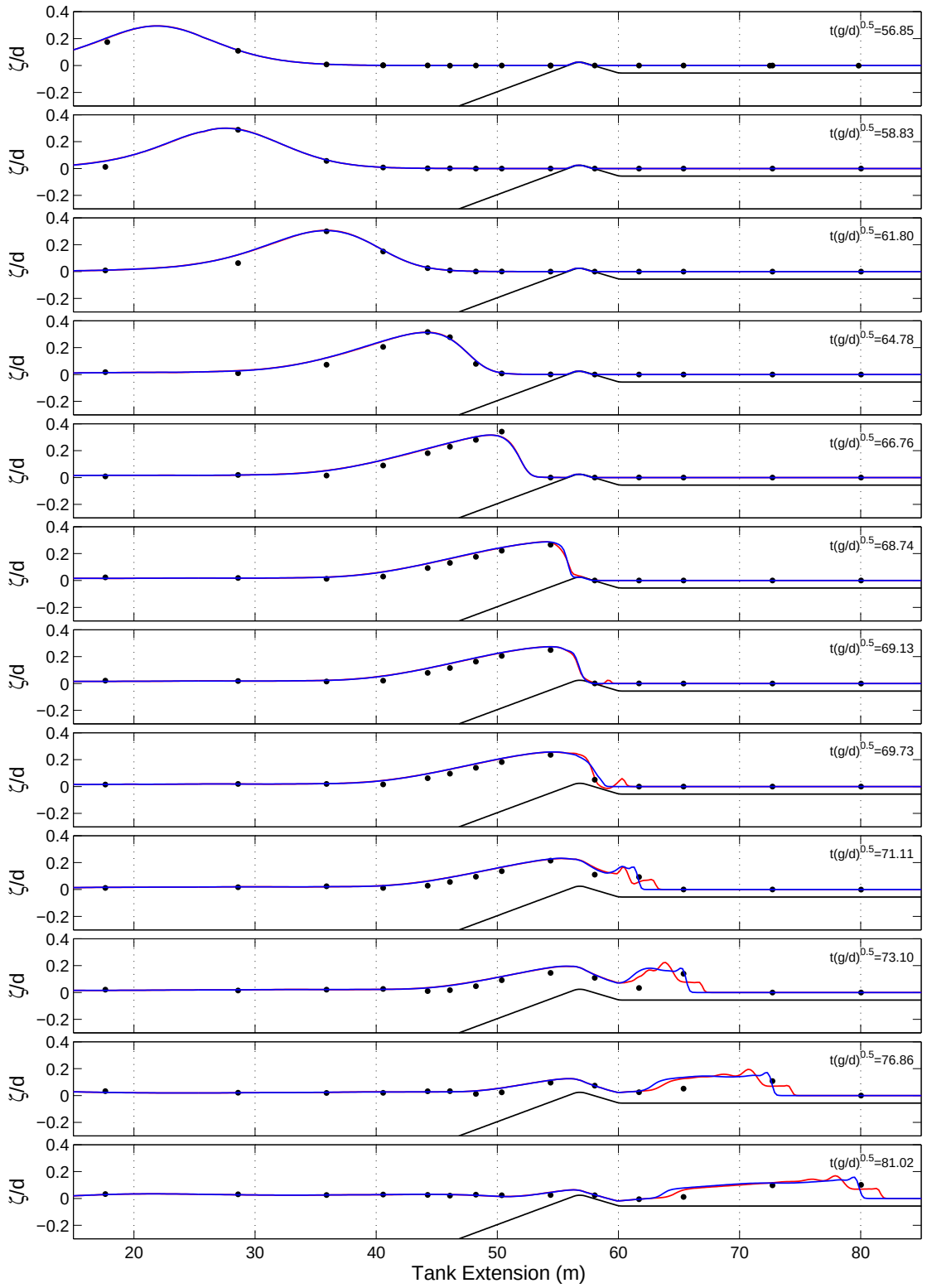

Figure 5.11. Surface profile of solitary wave propagation over an exposed fringing reef from the integrated two-layer model with (blue line) or without (red line) interfacial advection. Dots denote laboratory measurements.

advection is essential for a two or multilayer model to synchronize the flow over the water column at the wet-dry moving boundary.

Chapter 6

Conclusions and Recommendations

This study has introduced an alternate formulation for multi-layer non-hydrostatic flows and demonstrated its capabilities in handing discontinuous flows and moving wet-dry boundaries with a two-layer model. A linear transformation between the two layers recasts the governing equations into a flux-dominated and a dispersion-dominated system. The new governing equations maintain the dispersion characteristics of the conventional two-layer system. The removal of the layer interface from the governing equations simplifies the implementation of the momentum-conserving advection scheme for breaking wave approximation and a moving-waterline scheme for inundation calculation.

To lower the computational requirements, a predefined piecewise linear distribution of the non-hydrostatic pressure coverts the integrated two-layer flow system into a hybrid system with a free parameter, which in turn is optimized for a specific range of water depth parameters. The approximation to the non-hydrostatic pressure reduces the non-symmetric 9-band sparse matrix in the integrated two-layer system into a non-symmetric tridiagonal matrix with one half of the rank as in a one-layer model, while maintaining necessary dispersion characteristics for practical application. A one-layer system can be recovered by setting the tuning parameter as 0.5.

A perturbation procedure develops the first and second-order governing equations for a systematic analysis of the linear and nonlinear wave properties associated with the two-layer, hybrid, and one-layer models. Dispersion is fundamental to the non-hydrostatic formulation of free surface flows. The two-layer model reproduces the exact linear dispersion relation within a 5% error for water depth parameter up to $kd = 11$. The hybrid model can be satisfactorily tuned for the water depth parameter $0 < kd \leq 3$ as in the extended Boussinesq model of Nwogu (1993), while the one-layer model produces better performance than the classical Boussinesq model. In terms of the linear shoaling gradient, the one and two-layer models provide slightly better performance than the hybrid model, which is optimized to reproduce the linear dispersion relation. However, the hybrid model exhibits better performance than the two-layer model in reproducing super-harmonics and sub-harmonics in nonlinear wave-wave interactions.

Numerical implementation of the integrated two-layer system is conducted on a staggered grid by a finite difference scheme in the horizontal direction with the θ-method for time integration. A finite volume scheme resolves the vertical velocity distribution with the Keller box method and gives rise to a Poisson-type equation for the non-hydrostatic pressure. The pressure correction technique of Zijlema and Stelling (2005), which consists of a hydrostatic and a non-hydrostatic step in the solution procedure, works well for the integrated two-layer model. The numerical solution remains stable and accurate with proper temporal and spatial resolution. The numerical framework reduces to the hybrid and one-layer models through adjustment of the tuning parameter in the non-hydrostatic pressure distribution.

The integrated two-layer and hybrid models provide an accurate description of dispersive waves in a series of test cases without compromising the capability to describe flux-dominated processes such as wave breaking, bore propagation, and sheet flow. The computed results give very good agreement with laboratory measurements for wave transformation over a submerged bar, a plane beach, and fringing reefs. The submerged

bar experiment with weak nonlinearity demonstrates the important role of dispersion in coastal wave transformation. The plane beach experiment confirms both dispersion and nonlinearity play a primary role in defining shoaling processes. The fringing reef tests illustrate the vertical flow structure is crucial in describing the advection across discontinuities associated with bore formation and propagation. Interfacial advection is essential for a multi-layer models to describe rotational flows at the wet-dry moving boundary.

The analytical and numerical studies have shown the advantages of the hybrid model in describing coastal wave transformation. The hybrid model provides comparable or better results as the two-layer model partly due to its good nonlinear properties, but at substantially lower computational requirements. Its non-hydrostatic formulation is identical to the one-layer model, NEOWAVE, of Yamazaki et al. (2009, 2011). A logical next step is to extend NEOWAVE with the hybrid formulation for modeling of coastal and surf-zone processes. Future research on the multi-layer non-hydrostatic models should be directed toward quantification of the rotational flow across flow discontinuities and at the moving wet-dry boundary.

Bibliography

Agnon, Y., Madsen, P. A. and Schäffer, H. A. 1999 A new approach to high order Boussinesq models. *Journal of Fluid Mechanics* **399**, 319 – 333.

Ai, C. and Jin, S. 2012 A multi-layer non-hydrostatic model for wave breaking and runup. *Coastal Engineering* **62**, 1 – 8.

Beji, S. and Battjes, J. A. 1993 Experimental investigation of wave propagation over a bar. *Coastal Engineering* **19**, 151 – 162.

Beji, S. and Nadaoka, K. 1996 A formal derivation and numerical modelling of the improved boussinesq equations for varying depth. *Ocean Engineering* **23**, 691 – 704.

Casulli, V. 1995 Recent developments in semi-implicit numerical methods for free surface hydrodynamics, Vol.2, Part B, advances in Hydroscience and Engineering. *Proceedings of the Second International Conference on Hydroscience and Engineering at Beijing* pp. 2174 – 2181.

Casulli, V. 1999 A semi-implicit finite difference method for non-hydrostatic, free-surface flows. *International Journal for Numerical Methods in Fluids* **30**, 425 – 440.

Casulli, V. and Stelling, G. S. 1998 Numerical simulation of 3D quasi-hydrostatic, free-surface flows. *Journal of Hydraulic Engineering* **124**, 678 – 686.

Chen, Y. and Liu, L. F. 1995 Modified boussinesq equations and associated parabolic models for water wave propagation. *Journal of Fluid Mechanics* **288**, 351 – 381.

Dean, R. G. and Sharma, J. N. 1981 Simulation of wave systems due to nonlinear directional spectra. *Proceedings of the Internatioinal Symposium Hydrodynamics in Ocean Engineering, The Norwegian Institue of Technlogy* **2**, 1211 – 1222.

Dutykh, D., Katsaounis, T. and Mitsotakis, D. 2011 Finite volume scheme for dispersive wave propagation and runup. *Journal of Computational Physics* **230**, 3035 – 3061.

Gobbi, M. F., Kirby, J. T. and Wei, G. 2000 A fully nonlinear boussinesq model for surface waves Part 2. Extension to $o(kh)^4$. *Journal of Fluid Mechanics* **405**, 181 – 210.

Kennedy, A. B., Chen, Q., Kirby, J. T. and Dalrymple, R. A. 2000 Boussinesq modeling of wave transformation, breaking, and runup. 1: 1d. *Journal of Waterway, Port, Coastal and Ocean Engineering* **126**, 39 – 47.

Kim, D. H., Lynett, P. J. and Socolofsky, S. A. 2009 A depth-integrated model for weakly dispersive, turbulent, and rotational fluid flows. *Ocean Modelling* **27**, 198 – 214.

Lay, T., Ammon, C. J., Yamazaki, Y., Cheung, K. F. and Hutko, A. R. 2011a The 25 October 2010 Mentawai tsunami earthquake and the tsunami hazard presented by shallow megathrust ruptures. *Geophysical Research Letters* **38**, L06302, doi:10.1029/2010GL046552.

Lay, T., Yamazaki, Y., Ammon, C. J., Cheung, K. F. and Kanamori, H. 2011b The 2011 M(w) 9.0 off the Pacific coast of Tohoku Earthquake: Comparison of deep-water tsunami signals with finite-fault rupture model predictions. *Earth Planets and Space* **63**, 797 – 801.

Luth, H. R., Klopman, G. and Kitou, N. 1994 Project 13G. kinematic of waves breaking partially on an offshore bar; LDV measurements for waves with and without a net onshore current. H 1573, Delft Hydraulics.

Lynett, P. J., Wu, T. R. and Liu, P. 2002 Modeling wave runup with depth-integrated equations. *Coastal Engineering* **46**, 89 – 107.

Madsen, P. A., Bingham, H. B. and Schäffer, H. A. 2003 Boussinesq-type formulation for fully nonlinear and extremely dispersive water waves: derivation and analysis. *Proceedings of the Royal Society of London* **A**, 1075 – 1104.

Madsen, P. A., Fuhrman, D. R. and Wang, B. 2006 A Boussinesq-type method for fully nonlinear waves interacting with a rapidly varying bathymetry. *Coastal Engineering* **53**, 487 – 504.

Madsen, P. A., Murray, R. and Sørensen, O. R. 1991 A new form of boussinesq equations with improved linear dispersion characteristics. *Coastal Engineering* **15**, 371 – 388.

Madsen, P. A. and Sørensen, O. R. 1992 A new form of the Boussinesq equations with improved linear dispersion characteristics. part A: slowly-varying bathymetry. *Coastal Engineering* **18**, 183 – 204.

Madsen, P. A. and Sørensen, O. R. 1997 Surf zone dynamics simulated by a Boussinesq type model. Part I. Model description and cross-shore motion of regular waves. *Coastal Engineering* **32**, 255 – 287.

Mahadevan, A., Oliger, J. and Street, R. L. 1996a A non-hydrostatic mesoscale ocean model, Part I: Well-posedness and scaling. *Journal of Physical Oceanography* **269**, 1868 – 1880.

Mahadevan, A., Oliger, J. and Street, R. L. 1996b A non-hydrostatic mesoscale ocean model, Part II: Numerical implementation. *Journal of Physical Oceanography* **269**, 1881 – 1900.

Marshall, J., Hill, C., Perelman, L. and Adcroft, A. 1997 Hydrostatic, quasi-hydrostatic, and non-hydrostatic ocean modeling. *Journal of Geophysical Research* **102**, 5733 – 5752.

Nwogu, O. 1993 Alternative form of Boussinesq equations for nearshore wave propagation. *Journal of Waterway, Port, Coastal and Ocean Engineering* **119**, 618 – 638.

Ottesen-Hansen, N. E. 1978 Long period waves in natural wave train. *Progress report no. 46 Institute Hydrodyn. and Hydraulic Engineering, Technical University of Denmark* **46**, 13 – 24.

Peregrine, D. H. 1967 Long waves on a beach. *Journal of Fluid Mechanics* **27**, 815 – 827.

Roeber, V. 2010 Boussinesq-type Model for Nearshore Wave Processes in Fringing Reef Environment. Ph.D Dissertation, University of Hawaii, Honolulu.

Roeber, V., Cheung, K. F. and Kobayashi, M. H. 2010a Shock-capturing Boussinesq-type model for nearshore wave processes. *Coastal Engineering* **57**, 407 – 423.

Roeber, V., Yamazaki, Y. and Cheung, K. F. 2010b Resonance and impact of the 2009 samoa tsunami around Tutuila, American Samoa. *Geophysical Research Letters* **37**, L21604, doi:10.1029/2010GL044419.

Sand, S. E. and Mansard, E. P. D. 1986 Reproducetion of higher harmonics in irregular waves. *Ocean Engineeing* **13**, 57 – 83.

Schäffer, H. A., Madsen, P. and Deigaard, R. 1993 A Boussinesq model for wave breaking in shallow water. *Coastal Engineering* **20**, 185 – 202.

Schäffer, H. A. and Madsen, P. A. 1995 Further enhancements of Boussinesq-type equations. *Coastal Engineering* **26**, 1 – 14.

Stansby, P. K. and Zhou, J. G. 1998 Shallow-water flow solver with non-hydrostatic pressure: 2D vertical plane problems. *International Journal for Numerical Methods in Fluids* **28**, 541 – 563.

Stelling, G. S. and Duinmeijer, S. P. A. 2003 A staggered conservative scheme for every Froude number in rapidly varied shallow water flows. *International Journal for Numerical Methods in Fluids* **43**, 1329 – 1354.

Stelling, G. S. and Zijlema, M. 2003 An accurate and efficient finite-difference algorithm for non-hydrostatic free-surface flow with application to wave propagation. *International Journal for Numerical Methods in Fluids* **43**, 1 – 23.

Synolakis, C. E. 1987 The runup of solitary wave. *Journal of Fluid Mechanics* **185**, 523 – 545.

Titov, V. V. and Synolakis, C. E. 1995 Modeling of breaking and nonbreaking long-wave evolution and runup using VTCS-2. *Journal of Waterway, Port, Coastal and Ocean Engineering* **121**, 308 – 316.

Tonelli, M. and Petti, M. 2009 Hybrid finite volume - finite difference scheme for 2DH improved Boussinesq equations. *Coastal Engineering* **56**, 609 – 620.

Veeramony, J. and Svendsen, I. A. 2000 The flow in surf-zone waves. *Coastal Engineering* **39**, 93 – 122.

Wei, G., Kirby, J. T. and Grilli, S. T. 1995 A fully nonlinear boussinesq model for surface waves. Part 1. Highly nonlinear unsteady waves. *Journal of Fluid Mechanics* **294**, 71 – 92.

Wei, Y., Mao, X. Z. and Cheung, K. F. 2006 Well-balanced finite-volume model for long-wave runup. *Journal of Waterway, Port, Coastal and Ocean Engineering* **132**, 114 – 124.

Yamazaki, Y. 2010 Depth-integrated, Non-hydrostatic Model with Grid-nesting for Tsunami Generation, Propagation and Runup. Ph.D Dissertation, University of Hawaii, Honolulu.

Yamazaki, Y. and Cheung, K. F. 2011 Shelf resonance and impact of near-field tsunami generated by the 2010 Chile earthquake. *Geophysical Research Letters* **38**, L12605, doi:1029/2011GL047508.

Yamazaki, Y., Cheung, K. F. and Kowalik, Z. 2011 Depth-integrated, non-hydrostatic model with grid nesting for tsunami generation, propagation and runup. *International Journal for Numerical Methods in Fluids* **67**, 2081 – 2107.

Yamazaki, Y., Kowalik, Z. and Cheung, K. F. 2009 Depth-integrated, non-hydrostatic model for wave breaking and runup. *International Journal for Numerical Methods in Fluids* **61**, 473 – 497.

Zelt, J. A. 1991 The runup of non-breaking and breaking solitary waves. *Coastal Engineering* **15**, 205 – 246.

Zhou, J. G. and Stansby, P. K. 1999 An arbitary Lagrangian-Eulerian σ (ALES) model with non-hydrostatic pressure for shallow water flows. *Computer Methods in Applied Mechanics and Engineering* **178**, 199 – 214.

Zijlema, M. and Stelling, G. S. 2005 Further experiences with computing non-hydrostatic free-surface flows involving water waves. *International Journal for Numerical Methods in Fluids* **48**, 169 – 197.

Zijlema, M. and Stelling, G. S. 2008 Efficient computation of surf zone waves using the nonlinear shallow water equations with non-hydrostatic pressure. *International Journal for Numerical Methods in Fluids* **55**, 780 – 790.

Zijlema, M., Stelling, G. S. and Smit, P. 2011 SWASH: An operational public domain code for simulating wave fields and rapidly varied flows in coastal waters. *Coastal Engineering* **58**, 992 – 1012.